A Stochastic Approach to Broadband Control of Parametrically Uncertain Structures

by

Douglas G. MacMartin

B.A.Sc. University of Toronto (1987)
S.M. Massachusetts Institute of Technology (1990)

SUBMITTED TO THE DEPARTMENT OF
AERONAUTICS AND ASTRONAUTICS
IN PARTIAL FULFILLMENT OF THE REQUIREMENTS
FOR THE DEGREE OF
Doctor of Philosophy
at the
Massachusetts Institute of Technology
June, 1992

Signature of Author _____
Department of Aeronautics and Astronautics
May 6, 1992

Certified by _____
Professor Steven R. Hall
Thesis Committee Chairman, Department of Aeronautics and Astronautics

Certified by _____
Professor Dennis S. Bernstein
Department of Aerospace Engineering, The University of Michigan

Certified by _____
Professor Andreas von Flotow
Department of Aeronautics and Astronautics

Certified by _____
Professor Michael Athans
Department of Electrical Engineering and Computer Science

Certified by _____
Professor Edward F. Crawley
Department of Aeronautics and Astronautics

Accepted by _____
Professor Harold Y. Wachman
Chairman, Department Graduate Committee

A Stochastic Approach to Broadband Control of Parametrically Uncertain Structures

by

Douglas G. MacMartin

SUBMITTED TO THE DEPARTMENT OF AERONAUTICS AND ASTRONAUTICS
ON MAY 6, 1992, IN PARTIAL FULFILLMENT OF THE
REQUIREMENTS FOR THE DEGREE OF
DOCTOR OF PHILOSOPHY

This thesis describes an approach for designing optimal low authority controllers for flexible structures with collocated sensors and actuators. The parametric uncertainty in the structural model is treated as stochastic, and the cost is averaged with respect to the uncertain parameters. The Statistical Energy Analysis assumptions of equipartition and incoherence can be shown to hold for the average covariance of a structure with uncertain modal frequencies. Using these properties, and conservation of energy, the average value of a global $\mathcal{H}_2$ performance metric can be expressed in terms of the power dissipation of the compensator. This power dissipation can be represented using the dereverberated mobility; an experimentally determined local structural model which ignores the effect of the reverberant field. Minimizing the resulting cost yields controllers with good performance which are guaranteed to be stabilizing. The approach is demonstrated on several examples, and experimentally verified on the M.I.T. Space Engineering Research Center interferometer testbed. This stochastic approach achieved a performance reduction that was approximately 30% greater than the constant gain "rate feedback" approach.

Thesis Committee: Dr. Steven R. Hall
Associate Professor of Aeronautics and Astronautics
Dr. Dennis S. Bernstein
Professor of Aerospace Engineering, The University of Michigan
Dr. Andreas H. von Flotow
Associate Professor of Aeronautics and Astronautics
Dr. Michael Athans
Professor of Electrical Engineering and Computer Science
Dr. Edward F. Crawley
Professor of Aeronautics and Astronautics

Acknowledgements

There are many people who contributed in some way to the research in this thesis, and it is certainly not possible to thank every single person whose conversations and suggestions helped solve some problem, or sparked some idea. There are, however, a number of people whose contributions were particularly significant, and who should be recognized. First, I would like to thank my advisor, Professor Steven R. Hall, whose ideas, intuition and guidance were invaluable. He also made sure that I consistently misspelled words like "behaviour" and "centre" throughout the thesis. The rest of the members of my thesis committee were also invaluable. Professor Dennis Bernstein and I worked at length during his frequent visits, and the results of that research are particularly evident in Chapter 3 and in the multiple-model paper. Professor Andy von Flotow gave a valiant effort to keep me connected with reality, and his insight was tremendous. He also pointed me towards SEA literature in the first place. Professor Michael Athans gave me the opportunity to teach a section of MCS I, which was both a valuable and an enjoyable experience. While not on my committee, Dr. David Miller certainly contributed significantly, particularly to the implementation issues discussed in Chapter 7. Dr. Denis Mustafa helped me understand $\mathcal{H}_\infty$ theory, particularly while trapped on his exercise bicycle, and helped provide theoretical rigour, particularly in Chapter 5. Thanks also to the patience of Dina, Sam, Gary, Eric and the rest of the interferometer team with my experimental questions; Jon and others with the rest of my questions.

In addition to the help I received on the research in this thesis, I am also grateful to all the friends who made being a student fun. First, Dr. Andrew K. Gunstensen for lunch, dinner, games, *et al.* (have fun on Wall Street, eh?), and his *beautiful* wife

Sheilagh, for putting up with us so often during random discussions. Also, my room-mate Jon and former room-mates Denis (stick to control theory, not pizza-making), and Simon. Thanks to everyone in SERC; especially the Thirsty crowd, for about 200 Friday evenings. And V-rah (ex-jogging partner, friend, E-mail witticist at large), and everyone else on E-mail, and of course, (who could forget!), Belle, for being so cute. (Not that that's everyone, but the rest of you know who you are.) And, of course, Leslie Lamport, and Bartlett's Famous Quotations, and anyone else I may have forgotten...

This work was sponsored by Sandia National Laboratory under contract 69-4391 and by the M.I.T. Space Engineering Research Center under NASA grant NAGW-1335.

Contents

1 Introduction 13
- 1.1 Motivation and Approach . . . 13
- 1.2 Overview . . . 19

2 Previous Research 21
- 2.1 Impedance Matching . . . 22
  - 2.1.1 Modelling . . . 23
  - 2.1.2 Control . . . 25
- 2.2 Parameter Robust Control Design . . . 27

3 Stochastic Modelling 31
- 3.1 Introduction . . . 31
- 3.2 Average Covariance . . . 33
- 3.3 Single Mode Oscillator . . . 36
- 3.4 Examples . . . 41
  - 3.4.1 Discrete Uncertainty . . . 42
  - 3.4.2 Uniform Distribution . . . 43
  - 3.4.3 Cauchy Distribution . . . 44
  - 3.4.4 Rational Distributions . . . 46
- 3.5 Multiple Mode Results . . . 50
- 3.6 Summary . . . 52

4 Performance Metric for Uncertain Structures 53
- 4.1 Motivating Example . . . 54
- 4.2 Power Flow . . . 58
  - 4.2.1 Dereverberated Mobility . . . 58
  - 4.2.2 State Space Representation . . . 63
- 4.3 Arbitrary Structures . . . 64
- 4.4 Possible Extensions . . . 70
  - 4.4.1 Reverberant Information . . . 70
  - 4.4.2 $\mathcal{H}_\infty$ Performance . . . 71
- 4.5 Summary . . . 71

5 Optimization of Performance **73**
5.1 Properties 75
5.2 Evaluation 76
5.3 Optimization 81
5.3.1 Necessary Conditions 81
5.3.2 Numerical Optimization 84
5.4 Time Domain Interpretation 88
5.5 Summary 89

6 Examples **91**
6.1 Two Mass Oscillator 93
6.2 Bernoulli-Euler Beam 99
6.3 Summary 105

7 Experimental Verification **109**
7.1 Interferometer Testbed Description 110
7.1.1 Performance Metric 112
7.1.2 Control and Damping Hardware 113
7.2 Control System Design 116
7.2.1 Actuator Placement 116
7.2.2 Sensor Selection 117
7.2.3 Dereverberated Transfer Function 120
7.2.4 Impedance Matching 121
7.2.5 Stochastic Optimum 123
7.3 Implementation 131
7.4 Results 133

8 Conclusions and Recommendations **143**
8.1 Summary 143
8.2 Contributions and Conclusions 144
8.3 Recommendations 146

References **151**

List of Figures

1.1 Controlled Structures Technology problem. 15

2.1 Generic wave junction 24
2.2 Arbitrary structure 24

3.1 Uncertain state space trajectories 34
3.2 Equipartition behavior: average unforced covariance from initial conditions and corresponding probability density function 47
3.3 Incoherence behavior: average unforced covariance from initial conditions and corresponding probability density function 48

4.1 Rod with end-point control and unknown length. 55
4.2 Equivalent uncertainty block diagram for rod example. 57
4.3 Power minimization on an arbitrary structure. 60
4.4 Power flow model 63
4.5 Block diagram representation of cost. 69

5.1 Comparison of $L(H,\gamma)$, entropy, and $\mathcal{H}_2$ cost integrands for a scalar argument. 77
5.2 Block Diagram for M^*M 79
5.3 Feedback System 81

6.1 Compensator design procedure 92
6.2 Two mass oscillator. 93
6.3 Reverberant and dereverberated mobility for two mass oscillator example. 96
6.4 Compensators for two mass oscillator example. 97
6.5 Cost as a function of uncertain stiffness for two mass oscillator example. 98
6.6 Beam example with collocated force actuation and rate sensing at left end, and a disturbance force acting at the opposite end. 100
6.7 Reverberant and dereverberated mobility for beam example. 101
6.8 Modal costs and $C(\omega)$ for beam example 103
6.9 Compensators for beam example. 105
6.10 Cost as a function of uncertain length for beam example. 106
6.11 Fraction of power reflected for beam example. 107

7.1 Definition of geometry for testbed performance metric 110
7.2 The SERC Interferometer Testbed 111

7.3 Autospectrum of open-loop differential pathlength A–B 113
7.4 Active strut for the SERC interferometer testbed 114
7.5 Active strut placement in truss 117
7.6 Transfer function between active strut voltage and strain 119
7.7 Measured and dereverberated transfer function between active strut voltage and integrated force near plate A 122
7.8 Measured and dereverberated transfer function between active strut voltage and integrated force near plate B 123
7.9 Narrowband weighting function used in control design 124
7.10 Broadband weighting function used in control design, and transfer function from disturbance to siderostat B absolute pathlength 126
7.11 Compensators for active strut at plate A 127
7.12 Compensators for active strut at plate A 128
7.13 Relative power dissipation for compensators at plate A 129
7.14 Relative power dissipation for compensators at plate B 130
7.15 Comparison of implemented and desired broadband, stochastically optimal compensators at plate B 132
7.16 Measured loop transfer function for broadband, stochastically optimal compensators at plate B. 133
7.17 Differential pathlength error A–B 136
7.18 Differential pathlength error B–C 137
7.19 Differential pathlength error C–A 139
7.20 Differential pathlength error B–C, for open-loop, and stochastic optimum feedback 140
7.21 Differential pathlength error transfer function B–C, for rate feedback, and stochastic optimum feedback 141

List of Tables

7.1 Active strut sensor and actuator properties 115
7.2 Achieved performance, and relative improvement, for 10–500 Hz . . . 134
7.3 Achieved performance in frequency bands 135
7.4 Percentage reduction in performance, in frequency bands 135
7.5 Modal damping (%) on interferometer with active and passive damping 138

Notation

$G^*(s)$	Parahermitian conjugate; $G^T(-s)$
$\langle\cdot\rangle_w$	Expectation operator, with respect to white noise w
$\langle\cdot\rangle_\sigma$	Expectation operator, with respect to uncertain parameter σ
$\mathrm{vec}\{A\}$	Kronecker "vec" operator; the vector obtained by vertically stacking the columns of the matrix A
$A \otimes B$	Kronecker product of A and B
$A \oplus B$	Kronecker sum of A and B
$\mathbb{R}$	The set of real numbers
$\mathcal{H}_2$	Hardy space of square-integrable functions on the imaginary axis, with analytic coninuation into the right half-plane
$\mathcal{H}_\infty$	Hardy space of essentially bounded functions on the imaginary axis, with analytic coninuation into the right half-plane
$\mathcal{L}_2$	Lebesgue space of square-integrable functions on $(-\infty, \infty)$
$\mathcal{L}_\infty$	Lebesgue space of essentially bounded functions on $(-\infty, \infty)$
$\|\cdot\|_2$	Norm on $\mathcal{H}_2$ or $\mathcal{L}_2$; given by the square root of the square-integral
$\|\cdot\|_\infty$	Norm on $\mathcal{H}_\infty$ or $\mathcal{L}_\infty$; equal to the essential supremum
μ	Norm for structured uncertainty (see [27])
$\mathcal{RH}_2$	Real, rational functions in $\mathcal{H}_2$
$\mathcal{RH}_\infty$	Real, rational functions in $\mathcal{H}_\infty$
$\left[\begin{array}{c\|c} A & B \\ \hline C & D \end{array}\right]$	State space representation for system $C(sI - A)^{-1}B + D$

Chapter 1

Introduction

The beginning is the most important part of the work.

–Plato

1.1 Motivation and Approach

Active control of lightly damped, modally rich structures is difficult due to the parametric uncertainty that is inherent in any model of such a structure. The first few modes of the structure can usually be modelled with sufficient accuracy for many control design techniques; however, it may be necessary to have some control authority over many more modes of the structure. This might be due to stringent performance requirements [6], a need to control relatively high frequency modes that couple into audible acoustic modes [57], or a requirement to add active damping to structural modes in the roll-off region of a high authority controller [5]. The objective of this thesis is therefore to investigate the design of optimal compensators to achieve these goals. A major aspect of this investigation is the modelling of the uncertain structure in this frequency region to facilitate the control design.

In order to achieve acceptable performance over the first few modes of the structure without destabilizing less certain higher frequency modes due to spillover, a multiple level approach to the control design process has been suggested [5]. A High Authority Controller (HAC) would be designed to meet performance specifications using non-

collocated multiple-input, multiple-output (MIMO) feedback loops. This would be augmented with a Low Authority Control (LAC) loop, whose primary purpose (as envisioned in [5]) is to provide damping, and therefore robustness in the roll-off region of the HAC. Note that for lightly damped, modally dense structures, there may be several cross-over frequencies (where the loop gain is unity.) The roll-off region consists of the frequency range between the first and last cross-over frequencies. It is in this region that the HAC is most sensitive to uncertainties in the model, and thus it is this region in which added damping is most important. The LAC also reduces the sensitivity of the model to uncertainty, increases confidence in model reduction, and provides a direct performance benefit by reducing the peak magnitude of the transfer function.

The reason for making an explicit distinction between high and low authority controllers lies in the fact that the problems each faces, and the resulting solution techniques, are very different. The HAC is designed for a frequency region where a reasonably accurate structural model is available, and as a result, MIMO controllers can be designed that significantly alter both pole locations and mode shapes. The LAC, on the other hand, must operate in a frequency region in which modal uncertainty is significant. If the uncertainty in modal frequencies is comparable to the modal spacing, then phase uncertainty at cross-over in any non-collocated transfer function makes useful non-collocated compensation difficult. However, robust performance can still be achieved using collocated sensors and actuators, since the structural transfer function between these is known to be positive real, provided that the sensor and actuator are "dual." Duality implies that the product of the sensed and actuated variable is proportional to the power flow into the structure (as in force and collocated velocity, or moment and collocated angular rate.) Thus for broadband, or low authority control, restricting attention to the collocated case is not a severe limitation. Indeed, this is perhaps the fundamental distinguishing characteristic between HAC and LAC.

The complete controlled structures technology problem, with the explicit distinction made between HAC and LAC, can be viewed as in Figure 1.1 (from [17, 22].)

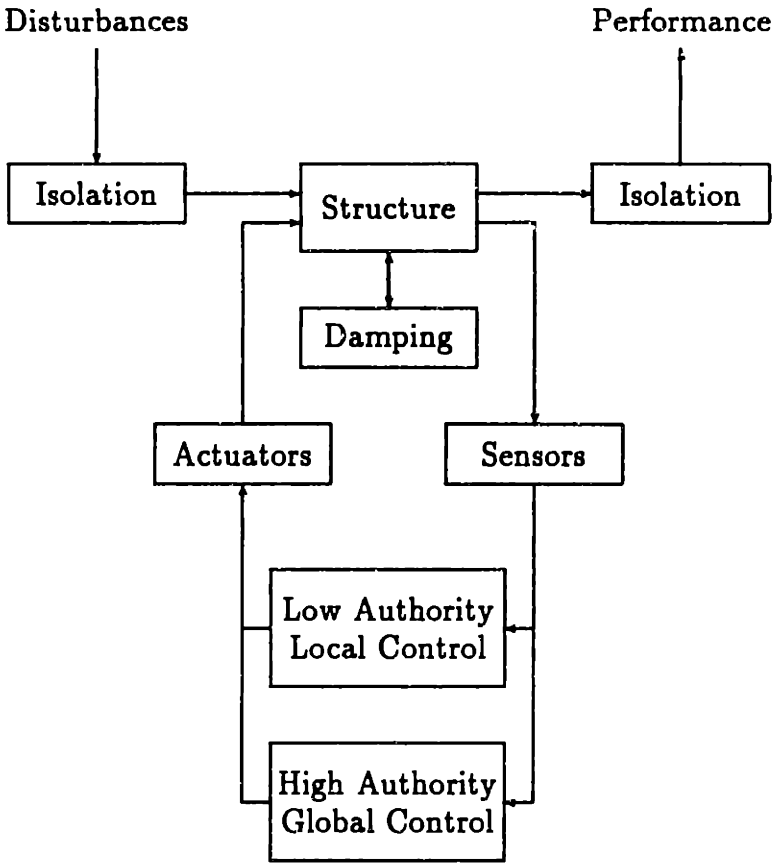

Figure 1.1: Controlled Structures Technology problem.

There is a considerable amount of literature on most of the blocks in this figure. This thesis concentrates on the LAC block, and attempts to achieve a comprehensive theoretical and experimental treatment of this problem.

The damping of the LAC loop can be provided actively or passively. Passive damping augmentation should certainly be used; however, it may be useful or necessary to augment this with active damping. Active techniques are capable of adding greater damping in a narrow frequency band. The hardware required to implement an active approach would almost certainly incur a greater weight penalty than a passive approach. However, if this hardware is already present on the structure to implement the HAC, there may be very little additional weight penalty associated with the LAC, since much of the same hardware can be used.

Typically, collocated rate feedback has been used for the LAC. However, it has been shown [68] that greater damping can be added using an impedance matching

approach, based on a local model of the structure. The local model attempts to describe the local power flow properties at a collocated and dual actuator/sensor pair, and can be obtained, for example, from a wave-based, or dereverberated model of the structure. The dereverberated mobility is the transfer function of the system with only the direct response, and not the reverberant response included [57]; this concept will be discussed in greater detail in Sections 2.1 and 4.2.1.

Previous research with a dereverberated mobility model for control design [61,62, 64], and with a related wave-based model [96, 64, 68, 69], has shown that the best possible compensator is the complex conjugate of the structure's dereverberated impedance. That is, the desired compensator can be thought of as an optimal impedance match, subject to the constraint that the compensator be causal and stable. The impedance matching solution is only valid if the dereverberated, or local model of the structure is used. The impedance match to the reverberant transfer function is generally undesirable, as shown in Section 4.2.1. The previous control design approaches with local models used several approaches to obtain stable, causal compensators, including *ad hoc* approximations to the non-causal compensator, or optimizations. Both $\mathcal{H}_2$ [69] and $\mathcal{H}_\infty$ [61] optimizations of the power flow have been used. The $\mathcal{H}_2$ approach suffers from the lack of a stability guarantee, since the dereverberated model does not include the fact that any departing energy will eventually return; that is, that the structure is approximately conservative. As a result, there is nothing that prevents the controller from adding energy to the structure at some frequencies. The $\mathcal{H}_\infty$ approach [61] fixes this problem, but loses the advantages of minimizing the true quantity of interest, which is better represented by an $\mathcal{H}_2$ cost.

The difficulty with both of these approaches is that they do not incorporate sufficient information about the structure into the control design process. The $\mathcal{H}_2$ approach ignores the conservative nature of the structure, while the $\mathcal{H}_\infty$ approach does not correctly approximate the actual global $\mathcal{H}_2$ cost functional. The real goal of the control system is to minimize a "global" cost that involves contributions from the deflections of the structure at points other than the actuator/sensor location, as opposed to a "local" cost that could be described in terms of only the structural motion

at the sensor. In order to incorporate more information into the design process, a better approach to modelling a highly uncertain, modally dense structure must be investigated.

Because of the number of modes in the bandwidth of these problems and the uncertainty in their frequencies and mode shapes, it may be more useful to model only some statistical aspects of the response, rather than attempting to model the detailed modal behavior of the structures. The viewpoint taken in this thesis is that the structure is taken from an ensemble of possible systems, the statistics of which are known. In recent years, however, the predominant trend in robust analysis and synthesis of feedback control systems has been toward deterministic techniques over stochastic methods [15]. One motivation for this trend is the ability of deterministic techniques to provide worst-case measures of performance under uncertainty rather than average case results. One reason for studying stochastic models is that worst-case behavior may be so highly unlikely as to lead to undue conservatism in engineering design. For such systems, an average case model may be a more practically useful representation of system behavior. A rather extreme example of this is the probabilistic phenomenon of thermodynamics in which heat flows with virtual certainty from hot objects to cold objects.

One field of research that uses a stochastic approach to the modelling of flexible structures is Statistical Energy Analysis [14, 25, 47, 53, 58, 77], or SEA. SEA has been successfully applied to both acoustic and structural systems. The purpose behind SEA is to model the expected response of the structure using minimal information about the system. In order to obtain accurate response estimates, SEA makes use of conservation of energy, and also makes several other assumptions about the structural response; namely incoherence and equipartition. Incoherence requires that different modal amplitudes are uncorrelated, and equipartition requires that modes closely spaced in frequency have similar energy. These assumptions will be shown in Chapter 3 to be derivable from averaging the state space covariance with respect to a stochastic parametric uncertainty description [46]. Asymptotic Modal Analysis [25] obtains incoherence and equipartition in the limit of high modal density.

These properties have been shown elsewhere to occur for time-averaged steady state covariances [58], or for specific assumptions on the nature of the forcing [77], while this behavior is obtained here as a result of averaging over uncertainty for arbitrary forcing.

The incoherence property allows one to relate the mean-square displacement or velocity at any point in the structure to the average modal energy. The average energy in each frequency band is determined from a power flow, or energy balance, with input power flows being determined through average input mobilities. In the limit of large uncertainties, the average input mobility is the aforementioned dereverberated mobility [56]; the same transfer function as that obtained by considering only the direct field. If the uncertainty is large, then the phase of the reverberant field is unknown. Averaging over the uncertainty therefore gives that the average response is simply the direct field response.

The structural modelling principles used in this thesis are strongly motivated by SEA. The structure is assumed to be stochastic, and equipartition and incoherence are proven to hold. This allows the expected value of the desired quadratic cost to be computed in terms of known, local structural properties. Note that the cost is averaged over both the statistics of the driving noise, and over the uncertainty in the structure. This cost can then be expressed as a particular mixed $\mathcal{H}_2/\mathcal{H}_\infty$ cost functional of the power flow properties. This cost incorporates an $\mathcal{H}_\infty$ constraint, similar to that in [61], which guarantees that the optimal compensators will be positive real, and hence stabilizing for any uncertainty in the structure. The essential difference between this and other impedance matching approaches is that it includes the knowledge that the structure conserves energy directly into the derivation of the cost functional.

The mixed $\mathcal{H}_2/\mathcal{H}_\infty$ cost that represents the expected value of the performance can be evaluated using the state space representation of both the dereverberated structural mobility and the compensator. The compensator that minimizes this cost can be obtained from a numerical optimization. The resulting controllers are illustrated for several simple analytical examples, and have been demonstrated experimentally

on the M.I.T. Space Engineering Research Center interferometer testbed. The resulting performance was better than that of the usual low authority approach of using rate feedback, although the performance improvement may not justify the use of more complicated controllers in all structural control problems.

1.2 Overview

The body of the thesis builds upon the previous impedance matching theory. The most relevant of these results will be summarized in the following chapter. A similar summary can be found in [64]. The fundamental problem that must be dealt with in designing controllers for uncertain structures is the parametric uncertainty that is present in any model of the structure. The approach of this thesis is to average the global performance metric over the set of possible uncertainties. Other cost averaging approaches have been examined before for dealing with parametric uncertainty. Furthermore, the "maximum entropy" control design approach of Hyland [52] can be shown to have a cost averaging interpretation. In order to place the current results in perspective, several of these related parameter robust control design techniques will also be discussed in Chapter 2.

In Chapter 3, the stochastic approach to modelling is presented. The effects of parametric uncertainty are investigated by averaging the state space covariance over a parametric uncertainty distribution. Only uncertainty in the natural frequencies of the structure is considered. This material justifies the SEA assumptions of equipartition and incoherence by demonstrating that they are satisfied by the average covariance. In addition, the average covariance under a Cauchy distribution is shown to satisfy the same modified Lyapunov equation as the "maximum entropy" Stratonovich multiplicative white noise model. Much of the material in this chapter can be found in [46].

The properties of stochastic systems found in Chapter 3 are then used in Chapter 4 to derive a cost functional that reflects the available knowledge about the structure, the disturbances, and the true cost. The average value of the global $\mathcal{H}_2$ performance

metric is represented in terms of the local structural properties. The key to this impedance matching result is the fact that lightly damped structures approximately conserve energy. The local model is based upon the dereverberated mobility used in [61].

The compensator that minimizes the average cost in the structure can be obtained by minimizing the cost functional obtained in Chapter 4. For a state space representation of the structural model, the evaluation and optimization of the cost functional is given in Chapter 5. The cost functional is related to other $\mathcal{H}_2/\mathcal{H}_\infty$ costs, and to differential games. While a closed-form solution for the optimal compensator has not been found, a numerical optimization approach is presented. Parts of the material in this chapter can be found in [63].

Chapter 6 demonstrates the approach for several examples, including a two-mass oscillator, and a free-free beam. The results are compared with those of other existing parameter robust and impedance matching control design approaches.

Experimental results on the M.I.T. SERC interferometer are presented in Chapter 7. Constant gain feedback, and compensators designed using the stochastic optimization approach of this thesis have been implemented using two active struts. The stochastic optimization is shown to provide better performance than the simple constant gain low authority compensator, while guaranteeing closed-loop stability.

Chapter 8 presents the main conclusions and contributions of the thesis, and discusses a number of possible extensions to this research.

Chapter 2

Previous Research

Sail away, away
Ripples never come back...

–Genesis *Ripples*

This thesis considers the design of optimal low authority compensators. This problem has been considered before [61, 69]; the ideal compensator is an impedance match. In general, this ideal compensator has right-half plane dynamics, which correspond to either an unstable, or a non-causal compensator. There has been some previous research on obtaining stable, causal approximations to the ideal compensator, and on modelling the local structural properties in order to obtain the correct driving point impedance to match. This thesis builds upon earlier work by MacMartin and Hall in [61, 62], which in turn built upon the work of Miller and others in [68, 69, 71, 95, 96]. These previous approaches to solving the problem will be summarized here. The impedance matching approaches obtain robust stability by constraining the compensator to be positive real. Since the transfer function between collocated and dual sensors and actuators is positive real, any positive real compensator will be guaranteed to be stabilizing for any uncertainty in the structure that does not destroy the positivity property.

An alternative approach to guaranteeing stability is to model the details of the structure, and include information about the parametric uncertainty of the model in the control design procedure. Some existing parameter-robust control design proce-

dures will also be discussed. In particular, cost or covariance averaging approaches are considered. These are of particular relevance to this research, since the impedance matching approach obtained in Chapter 4 is based upon averaging the global $\mathcal{H}_2$ performance metric. Furthermore, it is shown in Chapter 3 that the maximum entropy approach of Hyland [52] can also be interpreted as a cost averaging approach.

2.1 Impedance Matching

The formulation of control algorithms for active dissipation of vibrational energy generally requires an accurate model of the structural system. Global models of complex structures, perhaps acquired through finite element methods, are prone to inaccuracy, while global measurement-based (identified) models are time consuming to generate, and often unreliable due to suspension coupling during testing. Instead of using a high-order, inaccurate model, one could instead include only the information that can be accurately modelled in the description of the plant. The local information that describes the dynamics of the structure within a few wavelengths of a collocated and dual sensor and actuator pair is much easier to model, since this local model does not require knowledge of all of the reflections from other parts of the structure. Furthermore, since the power dissipation properties of the control system can be described in terms of only a local structural model, the local model is sufficient to design compensators with the goal of only adding damping.

There are several ways in which a local model of the structure can be obtained. One approach is to model the control location in terms of waves. Early work in this field includes that of Vaughan [94], who identified a matched termination as being an appropriate control law for a beam, and gave suitable approximations for the implementation of the irrational transfer functions required. More recently, a number of researchers have done both theoretical [43, 59, 69, 86] and experimental [68, 80, 96] work in wave-based control for structures. An alternative approach for obtaining a local model is to use the dereverberated driving point mobility [61,62] at the actuator location. This model can be obtained from a wave model, or directly

from experimental data. A similar average impedance model has also been used by Chen *et al.* [19]. The optimal control law for a local objective can be derived in terms of the local model, so that the closed loop system will be stable for any uncertainties in the rest of the structure.

Maximizing the power dissipated by the control action corresponds to matching the structure's driving point impedance as closely as possible, given the available actuators [19,20,40]. An exact match at every frequency is not always possible [30], as the required compensator is in general non-causal and cannot be implemented. If the frequency weighted power flow is minimized using a Wiener-Hopf or LQG approach [69], then the resulting compensator will be causal. The main disadvantage of this $\mathcal{H}_2$ formulation is that because the local model does not include the reverberances present in the real structure, the optimal compensator may generate power at one frequency in order to better dissipate power at another, which could lead to instability when implemented on the real structure. If the worst case power flow, rather than the average power flow, is minimized, then stability is guaranteed [61]. This can be formulated as a standard $\mathcal{H}_\infty$ optimal control problem. Both the $\mathcal{H}_2$ and $\mathcal{H}_\infty$-optimal control laws developed with local models have been implemented, and the achievable performance verified on a pinned-free beam in the laboratory [68,62].

2.1.1 Modelling

Using the travelling wave model in [69], the structure is modelled as a network of waveguides, such as beams, rods, etc. The control input is applied at a junction, where these waveguides intersect, as shown in Figure 2.1. The cross-sectional variables (displacements and forces) in each member can be related to the amplitudes of independently travelling wave modes. The junction can then be described by a matrix S of scattering coefficients, which relate outgoing waves w_o to incoming waves w_i, and a generation matrix Ψ that relates the outgoing waves to the control input u.

For arbitrarily complex junctions, such as that in Figure 2.2, deriving a wave model can be impractical. An alternative to a wave model for obtaining a local model of the structure near the actuator is to use the dereverberated driving point mobility [61].

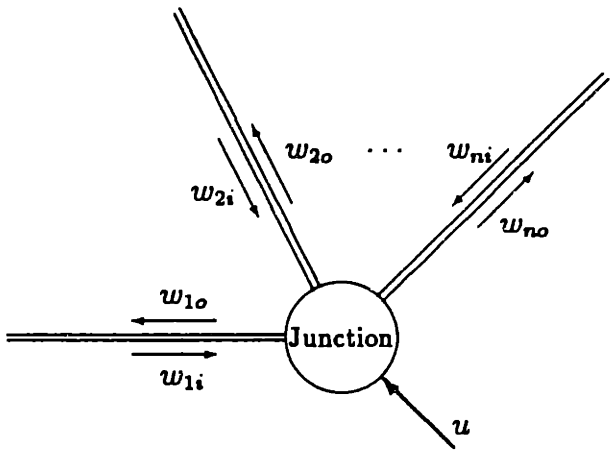

Figure 2.1: Generic wave junction

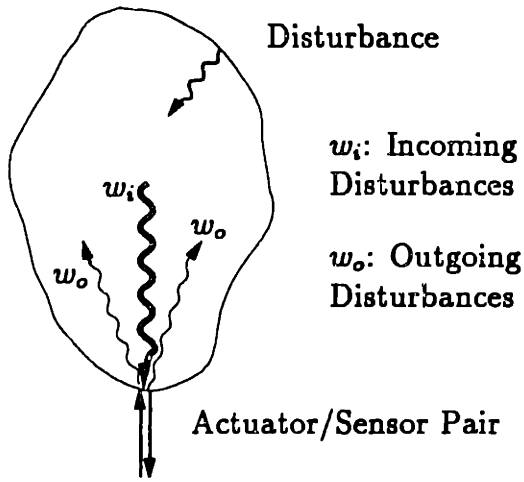

Figure 2.2: Arbitrary structure

The structural response due to the actuator can be divided into two parts: a *direct field*, due to the local dynamics; and a *reverberant field*, which is created by reflections from other parts of the structure. The direct field corresponds to that part of the outgoing waves w_o which is due to the control u, while the reverberant field consists of the incoming waves w_i, and that part of w_o which is due to w_i. The term "dereverberated" implies that the "reverberant" part of the response has been removed before computing the mobility. The dereverberated mobility may be approximated by taking a logarithmic average of the reverberant driving point mobility [47], or obtained from a wave model [64]. If $G(s)$ is the dereverberated mobility, then the response is of the form

$$y(s) = G(s)u(s) + d(s) \tag{2.1}$$

where d is a disturbance input.

The wave model provides more physical insight, and a more complete description of the junction than the dereverberated mobility. The junction wave model can also be combined with a wave description of transmission along members to generate a model of the entire structure [71]. The dereverberated mobility approach is motivated by a wave model, but does not require the wave modes of the structure to be identified, as the model can be obtained directly from experimental data by averaging, as will be demonstrated in Chapter 7. As a result, it may be easier to apply to complicated

structures. Some of the analytical results are also simpler using this model, since all of the relevant information about the junction is contained in a single transfer function matrix.

2.1.2 Control

A possible control objective that requires only a local model is to maximize the power that is dissipated by the control. Since y and u in Equation (2.1) are collocated and dual, the average power flow into the structure at each frequency is of the form [71]:

$$\mathsf{P}(\omega) = \frac{1}{2}\left(y^H(j\omega)u(j\omega) + u^H(j\omega)y(j\omega)\right) \tag{2.2}$$

Optimal compensators of the form $u(s) = -K(s)y(s)$ are desired.

A standard result from electric circuits (e.g. [93]) is that the optimal impedance to maximize power dissipation is the conjugate of the load impedance. If this condition is achieved, then one has a "matched termination," and there is no reflected signal. The same result is true in structures. The load impedance is the inverse of the mobility of the structure, and the transfer function of the compensator (from velocity to force) is itself an impedance function. Hence the optimal compensator is

$$K(s) = (G^*(s))^{-1} \tag{2.3}$$

where $G^*(s) = G(-s)^T$ is the parahermitian conjugate [33]. This compensator can also be obtained by optimizing Equation (2.2) at each frequency.

The matched termination condition is equivalent to continuing the structure at the junction with an identical structure, so that there is no effective discontinuity. If, at the end of a beam, the control mimics the forces and moments that would be present if the beam continued indefinitely, then there will be no reflection, and all of the incoming power will be absorbed. The required MIMO compensator is causal; however, this solution requires that all of the cross-sectional forces at the junction can be independently controlled. If this is not true, then all of the incoming power cannot be absorbed with a stable, causal compensator.

Indeed, unless the dereverberated mobility is a constant, the compensator in Equation (2.3) has right-half plane dynamics. As both the compensator and plant are

positive real, there are no encirclements of the -1 point in the Nyquist plot. Hence, the closed-loop system is only stable if the compensator is stable. The frequency by frequency optimization that yields Equation (2.3) only represents a minimum cost if the system is stable, and therefore it is reasonable to associate the right-half plane dynamics with a non-causal compensator. A non-causal compensator requires future information, and cannot be implemented.

The control design procedure must therefore find the best causal approximation to the non-causal impedance match. One approach to obtaining an optimal causal compensator is to minimize the integral over frequency of the power flow in Equation (2.2) using a Wiener-Hopf or LQG approach. This is a standard $\mathcal{H}_2$ problem. A penalty on the control effort could also be included. As was noted in Reference [69], the $\mathcal{H}_2$ approach suffers from the fact that it does not guarantee a stabilizing compensator. This is because the local model does not include knowledge of the fact that departing energy will eventually return; that is, that the incoming disturbance is correlated with the outgoing waves, and therefore with the control. As a result, the approach will allow power to be generated at some frequencies in order to allow greater dissipation at other frequencies.

To guarantee dissipation at all frequencies, the worst case power dissipation could instead be minimized, which can be cast as an $\mathcal{H}_\infty$ minimization problem.

With the optimal non-causal compensator from Equation (2.3), the closed loop power flow into the structure is

$$\mathsf{P} = -d^*(G + G^*)^{-1}d \tag{2.4}$$

If $d = G_0 w$ where

$$G_0 G_0^* = G + G^* \tag{2.5}$$

then the optimal non-causal compensator will dissipate power w^*w. Since this is the maximum power that can be dissipated, adding it to the power flow into the structure at each frequency yields a positive cost, given by

$$\text{Cost}(\omega) = w^*w + u^*y + y^*u \tag{2.6}$$

$$= |G_0^*u + w|^2 = |z|^2 \tag{2.7}$$

where $z = G_1 G_0^* u + G_1 w$, and $G_1(s)$ is an inner function ($G_1^* G_1 = I$) defined so that $G_1 G_0^*$ is stable. Combining this with the system equation (2.1) and the definition of w yields:

$$\begin{Bmatrix} z \\ y \end{Bmatrix} = \begin{bmatrix} G_1 I & G_1 G_0^* \\ G_0 & G \end{bmatrix} \begin{Bmatrix} w \\ u \end{Bmatrix} \tag{2.8}$$

The input w can be interpreted as the normalized incoming wave, and the performance variable z is the resulting reflected outgoing wave. The compensator from y to u that minimizes the $\mathcal{H}_\infty$ norm of the transfer function T_{zw} from w to z will minimize the maximum power flow into the structure. Because of the definition of the cost in Equation (2.6), if power is being dissipated at a particular frequency ω, then $T_{zw}(\omega) < 1$. Hence $\|T_{zw}\|_\infty < 1$ implies that power is dissipated at all frequencies, which implies that the closed loop system will be stable.

A compensator K which satisfies the $\mathcal{H}_\infty$ constraint $\|T_{zw}\|_\infty < 1$ can be found from a standard $\mathcal{H}_\infty$ optimization problem [28]. Any compensator that satisfies this constraint will be positive real. From [42], a stable transfer function $H(s)$ has bounded magnitude $\|H(s)\|_\infty < 1$ if and only if the function $(I - H)^{-1}(I + H)$ is positive real. Applying this result to T_{zw} yields that $\|T_{zw}\|_\infty < 1$ if and only if the compensator K is positive real. Hence, closed loop stability can also be shown using a positivity argument. Since the structural transfer function between collocated and dual actuators and sensors is also positive real, the closed loop system will be stable.

Note that the $\mathcal{H}_2$ problem solved in [69] by a Wiener-Hopf approach can also be represented by Equation (2.8); the $\mathcal{H}_2$ optimal compensator is that which minimizes $\|T_{zw}\|_2$, which is a standard LQG problem.

2.2 Parameter Robust Control Design

Impedance matching techniques are one way of obtaining compensators with stability and performance properties that are relatively insensitive to variations in structural parameters. The existing methods which have just been discussed, however, suffer from limitations in dealing with the performance of the real structure explicitly.

Since the goal of this thesis is to develop a technique for designing parameter-robust broadband compensators, it is relevant to examine existing approaches for parameter-robust control design for structures. In particular, the following chapters develop a cost averaging approach to control design, and hence existing approaches that are related to cost averaging will be discussed.

Cost averaging for robust control design encompasses a variety of techniques, all of which correspond explicitly or implicitly to averaging the state space covariance over some distribution of uncertainty. The resulting averaged covariance is then a statistical quantity that is useful in understanding the effects of parametric uncertainty. Explicit covariance averaged solutions are obtained in Chapter 3 for discrete, uniform, and Cauchy probability distributions for an uncertain modal frequency. For a single uncertainty, the discrete distribution leads to the Bourret approximation to the average cost studied in [44,45].

The idea of covariance averaging for control design has been investigated in [38, 44, 45, 48]. Hagood demonstrated in [44, 45] that the average cost over a uniform distribution of uncertainty can be approximated by means of Bourret equations [32]. A Monte Carlo simulation technique has also been investigated [92]. In addition to the continuously varying parameter problem, cost averaging over a finite set of models has been investigated; see for example [4,34,35,72]. While stability is not guaranteed for parameter values in between those chosen for design, this approach is conceptually straightforward, and can be a powerful design tool [39].

Also of interest is the discussion in [18, p. 114], where averaging an $\mathcal{H}_2$ cost over a bounded scalar complex parameter uncertainty is shown to yield the entropy cost of [74]. This cost combines features of both $\mathcal{H}_2$ and $\mathcal{H}_\infty$ cost functionals, and hence this result links the $\mathcal{H}_2$ and $\mathcal{H}_\infty$ optimization approaches more closely. A similar average over uncertainty with norm equal to unity, rather than bounded by one is shown in Section 4.1 to yield the $\mathcal{H}_2/\mathcal{H}_\infty$ cost functional studied in Chapter 5 of this thesis.

One approach that has had considerable success in designing parameter-robust controllers for structures is the maximum entropy optimal projection (MEOP) ap-

proach, developed originally by Hyland in [52] and reviewed in [13]. While originally justified by means of a Stratonovich multiplicative white noise model, this approach has proven to be useful in designing robust controllers for flexible structures with parametric uncertainty [10,11,37,51]. In Reference [52], Hyland discusses the equipartition and incoherence assumptions of Statistical Energy Analysis, and obtains a covariance equation for uncertain systems that yields similar behavior for modal systems with large uncertainty. The justification for this equation is based on assuming that the state space model is

$$\dot{x}(t) = \left(A_0 + \sum_{i=1}^{r} \sigma_i(t) A_i \right) x(t) + B w(t) \tag{2.9}$$

where each $\sigma_i(t)$ is a unit intensity white noise process, and $w(t)$ is white with intensity V. More precisely, the state satisfies the stochastic differential equation

$$\mathrm{d}x = \left(A_0 + \sum_{i=1}^{r} \mathrm{d}\sigma_i A_i \right) \mathrm{d}t + B\,\mathrm{d}w \tag{2.10}$$

That is, state dependent noise is used to model the effect of parametric uncertainty. Heuristically, the compensator must stabilize the system for variations in σ, but is not allowed to use information about the actual value of σ.

When Equation (2.9) is interpreted in the sense of Stratonovich, rather than in an Itô fashion, the covariance $Q = \left\langle x x^T \right\rangle_w$ satisfies the modified Lyapunov equation

$$\dot{Q} = (A_0 + \tfrac{1}{2}\sum_{i=1}^{r} A_i^2)Q + Q(A_0 + \tfrac{1}{2}\sum_{i=1}^{r} A_i^2)^T + \sum_{i=1}^{r} A_i Q A_i^T + V \tag{2.11}$$

Parameter robust control design is accomplished by minimizing the resulting expected $\mathcal{H}_2$ cost; that is, using Equation (2.11) to describe the covariance, rather than a standard Lyapunov equation. A fixed form parameter optimization approach is then used to derive Riccati and Lyapunov equations that describe the first order necessary conditions that an optimal solution must satisfy.

One of the difficulties this technique has had in gaining acceptance is that the multiplicative white noise model in Equation (2.9) is difficult to justify as being a reasonable approach to treating constant but unknown parameters. To provide a more rigorous foundation for this technique, it is shown in Chapter 3 that covariance

averaging in the presence of a Cauchy distribution yields precisely the maximum entropy model used in [13]. This result is obtained only for a single mode oscillator with natural frequency uncertainty. The interpretation of Equation (2.11) in terms of energy conservation will also be discussed in Section 3.4.3.

There has been some literature on the use of $\mathcal{H}_\infty$ bounds to treat parametric uncertainty (e.g. [91].) While this may be tempting due to the existence of clean theoretical results on the $\mathcal{H}_\infty$ problem, such an approach may not be able to obtain as much performance as possible, due to the inherent conservatism. Bounding transfer function error due to parametric uncertainty with an $\mathcal{H}_\infty$ bound assumes total ignorance of the phase of the error, which is an unrealistic assumption for structural systems. A μ-synthesis approach [27] reduces conservatism in the stability test by allowing a block structure to the uncertainty, but individual blocks are still assumed to have arbitrary phase. There is also some current research on the "real-μ" problem, which addresses the conservatism in applying complex-μ to parametric uncertainty problems [29,50,100].

One difficulty with applying many norm-based robust control design approaches to structural control problems is that the phase information in the parametric uncertainty of the structure is extremely important, and cannot be ignored [9]. The open loop system is known to be stable, and to approximately conserve energy, although the imaginary part of its eigenvalues may be highly uncertain. Thus it is also worth noting that because the multiple-model, Bourret, and maximum entropy approaches evaluate the cost as the average covariance over a set of conservative systems, they all incorporate into the design approach the knowledge that the structure is inherently conservative.

A survey of many current approaches to dealing with parametric uncertainty can be found from the recent American Control Conference sessions on the "Benchmark Problem" [97,98].

Chapter 3

Stochastic Modelling

Stochastic: *adj* [Στοχαστικος: skillful in aiming] ...
Involving chance or probability: PROBABILISTIC

–Webster's New Collegiate Dictionary

3.1 Introduction

This chapter studies the effects of parametric uncertainty in state space systems. There are several reasons for investigating parametrically uncertain structures. First, a detailed modal description of a highly uncertain, modally dense system is both unwieldy, and inaccurate. Instead, one would like to describe the system in terms of only some statistical properties of the response, rather than the exact details. This is the approach used by Statistical Energy Analysis [58]. Many of the conclusions reached by SEA are based upon the assumptions of incoherence and equipartition [47,77]. The incoherence property implies that the amplitudes of different modes are uncorrelated; equipartition implies that the energy in closely spaced modes is similar, and that the kinetic and potential energy of a given mode is the same. In [58] and in other SEA literature, these assumptions are justified heuristically, using arguments about the frequency content and spatial distribution of disturbances. One of the goals of this chapter is to justify these assumptions more rigourously by demonstrating that they are satisfied by the average covariance of an uncertain structure. These

properties can then be used in Chapter 4 to obtain the expected value of a global performance metric in terms of local structural information.

A second reason for investigating parametrically uncertain systems is to draw connections between existing parameter-robust control design techniques and the approach of this thesis. Both the Bourret equation approach of Hagood [44, 45], and the "maximum entropy" approach of Hyland [52] can be demonstrated to be equivalent to cost averaging techniques, wherein the uncertain parameters of the structure are assumed to be stochastic. This lends insight into both approaches, and further justification for the maximum entropy approach in particular. This connection also demonstrates that both the Bourret and the maximum entropy approach implicitly take advantage of conservation of energy for lightly damped structures, which implies that they are potentially much less conservative than many other robust control approaches for dealing with uncertainty in structures. Finally, since the approach of this thesis is to compute the average performance over the uncertainty from a frequency domain, impedance matching perspective, this conclusion indicates a strong connection between the current work and the maximum entropy approach.

The effect of parametric uncertainty is investigated in this chapter by averaging the state covariance over the statistics of the uncertain parameters. For natural frequency uncertainty, this computation is shown to be related to the Fourier transform of the probability density function of the uncertain parameter. In the case of a single mode oscillator, the average covariance is then shown to exhibit both equipartition and incoherence phenomena. The analysis is carried out for several probability distributions. Averaging over a discrete uncertainty model yields the Bourret design equations [44], while averaging over a Cauchy uncertainty distribution yields the "maximum entropy" covariance equation [52]. For arbitrary rational distributions, the average covariance can be evaluated as the solution of a set of coupled Lyapunov equations. In addition, incoherence is demonstrated for the case of multiple modes, which is a key result, since this is the case of interest for modally dense structures.

3.2 Average Covariance

Consider the linear state space system in which the state $x \in \mathbb{R}^n$ evolves according to the differential equation

$$\dot{x} = Ax + w \qquad x(0) = x_0 \tag{3.1}$$

for some white driving noise w. The goal is to analyze Equation (3.1) for the case in which the system matrix A is uncertain. Specifically, assume that uncertainty in A is represented by

$$A = A_0 + \sum_{i=0}^{r} \sigma_i A_i \tag{3.2}$$

where σ_i are the uncertain parameters with joint probability density function $p(\sigma_1, \ldots, \sigma_r)$, and the given matrices A_i describe the structure of each uncertain parameter.

The effect of uncertainty on the state space trajectories of an undamped single mode oscillator can be visualized by examining Figure 3.1. The probability of the state being at a particular location in the phase plane at a given time is plotted, assuming that the initial state is known. As time increases, the location becomes more and more uncertain. Note, however, that while the precise location of the state is highly uncertain, information about the location can still be obtained. Since the system is undamped, the total energy remains constant.

For simplicity, the following development will concentrate on the case of a single uncertain parameter, $\sigma = \sigma_1$. As will be seen, most of the results generalize to the case of multiple uncertain parameters. It will also be required that the uncertainty structure A_1 commute with the nominal system matrix A_0. If the eigenvalues of either A_0 or A_1 are all distinct, or if both are diagonalizable, then A_1 and A_0 commute if and only if both are simultaneously diagonalizable by the same eigenvector matrix [49, pp. 50, 135]. This implies that, in general, the uncertainty can change the eigenvalues, but not the eigenvectors (or mode shapes) of the original system. Although this assumption is confining, it encompasses nontrivial problems having practical ramifications.

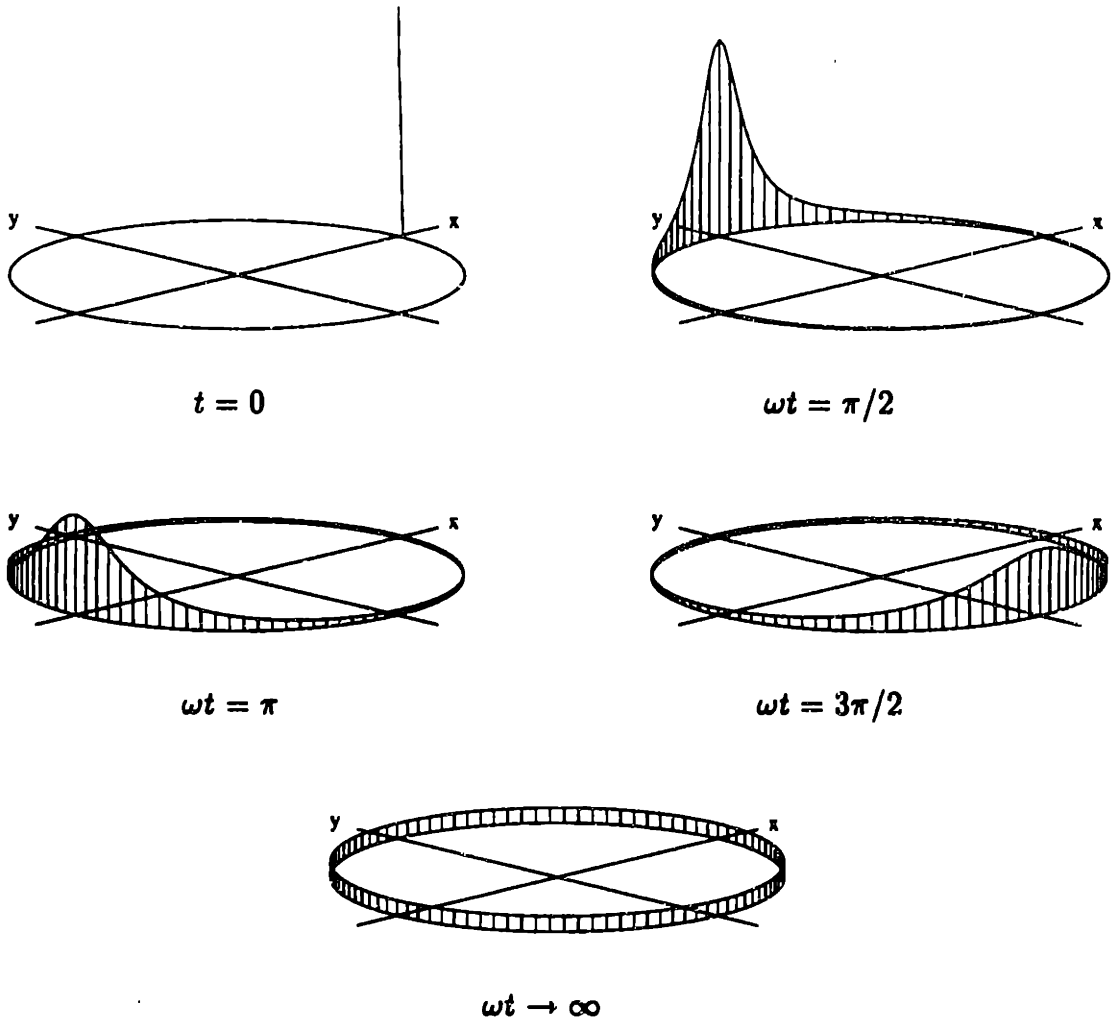

Figure 3.1: Uncertain state space trajectories; probability distribution of single mode oscillator states with a Cauchy distribution of uncertain frequency, for increasing time.

For collocated control, the mode shape uncertainty only influences the magnitude of the residues, and not their sign, and hence it is the modal frequency uncertainty that is likely to have the greatest effect on closed-loop performance. More generally, performance in many structural control problems is often limited by uncertainty in the natural frequencies, rather than uncertainty in the residues or zero locations that result from eigenvector perturbations [21, 54, 70]. Furthermore, the equipartition and incoherence properties that result from the effects of eigenvalue uncertainty are certainly a subset of those properties caused by both eigenvector and eigenvalue uncertainty. A control design approach that takes advantage of these properties is

therefore at worst, unnecessarily conservative, as it does not take advantage of all of the properties of the system in question.

The covariance matrix $Q(t) \triangleq \left\langle x(t)x^T(t)\right\rangle_w$ associated with the system in Equation (3.1) is given by

$$\dot{Q} = AQ + QA^T + V \qquad Q(0) = Q_0 = \left\langle x_0 x_0^T \right\rangle \tag{3.3}$$

where the constant matrix V is the intensity of the driving noise w, and $\langle\cdot\rangle_w$ denotes expectation over the white noise w. This covariance equation can be solved explicitly using Kronecker algebra [36]. The vector obtained by stacking the columns of Q is denoted by $\mathrm{vec}\{Q\}$. Similarly, define $q_0 \triangleq \mathrm{vec}\{Q_0\}$, and $v \triangleq \mathrm{vec}\{V\}$. The symbols $\otimes$ and $\oplus$ denote, respectively, the Kronecker product and sum operators. Equation (3.3) can then be written as as

$$\dot{q} = (A \oplus A)q + v \qquad q(0) = q_0 \tag{3.4}$$

where $q \triangleq \mathrm{vec}\{Q\}$, $q_0 \triangleq \mathrm{vec}\{Q_0\}$, and $v \triangleq \mathrm{vec}\{V\}$. Hence,

$$q(t) = e^{(A\oplus A)t}q_0 + \int_0^t e^{(A\oplus A)(t-\tau)}v\,d\tau \tag{3.5}$$

The following facts are required to proceed further.

Lemma 3.1

(i) $A = A_0 + \sigma_1 A_1 \;\Rightarrow\; A \oplus A = (A_0 \oplus A_0) + \sigma_1(A_1 \oplus A_1)$

(ii) $A_0A_1 = A_1A_0 \;\Rightarrow\; (A_0 \oplus A_0)(A_1 \oplus A_1) = (A_1 \oplus A_1)(A_0 \oplus A_0)$

(iii) *If* A_1 *is diagonalizable with* $A_1 = \Psi\Lambda\Psi^{-1}$, *where* $\Lambda = diag\{\lambda_i\}$, *then* $A_1 \otimes A_1$ *and* $A_1 \oplus A_1$ *are both diagonalizable, and*

$$A_1 \otimes A_1 = (\Psi \otimes \Psi)(\Lambda \otimes \Lambda)(\Psi \otimes \Psi)^{-1}$$

$$A_1 \oplus A_1 = (\Psi \otimes \Psi)(\Lambda \oplus \Lambda)(\Psi \otimes \Psi)^{-1}$$

(iv) $e^{(X+Y)t} = e^{Xt}e^{Yt}\ \forall\, t \iff XY = YX$

Proof: Results (i) through (iii) follow from the definitions of the Kronecker operators [36]. The final assertion is from [8, p. 171]. □

Now define

$$\mathcal{Q}(t) \triangleq e^{(A_0 \oplus A_0)t} \left(\int_{-\infty}^{\infty} e^{\sigma(A_1 \oplus A_1)t} p(\sigma)\, \mathrm{d}\sigma \right) \tag{3.6}$$

Then from Lemma 3.1 the average covariance is given by

$$\langle q(t) \rangle_\sigma = \mathrm{vec}\{\langle Q(t) \rangle_\sigma\} = \mathcal{Q}(t) q_0 + \int_0^t \mathcal{Q}(t-\tau) v\, \mathrm{d}\tau \tag{3.7}$$

This involves an expectation over both the uncertainty and the driving noise. The assumption that A_0 and A_1 commute is required by Lemma 3.1(iv). If $A_1 = \Psi \Lambda \Phi^T$ is diagonalizable with $\Lambda = \mathrm{diag}\{\lambda_i\}$, $\Psi = [\ \psi_1 \ \cdots \ \psi_n\ ]$, $\Phi = [\ \phi_1 \ \cdots \ \phi_n\ ]$, then Equation (3.6) can be written as

$$\mathcal{Q}(t) = e^{(A_0 \oplus A_0)t} \sum_{i=1}^{n} \sum_{j=1}^{n} (\psi_i \otimes \psi_j)(\phi_i^T \otimes \phi_j^T) \int_{-\infty}^{\infty} e^{\sigma(\lambda_i + \lambda_j)t} p(\sigma)\, \mathrm{d}\sigma \tag{3.8}$$

If only the modal frequencies of the system are uncertain, then the eigenvalues λ_i of A_1 are purely imaginary, and hence the integrals in Equation (3.8) are the Fourier transforms of $p(\frac{\sigma}{|\lambda_i + \lambda_j|})$.

Remark 3.2 *For modal frequency uncertainty, the average covariance can be evaluated in terms of the Fourier transform of the probability density function.*

Note that multiple uncorrelated uncertain parameters can be treated as easily as a single uncertain parameter as long as the uncertainty structure commutes. That is, with reference to Equation (3.2), every A_i must commute with A_0, and each A_i must commute with A_j, for all i and j. Additional uncertain parameters simply result in additional product terms in Equation (3.6).

3.3 Single Mode Oscillator

Of particular interest for understanding the effect of uncertainty in structures is whether the incoherence and equipartition assumptions of SEA [58] follow from averaging over uncertainty.

Definition 3.3 Equipartition *is said to occur at time t if the average energy in each state at time t is the same.* Incoherence *is said to occur if the average cross-correlation between the state coordinates is zero. Steady-state equipartition or incoherence is said to occur if equipartition or incoherence are satisfied in the limit as* $t \to \infty$.

To simplify the analysis, first consider the case of a single mode oscillator. Extensions to the multiple mode case will be examined in Section 3.5. Define

$$J = \begin{bmatrix} 0 & 1 \\ -1 & 0 \end{bmatrix} \tag{3.9}$$

so that $J^2 = -I$ and $J^T = -J$. This matrix is analogous to the imaginary number j, and has eigenvalues $\pm j$. Then for $\eta \geq 0$, consider the system

$$\begin{aligned} A &= A_0 + \sigma A_1 \\ A_0 = -\eta I + \omega J &\qquad A_1 = J \end{aligned} \tag{3.10}$$

The eigenvalues of the uncertain system are at $-\eta \pm j(\omega + \sigma)$, whereas the eigenvectors are independent of σ. In this state space basis, each element of the state vector corresponds to a normalized energy variable. Thus, if the system represents a mechanical oscillator, $\frac{1}{2}x_1^2(t)$ and $\frac{1}{2}x_2^2(t)$ are approximately the instantaneous kinetic and potential energy; in an electrical network, they would correspond to stored energy in an inductor and capacitor, and so forth.

The correspondence is only approximate because Equation (3.10) above implies equal dissipation rates from both energy storage states. In a spring-mass-damper system, only kinetic energy is dissipated, and a transformation is required from kinetic and potential energy states to the desired form. For the system

$$m\ddot{x} + c\dot{x} + kx = f \tag{3.11}$$

the normalized kinetic and potential energy states are $\xi_2 = \sqrt{m}\,\dot{x}$ and $\xi_1 = \sqrt{k}\,x$ respectively. The system matrix corresponding to $\dot{\xi} = A_\xi \xi$ is

$$A_\xi = \begin{bmatrix} 0 & \omega_n \\ -\omega_n & -2\eta \end{bmatrix} \tag{3.12}$$

where $\omega_n = \sqrt{k/m}$ and $\eta = \frac{1}{2}c/m$. The eigenvalues of A_ξ are the same as the eigenvalues of A_0 in Equation (3.10), with $\omega = \sqrt{\omega_n^2 - \eta^2}$. The frequency ω is the imaginary part of the poles, while the frequency ω_n is the distance of the pole from the origin. The system matrix A_0 in Equation (3.10) corresponds to the states $x = T\xi$ where

$$T = \begin{bmatrix} 1 & -\alpha \\ -\alpha & 1 \end{bmatrix} \tag{3.13}$$

and $\alpha = \eta/(\omega_n + \omega)$. For small damping, the resulting states still approximately correspond to kinetic and potential energy, and hence I will continue to refer to them as such.

With $\langle Q(t) \rangle_\sigma$ as the average covariance of the system in Equation (3.10), equipartition holds if $\langle Q_{11}(t) \rangle_\sigma = \langle Q_{22}(t) \rangle_\sigma$, while incoherence holds if $\langle Q_{12}(t) \rangle_\sigma = 0$. For an undamped system with σ fixed, the energy continually oscillates between Q_{11} and Q_{22}, and steady-state equipartition does not occur. Similarly, the state coordinates remain correlated, and steady state incoherence does not occur. Physically, equipartition and incoherence occur if the phase of the oscillation is uniformly distributed in the interval $[0, 2\pi]$, while the amplitude of the oscillation may be non-zero.

Rather than performing the eigen-decomposition indicated by Equation (3.8), complex algebra can be avoided by noting the decomposition

$$J \oplus J = \Phi \begin{bmatrix} 0 & 0 \\ 0 & 2J \end{bmatrix} \Phi^T \tag{3.14}$$

where the orthogonal transformation Φ is given by

$$\Phi \triangleq \frac{1}{\sqrt{2}} \left[\begin{array}{c|c} I & I \\ -J & J \end{array}\right] = \begin{bmatrix} \Phi_1 & \Phi_2 \end{bmatrix} \tag{3.15}$$

Also, a similar decomposition of $A_0 \oplus A_0$ yields

$$A_0 \oplus A_0 = \Phi \begin{bmatrix} -2\eta I & 0 \\ 0 & 2A_0 \end{bmatrix} \Phi^T \tag{3.16}$$

Using Equation (3.14), it follows that

$$\int_{-\infty}^{\infty} e^{\sigma(A_1 \oplus A_1)t} p(\sigma) \mathrm{d}\sigma = \Phi_1 \Phi_1^T + \Phi_2 \left(\int_{-\infty}^{\infty} e^{2\sigma J t} p(\sigma) \mathrm{d}\sigma \right) \Phi_2^T \tag{3.17}$$

Note that, analogous to Euler's formula for the scalar case,

$$e^{\sigma Jt} = (\cos \sigma t)I + (\sin \sigma t)J \tag{3.18}$$

Using this result, Equation (3.17) can be written in terms of the Fourier cosine and sine transforms of $p(\sigma/2)$:

$$f_c(t) \triangleq \int_{-\infty}^{\infty} \cos(2\sigma t)p(\sigma)\mathrm{d}\sigma \tag{3.19}$$

$$f_s(t) \triangleq \int_{-\infty}^{\infty} \sin(2\sigma t)p(\sigma)\mathrm{d}\sigma \tag{3.20}$$

Consider first the average covariance for the unforced case ($V = 0$).

Theorem 3.4 *The average covariance of the unforced single mode oscillator in Equation (3.10) satisfies both steady state equipartition and incoherence if the integral of $p(\sigma)$ is absolutely continuous. Furthermore, the average total energy decays at the same rate as the energy of the nominal system.*

Proof: Defining $\xi(t) \triangleq \Phi^T \langle q(t) \rangle_\sigma$, it follows that the four elements of ξ are related to the elements of the average covariance $\langle Q \rangle_\sigma$ via

$$\xi_1 = \langle Q_{11} \rangle_\sigma + \langle Q_{22} \rangle_\sigma \tag{3.21}$$

$$\xi_2 = \langle Q_{21} \rangle_\sigma - \langle Q_{12} \rangle_\sigma \tag{3.22}$$

$$\xi_3 = \langle Q_{11} \rangle_\sigma - \langle Q_{22} \rangle_\sigma \tag{3.23}$$

$$\xi_4 = \langle Q_{12} \rangle_\sigma + \langle Q_{21} \rangle_\sigma \tag{3.24}$$

Using Equations (3.16) and (3.17), Equation (3.7) for the average covariance can be written in terms of the ξ_i as

$$\xi_1(t) = e^{-2\eta t}\xi_1(0) \tag{3.25}$$

$$\xi_2(t) = e^{-2\eta t}\xi_2(0) \tag{3.26}$$

$$\begin{pmatrix} \xi_3(t) \\ \xi_4(t) \end{pmatrix} = e^{-2\eta t} \begin{bmatrix} \cos(2\omega t) & \sin(2\omega t) \\ -\sin(2\omega t) & \cos(2\omega t) \end{bmatrix} \begin{bmatrix} f_c(t) & f_s(t) \\ -f_s(t) & f_c(t) \end{bmatrix} \begin{pmatrix} \xi_3(0) \\ \xi_4(0) \end{pmatrix} \tag{3.27}$$

Recall that in the state space basis being used, Q_{11} and Q_{22} are the energies associated with the two state coordinates. Hence, ξ_1 given by Equation (3.21) is the

average total energy of the system. Equation (3.25) implies that the average total energy decays at the same rate as the energy of the nominal system. If the nominal system is undamped ($\eta = 0$), then conservation of energy holds for any uncertainty distribution.

From Equation (3.22), ξ_2 is the asymmetric part of $\langle Q \rangle_\sigma$. Since $\langle Q(0) \rangle_\sigma$ is symmetric, $\xi_2(0) = 0$. Equation (3.26) implies that $\xi_2(t) = 0 \; \forall \; t$, and hence that $\langle Q \rangle_\sigma$ remains symmetric for all time.

The third component, ξ_3 is the difference between the average energy in the two energy storage states, and ξ_4 is the average correlation between the two state coordinates. Steady state equipartition and incoherence occur if $\lim_{t\to\infty} \xi_3(t) = 0$ and $\lim_{t\to\infty} \xi_4(t) = 0$, which requires that in the undamped case, from Equation (3.27), $\lim_{t\to\infty} f_c(t) = 0$ and $\lim_{t\to\infty} f_s(t) = 0$. From the Riemann-Lebesgue Lemma [23], a sufficient condition for this is that the associated measure given by $\mathrm{d}\mu = p(\sigma)\mathrm{d}\sigma$ is absolutely continuous. □

Remark 3.5 *If there is a finite probability of a specific σ being achieved (a multiple-model uncertainty), then the Fourier transform of p does not tend to zero, and steady-state equipartition and incoherence do not occur.*

Now consider the steady state forced response; that is, the case $v = \mathrm{vec}\{V\} \neq 0$. Non-zero damping is required for a solution to exist. Defining $\mu = \Phi^T v$ gives

$$\lim_{t\to\infty} \begin{pmatrix} \xi_3(t) \\ \xi_4(t) \end{pmatrix} = \int_0^\infty e^{-2\eta t} \begin{bmatrix} \cos(2\omega t) & \sin(2\omega t) \\ -\sin(2\omega t) & \cos(2\omega t) \end{bmatrix} \begin{bmatrix} f_c(t) & f_s(t) \\ -f_s(t) & f_c(t) \end{bmatrix} \begin{pmatrix} \mu_3 \\ \mu_4 \end{pmatrix} \mathrm{d}t$$

$$= \int_{-\infty}^\infty p(\sigma) \begin{bmatrix} f_1 & f_2 \\ f_2 & f_1 \end{bmatrix} \begin{pmatrix} \mu_3 \\ \mu_4 \end{pmatrix} \mathrm{d}\sigma \tag{3.28}$$

where μ_3 and μ_4 are the third and fourth components of μ, and

$$f_1 \triangleq \frac{\eta}{\eta^2 + (\omega + \sigma)^2} \tag{3.29}$$

$$f_2 \triangleq \frac{\omega + \sigma}{\eta^2 + (\omega + \sigma)^2} \tag{3.30}$$

Both $|f_1|$ and $|f_2|$ are bounded by $1/\eta$, and also, $\forall \epsilon > 0 \; \exists \Delta > 0$ such that $|f_1| < \epsilon$ and $|f_2| < \epsilon \; \forall \; |\sigma| > \Delta$. If $p(\sigma)$ satisfies the conditions of Theorem 3.4, then p can be

parameterized by a scaling on the uncertainty such that $\forall \epsilon_2 > 0\ \exists k > 0$ such that $kp(k\sigma) < \epsilon_2 \quad \forall |\sigma| < \Delta$, and hence $\lim_{t\to\infty} \xi_3(t)$ and $\lim_{t\to\infty} \xi_4(t)$ can be made arbitrarily small. Hence, for any probability density with a continuous integral, equipartition and incoherence for the forced case will be achieved in the limit as the uncertainty level of the probability density is increased.

3.4 Examples

There are a variety of reasonable distributions that may be considered for the uncertainty. In addition to demonstrating equipartition and incoherence for several specific distributions, we wish to investigate whether the average covariance can be computed via a Lyapunov-like matrix equation similar to Equation (3.3) for the nominal covariance. To facilitate the calculations, note that

$$\Phi_1 \Phi_1^T = \tfrac{1}{2}(I + J \otimes J) \tag{3.31}$$

$$\Phi_2 \Phi_2^T = \tfrac{1}{2}(I - J \otimes J) \tag{3.32}$$

$$\Phi_2 J \Phi_2^T = \tfrac{1}{2} J \oplus J \tag{3.33}$$

It follows that the general solution for $\langle q(t) \rangle_\sigma$ with non-zero forcing v is given by Equation (3.7) where, from Equations (3.6) and (3.17),

$$\mathcal{Q}(t) = \tfrac{1}{2} e^{(A_0 \oplus A_0)t} [(I + J \otimes J) + (I - J \otimes J) f_c(t) + (J \oplus J) f_s(t)] \tag{3.34}$$

For convenience, henceforth denote the average covariance by $Q_a(t) \triangleq \langle Q(t) \rangle_\sigma$, and $q_a(t) \triangleq \mathrm{vec}\{Q_a(t)\}$.

The following identities will also be useful:

$$(J \oplus J)^2 = -2(I - J \otimes J) \tag{3.35}$$

$$(J \oplus J)(J \otimes J) = -(J \oplus J) \tag{3.36}$$

$$(I - J \otimes J)^2 = 2(I - J \otimes J) \tag{3.37}$$

$$(I - J \otimes J)(I + J \otimes J) = 0 \tag{3.38}$$

3.4.1 Discrete Uncertainty

First, consider the case involving only two possible values, $\sigma = \pm\Delta$, for the uncertain parameter. This is akin to the multiple model description of uncertainty used in [4].

Theorem 3.6 (Discrete Uncertainty) *Consider the system in Equation (3.10). If the probability density function for σ is given by*

$$p(\sigma) = \tfrac{1}{2}\delta(\sigma - \Delta) + \tfrac{1}{2}\delta(\sigma + \Delta) \tag{3.39}$$

where δ is the Dirac delta function, then the average covariance $Q_a(t)$ is the solution to

$$\dot{Q}_a = A_0 Q_a + Q_a A_0^T + \Delta(A_1 Q_b + Q_b A_1^T) + V \tag{3.40}$$

$$\dot{Q}_b = A_0 Q_b + Q_b A_0^T + \Delta(A_1 Q_a + Q_a A_1^T) \tag{3.41}$$

with initial conditions $Q_a(0) = Q_0$ and $Q_b(0) = 0$.

Proof: For this distribution,

$$f_c(t) = \cos(2\Delta t) \qquad\qquad f_s(t) = 0 \tag{3.42}$$

Note that neither equipartition nor incoherence will be achieved for this distribution since $\lim_{t\to\infty} f_c(t) \neq 0$, which corresponds to the fact as noted before that $\int p(\sigma)\,\mathrm{d}\sigma$ is discontinous.

The average covariance is given by Equation (3.7) with

$$\mathcal{Q}(t) = \tfrac{1}{2} e^{(A_0 \oplus A_0)t}\left[(I + J \otimes J) + (I - J \otimes J)\cos(2\Delta t)\right] \tag{3.43}$$

Differentiation yields that $q_a(t)$ satisfies

$$\begin{aligned} \dot{q}_a(t) = {} & (A_0 \oplus A_0) q_a(t) - \Delta e^{(A_0 \oplus A_0)t}(I - J \otimes J)\sin(2\Delta t) q_0 + v \\ & - \int_0^t \Delta e^{(A_0 \oplus A_0)(t-\tau)}(I - J \otimes J)\sin(2\Delta(t-\tau)) v\,\mathrm{d}\tau \end{aligned} \tag{3.44}$$

To characterize $q_a(t)$ in terms of Lyapunov-like matrix equations, define the auxiliary variable $q_b(t) = \mathrm{vec}\{Q_b(t)\}$ by

$$\begin{aligned} q_b(t) = {} & \tfrac{1}{2} e^{(A_0 \oplus A_0)t}(J \oplus J)\sin(2\Delta t) q_0 \\ & + \tfrac{1}{2}\int_0^t e^{(A_0 \oplus A_0)(t-\tau)}(J \oplus J)\sin(2\Delta(t-\tau)) v\,\mathrm{d}\tau \end{aligned} \tag{3.45}$$

Using Equation (3.36), one can therefore write

$$\dot{q}_a(t) = (A_0 \oplus A_0)q_a(t) + \Delta(J \oplus J)q_b(t) + v \tag{3.46}$$

with the initial condition $q_a(0) = q_0$. Similarly, $\dot{q}_b(t)$ can be expressed in terms of $q_a(t)$ and $q_b(t)$ using Equation (3.35), with initial condition $q_b(0) = 0$ from Equation (3.45). The result follows immediately. □

Remark 3.7 *Equations (3.40) and (3.41) are precisely the equations obtained in [45] for the Bourret approximation to the average covariance for a uniform distribution.*

The conclusion of Theorem 3.6 also applies to arbitrary A_0 and A_1; they may have arbitrary dimension, and need not commute. Denote the covariances corresponding to the two possible models, $A = A_0 \pm \Delta A_1$, by Q_1 and Q_2. Then $Q_a = \frac{1}{2}(Q_1 + Q_2)$ and $Q_b = \frac{1}{2}(Q_1 - Q_2)$; adding and subtracting the Lyapunov equations solved by Q_1 and Q_2 yields Equations (3.40) and (3.41).

3.4.2 Uniform Distribution

Perhaps the most common uncertainty assumption is that the parameter lies within some bounded interval, with uniform probability density within that interval. If the nominal plant is taken as the midpoint of this interval, then

$$p(\sigma) = \begin{cases} \frac{1}{2\Delta} & |\sigma| \leq \Delta \\ 0 & |\sigma| > \Delta \end{cases} \tag{3.47}$$

and

$$f_c(t) = \mathrm{sinc}(2\Delta t) = \frac{\sin(2\Delta t)}{2\Delta t} \qquad f_s(t) = 0 \tag{3.48}$$

Note that since $\lim_{t\to\infty} f_c(t) = 0$, both equipartition and incoherence will be achieved in the steady state, unforced case for this distribution. The average covariance is given by Equation (3.7) with

$$Q(t) = \tfrac{1}{2}e^{(A_0 \oplus A_0)t}\left[(I + J \otimes J) + (I - J \otimes J)\,\mathrm{sinc}(2\Delta t)\right] \tag{3.49}$$

3.4.3 Cauchy Distribution

Now consider the case where the uncertain parameter has a Cauchy probability density function. Although this distribution has neither compact support nor finite variance, it has the advantage of ease of computation. The conclusion in this case is particularly important due to its relationship to the maximum entropy design technique of Hyland [52].

Theorem 3.8 (Cauchy Distribution) *Consider the system in Equation (3.10). If the probability density function for σ is given by*

$$p(\sigma) = \frac{\Delta/\pi}{\sigma^2 + \Delta^2} \tag{3.50}$$

with $\Delta > 0$, then the average covariance is the solution to

$$\dot{Q}_a = (A_0 + \tfrac{1}{2}\Delta A_1^2)Q_a + Q_a(A_0 + \tfrac{1}{2}\Delta A_1^2)^T + \Delta A_1 Q_a A_1^T + V \tag{3.51}$$

with initial condition $Q_a(0) = Q_0$.

Proof: For this distribution,

$$f_c(t) = e^{-2\Delta|t|} \qquad f_s(t) = 0 \tag{3.52}$$

So for $t \geq 0$,

$$\mathcal{Q}(t) = \tfrac{1}{2}e^{(A_0 \oplus A_0)t}\left[(I + J \otimes J) + (I - J \otimes J)e^{-2\Delta t}\right] \tag{3.53}$$

Differentiating Equation (3.7) and using Equations (3.37) and (3.38) yields that the average covariance satisfies

$$\dot{q}_a(t) = (A_0 \oplus A_0)q_a(t) - \Delta(I - J \otimes J)q_a(t) + v \tag{3.54}$$

or

$$\dot{Q}_a = A_0 Q_a + Q_a A_0^T + \Delta\left(JQ_aJ^T - Q_a\right) + V \tag{3.55}$$

with initial condition $Q_a(0) = Q_0$. Setting $\alpha = \sqrt{\Delta}$, Equation (3.55) can be rewritten as Equation (3.51) on noting that $I = -A_1^2$. □

Remark 3.9 *Equation (3.51) is precisely the covariance equation in the maximum entropy design equations, Equation (2.11) or [13, Eq'n (212)], for a single uncertain parameter.*

The covariance of the state which satisfies Equations (3.1) and (3.10), where σ has a Cauchy distribution given by Equation (3.50), is precisely the same as the covariance of the state that satisfies a differential equation of the same form, but where σ is replaced by a white noise process of intensity $\sqrt{\Delta}$. This is a powerful result, as it relates two apparently different approaches, and demonstrates that the maximum entropy approach [52] can be interpreted as a cost averaging approach.

In the undamped, unforced case, the average covariance must satisfy conservation of energy, since each individual model does. This can be seen directly from the covariance equation, (3.51), by noting that since $A_1^2 = -I$ and $A_1^T A_1 = +I$,

$$\begin{aligned} \mathrm{tr}\left\{\dot{Q}_a\right\} &= \mathrm{tr}\left\{A_0 Q_a\right\} + \mathrm{tr}\left\{A_0^T Q_a\right\} + \alpha^2 \mathrm{tr}\left\{A_1^2 Q_a\right\} + \alpha^2 \mathrm{tr}\left\{A_1^T A_1 Q_a\right\} \\ &= 0 \end{aligned} \tag{3.56}$$

The various terms in the covariance equation can be interpreted as follows. The equivalent system matrix $(A_0 + \frac{1}{2}\alpha^2 A_1^2)$ is a left-shifted, or damped version of the original system matrix. This new system matrix corresponds to a transfer function that is smoother than the original transfer function, in order to reflect the uncertainty in the exact pole locations. The extra term $\alpha^2 A_1 Q_a A_1^T$ represents an additional driving noise that corresponds exactly to the energy lost due to the apparent damping that has been added in the new system matrix.

The behavior of the two average energy variables with the various probability distributions discussed so far is shown in Figure 3.2, starting from an initial condition where all of the energy is in the first state. Equipartition occurs for the uniform and Cauchy distribution, but not for the discrete uncertainty distribution. The parameter Δ of the discrete and uniform distributions are chosen so that they both have the same variance. The cross-correlation between the two state variables is shown for the same distributions in Figure 3.3, starting from an initial condition where the two states have unit cross-correlation. Again, incoherence occurs for the uniform and

Cauchy distributions, but not for the discrete distribution. In both plots, the Fourier transform of the probability density function is clearly visible in the envelope of the response.

3.4.4 Rational Distributions

In Section 3.4.3 it was shown that the average covariance for a Cauchy distribution can be computed by solving a single Lyapunov equation. More generally, it can be shown that it is possible to compute the average covariance for any rational and proper distribution from a set of coupled Lyapunov equations. Although not directly relevant to demonstrating equipartition and incoherence for parametrically uncertain systems, these results are included for completeness.

Theorem 3.10 (Rational Distribution) *Let $g(s) = c(sI - \mathcal{A})^{-1}b$ be positive real, where $\mathcal{A}$ is an arbitrary asymptotically stable $n \times n$ matrix with elements a_{ij}, and b, c^T are of dimension $n \times 1$, satisfying $cb = 1$. Consider the system in Equation (3.10). If the probability density function for σ satisfies*

$$p(\sigma) = \frac{1}{2\pi}\left(g(j\sigma) + g^*(j\sigma)\right) \tag{3.57}$$

then the average covariance satisfies $Q_a(t) = \sum_{i=1}^{n} c_i Q_i(t)$, where the $Q_i(t)$ solve

$$\dot{Q}_i = A_0 Q_i + Q_i A_0^T + \sum_{j=1}^{n} a_{ij}(Q_j - JQ_jJ^T) + b_i V \tag{3.58}$$

for $i = 1, \ldots, n$, with initial conditions $Q_i(0) = b_i Q_0$.

Proof: First note that $p(\sigma)$ is real, and positive since $g(s)$ is positive real. It follows that

$$f_c(t) = ce^{2\mathcal{A}|t|}b \qquad\qquad f_s(t) = 0 \tag{3.59}$$

For $p(\sigma)$ to be a probability density function, $f_c(0) = \int_{-\infty}^{\infty} p(\sigma)d\sigma = 1$, and hence the condition $cb = 1$ is required.

For $t \geq 0$, the average covariance is given by Equation (3.7) where

$$Q(t) = \tfrac{1}{2}e^{(A_0 \oplus A_0)t}\left[(I + J \otimes J) + (I - J \otimes J)ce^{2\mathcal{A}t}b\right] \tag{3.60}$$

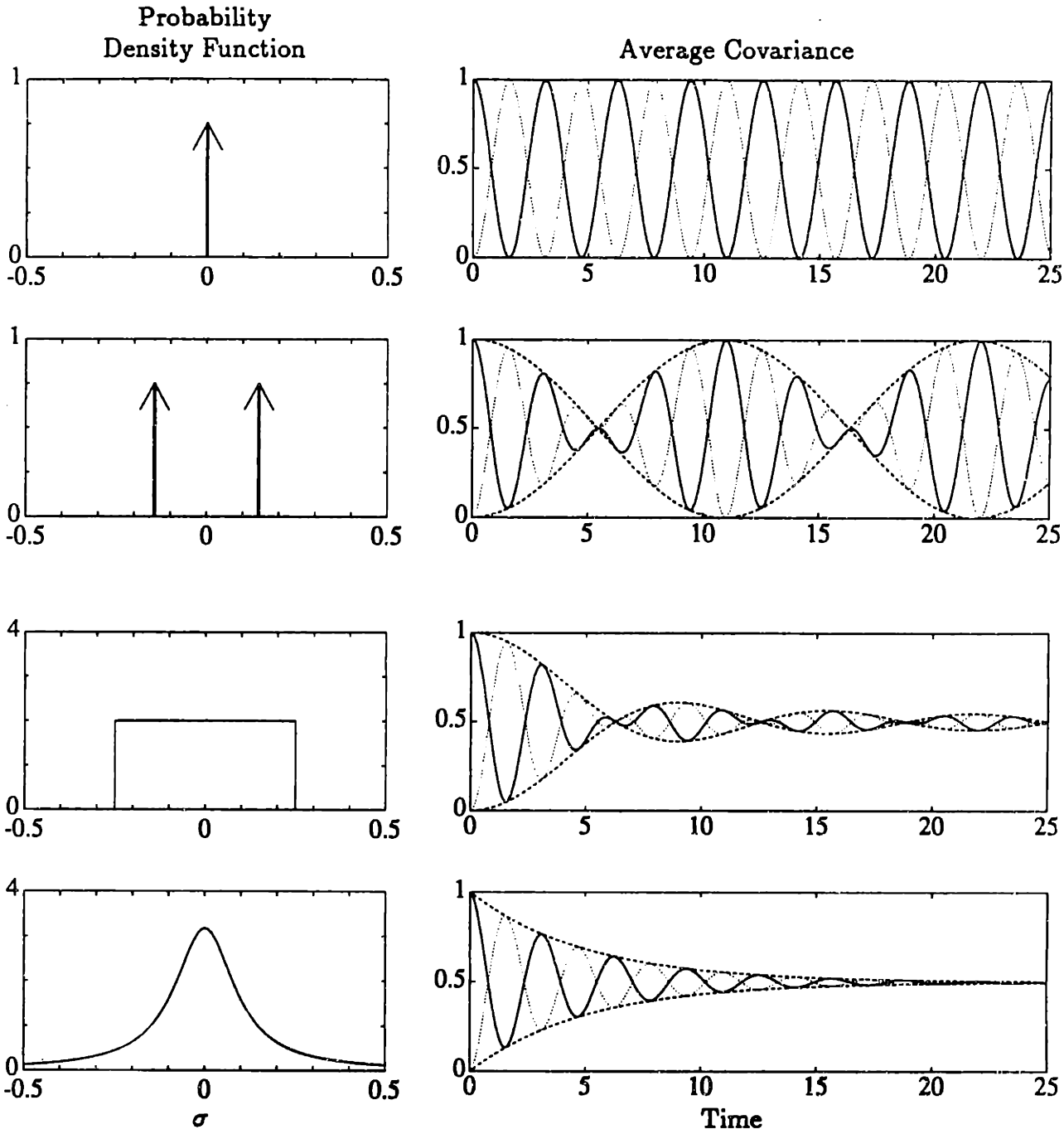

Figure 3.2: Equipartition behavior: average unforced covariance from initial conditions (right) and corresponding probability density function (left). On right, $\langle Q_{11} \rangle_\sigma$ (solid), $\langle Q_{22} \rangle_\sigma$ (dotted), and the envelope of the average (dashed), from Equations (3.42), (3.48), and (3.52). From top, nominal case, discrete uncertainty ($\Delta = .14$), uniform distribution ($\Delta = .25$), and Cauchy distribution of uncertainty ($\Delta = .10$).

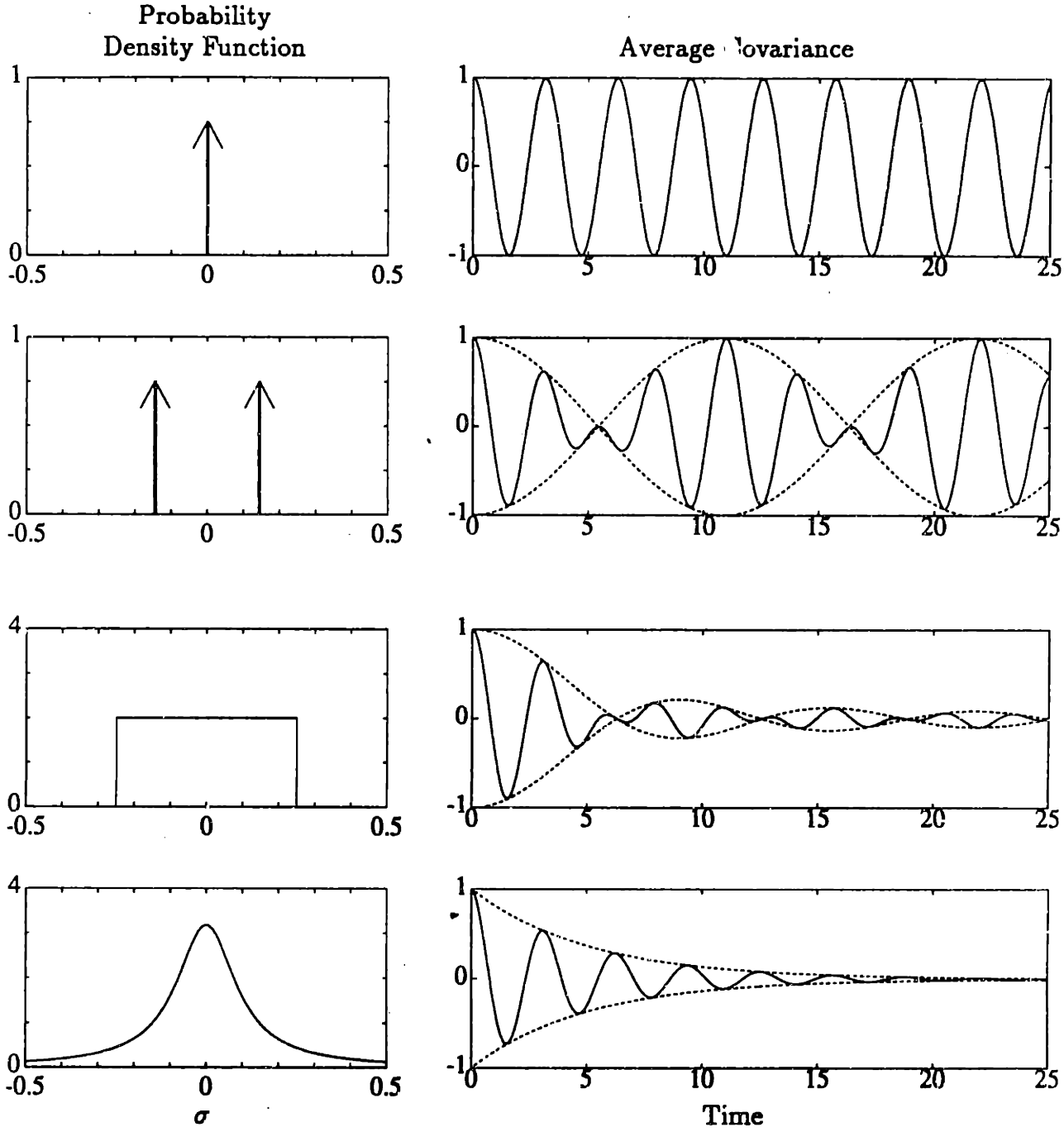

Figure 3.3: Incoherence behavior: average unforced covariance from initial conditions (right) and corresponding probability density function (left). On right, $\langle Q_{12} \rangle_\sigma$ (solid) and the envelope of the average (dashed), from Equations (3.42), (3.48), and (3.52). From top, nominal case, discrete uncertainty ($\Delta = .14$), uniform distribution ($\Delta = .25$), and Cauchy distribution of uncertainty ($\Delta = .10$)

With b_i as the i^{th} component of the vector b, and $\left[e^{2\mathcal{A}t}b\right]_i$ as the i^{th} component of the vector $e^{2\mathcal{A}t}b$, then for $i = 1, \ldots, n$ define

$$\begin{aligned} q_i(t) &= \tfrac{1}{2}e^{(A_0 \oplus A_0)t}\left\{(I + J \otimes J)b_i + (I - J \otimes J)\left[e^{2\mathcal{A}t}b\right]_i\right\} q_0 \\ &+ \tfrac{1}{2}\int_0^t e^{(A_0 \oplus A_0)(t-\tau)}\left\{(I + J \otimes J)b_i + (I - J \otimes J)\left[e^{2\mathcal{A}(t-\tau)}b\right]_i\right\} v \, d\tau \end{aligned} \tag{3.61}$$

with the initial conditions $q_i(0) = b_i q_0$. With this definition, $q_a(t) = \sum_{i=1}^{n} c_i q_i(t)$ since $\sum_{i=1}^{n} c_i b_i = 1$. Differentiating Equation (3.61) for each i yields

$$\dot{q}_i(t) = (A_0 \oplus A_0)q_i(t) + \sum_{j=1}^{n} a_{ij}(I - J \otimes J)q_j(t) + b_i v \tag{3.62}$$

where a_{ij} are the elements of the matrix $\mathcal{A}$. The conclusion follows. □

Remark 3.11 *The Cauchy distribution in Theorem 3.8 corresponds to* $\mathcal{A} = -\Delta$, $b = c = 1$.

The equations that describe the average covariance for a rational distribution can be written in a more compact form using Kronecker algebra. Define

$$\mathbf{Q} = \begin{bmatrix} Q_1 \\ Q_2 \\ \vdots \\ Q_n \end{bmatrix} \tag{3.63}$$

Then $Q_a(t)$ can be expressed in terms of $\mathbf{Q}(t)$ as

$$Q_a = (c \otimes I)\mathbf{Q} \tag{3.64}$$

$$\dot{\mathbf{Q}} = [I \otimes A_0]\mathbf{Q} + \mathbf{Q}A_0^T + [\mathcal{A} \otimes I]\left(\mathbf{Q} - [I \otimes A_1]\mathbf{Q}A_1^T\right) + [b \otimes I]V \tag{3.65}$$

$$\mathbf{Q}(0) = [b \otimes I]Q_0 \tag{3.66}$$

If one further defines the Lyapunov operator $\mathcal{L}_0(Q) = A_0Q + QA_0^T$ and the Stratonovich operator $\mathcal{S}_1(Q) = Q - A_1QA_1^T$, then one can write instead that

$$Q_a = (c \otimes I)\mathbf{Q} \tag{3.67}$$

$$\dot{\mathbf{Q}} = [I \otimes \mathcal{L}_0]\mathbf{Q} + (\mathcal{A} \otimes I)[I \otimes \mathcal{S}_1]\mathbf{Q} + (b \otimes I)V \tag{3.68}$$

$$\mathbf{Q}(0) = (b \otimes I)Q_0 \tag{3.69}$$

where the operators $I \otimes \mathcal{L}_0$ and $I \otimes \mathcal{S}_1$ are understood to imply that the Lyapunov or Stratonovich operator is repeated n times along the diagonal, with the off-diagonal operators being equal to zero.

If the probability density describing σ is a rational function of order $2n$, then the solution is described by n coupled Lyapunov equations.

3.5 Multiple Mode Results

Now consider the case in which the plant has multiple modes. The primary question of interest is whether incoherence and equipartition among different modes arise from averaging over uncertainty. Recall that the assumption that the uncertainty structure commutes with the nominal system implies that only modal frequency uncertainty can be considered, and not uncertainty in the mode shapes. Hyland [52] concluded that incoherence between modes results from uncertain frequencies, while equipartition between modes occurs only if the mode shapes themselves are uncertain.

To examine the interaction among different modes, consider a two mode system, with a single uncertain parameter that affects both modal frequencies. (Multiple uncorrelated uncertain parameters can be treated using the results of Section 3.3.) The system is then of the form

$$A_0 = \begin{bmatrix} -\eta_1 I + \omega_1 J & 0 \\ 0 & -\eta_2 I + \omega_2 J \end{bmatrix} \tag{3.70}$$

with uncertainty structure

$$A_1 = \begin{bmatrix} \lambda_1 J & 0 \\ 0 & \lambda_2 J \end{bmatrix} \tag{3.71}$$

where λ_1 and λ_2 are arbitrary real numbers.

Theorem 3.12 *The average covariance of the system $\dot{x} = (A_0 + \sigma A_1)x$ described by Equations (3.70) and (3.71) satisfies steady state incoherence between modes, provided $\mathrm{d}\mu = p(\sigma)\,\mathrm{d}\sigma$ is absolutely continuous and $|\lambda_1| \neq |\lambda_2|$.*

Proof: The proof is similar to that of Theorem 3.4. From Equations (3.7) and (3.6), the average covariance requires computation of

$$\mathcal{Q}(t) = e^{(A_0 \oplus A_0)t} \int_{-\infty}^{\infty} e^{\sigma(A_1 \oplus A_1)t} p(\sigma) \mathrm{d}\sigma \tag{3.72}$$

In a similar fashion to Equation (3.14), $A_1 \oplus A_1$ can be decomposed as

$$A_1 \oplus A_1 = \Phi \begin{bmatrix} 0 & \cdots & & & & & \\ \vdots & (\lambda_1+\lambda_1)J & & & & & \\ & & (-\lambda_1+\lambda_2)J & & & & \\ & & & (\lambda_1+\lambda_2)J & & & \\ & & & & (\lambda_1-\lambda_2)J & & \\ & & & & & (\lambda_1+\lambda_2)J & \\ & & & & & & 0 \\ & & & & & & & (\lambda_2+\lambda_2)J \end{bmatrix} \Phi^T \tag{3.73}$$

where Φ is the orthogonal transformation

$$\Phi \triangleq \frac{1}{\sqrt{2}} \begin{bmatrix} \Phi_1 & 0 \\ 0 & \Phi_1 \end{bmatrix} \tag{3.74}$$

$$\Phi_1 \triangleq \begin{bmatrix} I & -J & 0 & 0 \\ 0 & 0 & -I & -J \\ -J & I & 0 & 0 \\ 0 & 0 & J & I \end{bmatrix} \tag{3.75}$$

The matrix Λ has eigenvalues $\left((-1)^{\ell}\lambda_i + (-1)^m \lambda_k\right) j$ for $i,k,\ell,m = 1,2$. The zero eigenvalues ($\ell \neq m, i = k$) correspond to conservation of energy, and symmetry. Examining the eigenvectors corresponding to the remaining eigenvalues, one can conclude that in the unforced case, *every* off-diagonal element of $\langle Q(t) \rangle_\sigma$ decays with time, provided again that the Fourier transform of the probability density is zero at infinity, and with the additional requirement that $|\lambda_1| \neq |\lambda_2|$. If this extra condition is violated, then there are additional zero blocks in the block-diagonal matrix in

Equation (3.73), and some off-diagonal elements of the average covariance will not tend to zero. □

In general, not only is there incoherence between the two states of a given mode, but there is incoherence between modes; the states associated with one mode are uncorrelated with those of another when averaged over uncertainty. Conclusions in the forced case are similar to the conclusions for the single mode forced case.

3.6 Summary

The effect of parametric uncertainty on state space systems has been investigated by averaging the state covariance over the probability distribution of the uncertain parameters. The key observation is that for natural frequency uncertainty, the average covariance can be computed in terms of the Fourier transform of the probability density function of the uncertain parameter. This allows one to reach several conclusions. First, that the average covariance for a single mode oscillator exhibits both equipartition and incoherence phenomena for a large class of uncertainty distributions, and that incoherence between modes occurs for the multiple mode case as well. These properties of uncertain systems will be used in the next chapter to develop a cost functional that represents the average performance over the uncertainty in the structure. Similar properties have been assumed in Statistical Energy Analysis, but without rigourous justification based on averaging over uncertainty.

Second, the Bourret approximation of [44, 45] with a single uncertain parameter is the average covariance for a discrete (or multiple model) uncertainty distribution, while the maximum entropy cost evaluation in [52, 13] is precisely the average covariance for a Cauchy probability distribution. The interpretation of these robust control design techniques in terms of covariance averaging over uncertainty gives them added justification. This also illustrates a connection between the cost averaging approach developed in the next chapter, and other existing parameter-robust control design techniques.

Chapter 4

Performance Metric for Uncertain Structures

Order and simplification are the first steps toward the mastery of a subject — The actual enemy is the unknown.

– Thomas Mann, *The Magic Mountain*

The objective of this chapter is to develop an approach for designing optimal parameter robust collocated control laws for structures. In order to be successful, such an approach should take advantage of the properties of parametrically uncertain systems. One difficulty with many current robust control approaches is their inability to distinguish between a natural frequency uncertainty, which is not open-loop destabilizing, and an uncertainty in the real part of the pole, which for lightly damped systems is likely to be destabilizing. That is, they do not take advantage of the knowledge that the open-loop system approximately conserves energy. As shown in Chapter 3, there are several robust control design techniques that do use conservation of energy implicitly. Herein, this property will be used explicitly, along with other properties of stochastic systems that were obtained in Chapter 3.

The goal is to describe the average value of a global $\mathcal{H}_2$ performance metric in terms of only local information. This is made possible by knowing that the average covariance satisfies equipartition and incoherence. The local structural properties are described by the dereverberated mobility, and using this model, the relative power

dissipation of any controller can be simply represented. The average global performance metric can then be related to the power dissipation, giving a cost functional that depends only on the dereverberated mobility, and the compensator.

The approach to finding the compensator that optimizes this cost is given in Chapter 5. If the average cost is finite, then the cost must be finite for almost any value of the uncertainty within the set of uncertainty considered. Therefore, the optimal compensator that minimizes the average value of the global $\mathcal{H}_2$ performance will be guaranteed to be stabilizing. The ideal compensator for collocated and dual sensors and actuators is known to be a non-causal impedance match of the dereverberated transfer function, which must be approximated by a causal compensator. The impedance match of the reverberant transfer function may decrease, rather than increase the damping in the structure. Previous impedance matching approaches obtained a causal approximation that minimized an $\mathcal{H}_2$ cost, but did not guarantee stability [69], or minimized an $\mathcal{H}_\infty$ cost that guaranteed stability, but did not minimize the desired cost [61]. The cost functional derived in this chapter describes the relative importance of different frequency regions, and the relative importance of matching the magnitude and phase of the non-causal impedance match. Minimizing this cost yields the best causal impedance match that minimizes the average value of the global cost, and guarantees that the closed loop system will remain stable.

4.1 Motivating Example

The following sections examine how to describe the average $\mathcal{H}_2$ cost for an arbitrary, complex structure in terms of only local information. First, consider a much simpler example; the end-point control of a uniform rod in compression with uncertain length, as shown in Figure 4.1. This example illustrates the ability to describe the expected global mean-square cost in terms of only local structural information.

A disturbance force $f(s)$ acting at the left end of the rod will combine with the incoming wave to create a wave $w_L(s)$ leaving that end. The resulting wave incoming at the right end will be ξw_L, where $\xi = e^{\ell s}$ is the transmission coefficient from one

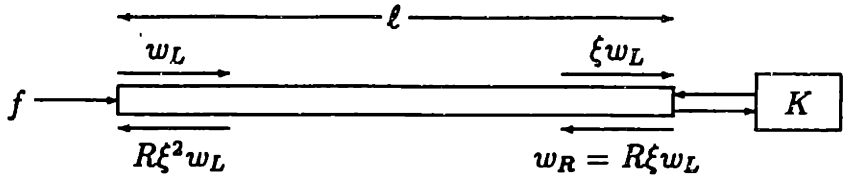

Figure 4.1: Rod with end-point control and unknown length.

end of the rod to the other. The fact that $|\xi(j\omega)| = 1$ is a consequence of conservation of energy. The effect of the control is to change the reflection coefficient at the right end of the rod to some value R. Thus if the incoming wave at this end is ξw_L, the outgoing wave w_R will be $\xi R w_L$. Finally, the incoming wave at the left end will be Hw_L, where $H = \xi^2 R$. With an appropriate scaling of the force, then

$$w_L = f + Hw_L \tag{4.1}$$

$$w_L = \frac{1}{1-H} f \tag{4.2}$$

For simplicity, let the cost be the rms amplitude of the wave leaving the actuator. Any other rms cost can be expressed in terms of $\langle w_R^2 \rangle$. If the force has mean square amplitude $\langle f^2 \rangle$, then the mean square amplitude of the outgoing wave at the disturbance end is

$$\langle w_L^2 \rangle = \frac{1}{(1-H^*)(1-H)} \langle f^2 \rangle \tag{4.3}$$

The mean square amplitude of the outgoing wave at the controlled end is

$$\langle w_R^2 \rangle = \frac{H^* H}{(1-H^*)(1-H)} \langle f^2 \rangle \tag{4.4}$$

Note that $H^*H = R^*R$, since $\xi^*\xi = 1$. Provided that the length of the rod is known exactly, it is the quantity in Equation (4.4) that should be minimized.

Now consider the case where there is some uncertainty in the length of the rod, and hence in ξ. This corresponds to knowing that, if a wave is allowed to reverberate throughout the structure, the returning wave will have the same amplitude as the original wave, due to conservation of energy, but the phase will be uncertain. In the limiting case where there is no knowledge about this phase, then

$$H = Re^{j\theta} \tag{4.5}$$

where θ is random with uniform probability density function $p(\theta) = \frac{1}{2\pi}$. This is now a stochastic description of the system.

The control design goal should now be to minimize the average value of the cost over the statistics of the uncertain parameter. The average mean-square magnitude of the wave outgoing from the controlled end of the rod is

$$\left\langle w_R^2 \right\rangle = \int_0^{2\pi} \frac{R^* R}{(1 - R^* e^{-j\theta})(1 - R e^{j\theta})} \frac{\mathrm{d}\theta}{2\pi} \left\langle f^2 \right\rangle \tag{4.6}$$

This integral can be evaluated using residue theory. Define $z = e^{j\theta}$, which yields $\mathrm{d}\theta = \frac{\mathrm{d}z}{jz}$. Then Equation (4.6) can be written as

$$\left\langle w_R^2 \right\rangle = \frac{1}{2\pi j} \oint \frac{R^*}{(1 - z^{-1} R^*)} \frac{R}{(1 - zR)} \frac{\mathrm{d}z}{z} \left\langle f^2 \right\rangle \tag{4.7}$$

where the contour of integration is around the unit circle. Evaluating this gives

$$\left\langle w_R^2 \right\rangle = \frac{R^* R}{1 - R^* R} \left\langle f^2 \right\rangle \tag{4.8}$$

provided that the reflection coefficient satisfies $|R| < 1$. (If not, then the system is unstable.) Thus the compensator that minimizes the *average* magnitude of the outgoing wave can be obtained by minimizing the cost functional in Equation (4.8). Note that this result depends on approximate conservation of energy, and requires only local knowledge; that is, knowledge of only the characteristics of the controlled end. Only the reflection coefficient R is needed to predict the average magnitude. The goal of Section 4.3 will be to justify a similar expression for arbitrary structures, using the properties obtained in the previous chapter.

This problem is similar to that considered in [18, p. 114]. The average cost in Equation (4.6) is also the average cost of the system shown in Figure 4.2, where the uncertainty block $\Delta = e^{j\theta}$ has known magnitude, but unknown phase. Reference [18] considers the same problem, motivated by a standard linear fractional description of uncertainty. The average $\mathcal{H}_2$ cost over uncertainty Δ of unknown phase and bounded magnitude is shown to be related to the entropy cost of [74], for a scalar system. Indeed, the result in Equation (4.8) is a step in the proof of the result in [18]. Rather

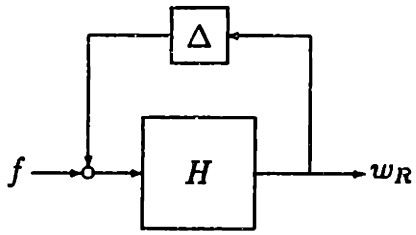

Figure 4.2: Equivalent uncertainty block diagram for rod example.

than integrating over the entire disk as in [18], the averaging that yields Equation (4.8) is performed only over the boundary of the disk.

If, instead of complete uncertainty on the phase of the returning wave, one has partial knowledge, then a similar analysis may still be performed. Assume now that the unknown phase angle is described by a nominal part, plus an error whose probability density function is

$$p(\theta) = \frac{1-\alpha^2}{(z-\alpha)(z^{-1}-\alpha)} \tag{4.9}$$

for some $\alpha < 1$. Applying a bilinear transformation that maps the unit circle to the $j\omega$ axis yields that if θ has the probability density function given in Equation (4.9), then the corresponding distribution along the $j\omega$ axis is Cauchy, given by Equation (3.50). With H being the nominal value of $Re^{j\theta_0}$, then the resulting contour integration yields the average mean square amplitude of the outgoing wave as

$$\left\langle w_R^2 \right\rangle = \frac{H^*H}{1-H^*H} \cdot \frac{1-\alpha^2 H^*H}{(1-\alpha H)(1-\alpha H^*)} \tag{4.10}$$

In the limiting case of complete uncertainty, $\alpha = 0$, this yields the same expression for the average cost as before. In the other limit, $\alpha \to 1$, the exact cost in Equation (4.4) is recovered except that the new cost retains the constraint that $|H| < 1$; that is, that power be dissipated in order to guarantee stability for arbitrary variations in the length of the rod.

4.2 Power Flow

The preceding example demonstrates that the average value of some global performance metric can be expressed in terms of only the local structural properties. In order to apply similar reasoning to an arbitrary structure, the notion of a reflection coefficient must be generalized. The appropriate reflection coefficient is the ratio of the power reflected back into the structure to the power in the incoming disturbance. For the rod, the simplest result was obtained by assuming the phase of the reverberant field to be completely uncertain. Applying this assumption to an arbitrary structure yields the dereverberated mobility as the average input mobility. This model has been used previously to describe the power dissipation and reflection characteristics of a compensator between collocated and dual actuators and sensors [61].

4.2.1 Dereverberated Mobility

As noted in Section 2.1.1, the structural response due to the actuator can be divided into two parts: a *direct field*, due to the local dynamics; and a *reverberant field*, which is created by reflections from other parts of the structure. The dereverberated mobility is defined to be the mobility associated with only the direct field; the effect of reflections (the reverberant field) is not included. There are a variety of equivalent interpretations of the dereverberated transfer function. It appears in [58] as an average mobility over frequency bands containing many modes, where the average is taken of the logarithmic magnitude. The logarithmic average has also been demonstrated to be equivalent to the limiting transfer function obtained as the damping is increased [47, 88]. Intuitively, the equivalence corresponds to the fact that increasing the damping eliminates the reverberant field entirely in the limit as the damping becomes critical. This leaves only the effects of the direct field, and hence yields the dereverberated mobility. The reverberant field can also be eliminated by considering the transfer function of the infinitely extended system. This approach allows the dereverberated mobility to be computed easily from a wave model [64], or directly from a partial differential equation representation of the structure. Another interpretation of the

dereverberated mobility is the large uncertainty limit of averaging the driving point mobility over uncertainty. Some early Statistical Energy Analysis research computed the average input mobility over the statistics of the uncertainty distribution, and demonstrated that with large uncertainty, this averaging yielded the mobility of the infinitely extended system, or the dereverberated mobility [56].

For certain assumptions on the uncertainty, the input power corresponding to the average system, computed from the dereverberated mobility, is the same as the average input power, where both averages are taken with respect to uncertainty. For a known structure with input mobility $G(s)$ at the actuator location, the average power flow at each frequency is given by

$$\Pi_{\text{in}}(\omega) = \tfrac{1}{2}(G(j\omega) + G^*(j\omega)) \left\langle u^2 \right\rangle_w \tag{4.11}$$

where $\langle u^2 \rangle_w$ is the mean-square input [47, 57]. Only the real part of the mobility contributes to the mean power flow, since only that part of the response that is in phase with the input can generate time-averaged power flow. Assuming that the mean-square input is independent of the structural uncertainty, the average power flow over both the input statistics and the uncertainty in the structure is

$$\langle \Pi_{\text{in}}(\omega) \rangle_\sigma = \tfrac{1}{2} \langle G(j\omega;\sigma) + G^*(j\omega;\sigma) \rangle_\sigma \left\langle u^2 \right\rangle_w \tag{4.12}$$

The equivalence between averaging the mobility over the uncertainty distribution, and the smoothing of the transfer function obtained by adding some damping to the system, can be seen by explicitly computing the average in a manner analogous to the covariance averaging in Chapter 3. Consider a single mode oscillator with natural frequency uncertainty and some white driving noise w, represented by Equations (3.1), (3.2), and (3.10), where the uncertain parameter σ has Cauchy probability density function $p(\sigma)$ given by Equation (3.50), and $A_1 = J$, with J defined by Equation (3.9). Averaging the impulse response $g(t;\sigma) = e^{At}$ over the statistics of the uncertain parameter σ yields

$$\langle g(t;\sigma) \rangle_\sigma = e^{A_0 t} \int_{-\infty}^{\infty} e^{\sigma J t} p(\sigma)\, d\sigma \tag{4.13}$$

$$= e^{A_\sigma t} \tag{4.14}$$

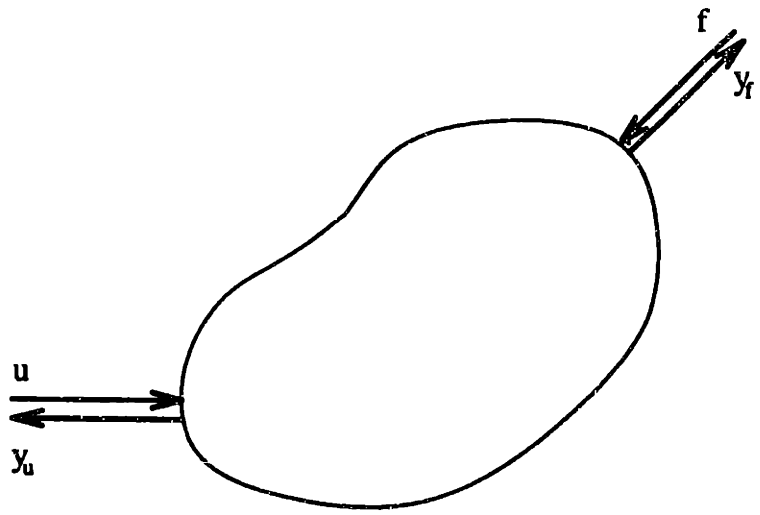

Figure 4.3: Power minimization on an arbitrary structure.

where

$$A_s = A_0 - \delta I \tag{4.15}$$

and I is the 2×2 identity matrix. That is, the average impulse response (and hence the average mobility) can be obtained by considering a state space model with the poles left-shifted. In the limit of large uncertainties, this left-shifted model will approach the dereverberated mobility. This left-shifted model is similar to that used in the maximum entropy technique [13,52].

One might think that one should simply use the best estimate of the transfer function to compute the expected power flow, rather than using the dereverberated mobility. However, the argument for impedance matching is based on maximizing the power dissipated by the control system. This optimization only makes sense for a dereverberated, or semi-infinite model, where there is only one chance to damp any passing disturbance. If the exact mobility were used, the optimal non-causal matched termination $1/G(-s)$ would achieve higher dissipation than the dereverberated optimal by making the structure *less* damped, so that more power is added to the structure by the disturbance, and hence more power is available to be dissipated. This conclusion is illustrated by the following example.

Consider an arbitrary structure with a control force u and a disturbance force f, and collocated velocities y_u and y_f as shown in Figure 4.3. This is similar to the

system of primary and secondary sources considered for acoustic potential energy minimization in [75]. The velocities are related to the forces by equations of the form

$$y_f = G_{ff} f + G_{fu} u \tag{4.16}$$

$$y_u = G_{uf} f + G_{uu} u \tag{4.17}$$

where, by reciprocity, the transfer functions G_{fu} and G_{uf} are transposes. In steady state, the total power input by both f and u is equal to the power dissipated by damping, which is proportional to the total structural energy via the loss factor. Thus the control law which minimizes the total power input also minimizes the energy in the structure. Note, though, that the power from both sources must be considered. That is, the cost functional at each frequency is

$$\Pi = \Pi_u + \Pi_f = \tfrac{1}{2}(u^* y_u + y_u^* u + f^* y_f + y_f^* f) \tag{4.18}$$

Minimizing this total power yields that the optimal control law (without regard to causality issues) is

$$u = -\frac{G_{uf} + G_{uf}^*}{G_{uu} + G_{uu}^*} f \tag{4.19}$$

and the net power flow into the structure with this control force is

$$\Pi_{\text{opt}} = \tfrac{1}{2} f^* \left((G_{ff} + G_{ff}^*) - \frac{(G_{fu} + G_{fu}^*)^2}{(G_{uu} + G_{uu}^*)} \right) f \tag{4.20}$$

This is strictly less than the open loop power flow, given by the first term in this equation. Also note an interesting feature of this solution; the control force dissipates no power, it instead achieves the reduction in total power by manipulating the velocity at the disturbance location. While this may be optimal, it seems unlikely that such an approach would be very robust if it were based upon feedback of the collocated velocity y_u. Similar solutions, however, are used in the noise control literature (e.g. [75].) Rather than using feedback, these solutions are almost always based upon feedforward of the disturbance frequency, and adaptation of the gains.

If, however, rather than minimizing the total power input $\Pi_u + \Pi_f$, one minimizes only the power input at the control force location Π_u, one gets quite a different result.

The optimal control law in this case is

$$u = -\frac{G_{uf}}{G_{uu} + G_{uu}^*} f \tag{4.21}$$

which can be rewritten as the standard impedance matching control law as a feedback on y_u:

$$u = -\frac{1}{G_{uu}^*} y_u \tag{4.22}$$

The net power flow into the structure with this compensator is

$$\Pi_{\text{im}} = \tfrac{1}{2} f^* \left((G_{ff} + G_{ff}^*) - \frac{(G_{fu} + G_{fu}^*)^2 - G_{fu}^* G_{fu}}{(G_{uu} + G_{uu}^*)} \right) f \tag{4.23}$$

The sign of the second term here depends on the whether the magnitude of the phase of G_{fu} is greater or less than 60°. For a lightly damped plant, the total closed loop power flow is greater than the open loop power flow. Although the compensator dissipates power, the effect of the control force at the disturbance location is to increase the disturbance input power, which more than counterbalances the dissipation.

Both of the previous results assumed full knowledge of the structural transfer functions. If there is sufficient uncertainty in the structure, then the phase of the cross transfer function G_{uf} will be unknown. As a result, the control force will be, on average, uncorrelated with the motion y_f at the disturbance location, and the power input by the disturbance, Π_f, can be assumed to be constant. This immediately yields the impedance matching solution, Equation (4.22), as the optimal control law for minimizing the total power. However, to then use the exact reverberant value for G_{uu} would be inconsistent. Since the phase of the cross transfer function G_{uf} has been assumed uncertain, the phase of the reverberant field contribution to G_{uu} must also be assumed uncertain, and uncorrelated with the input u. The reverberant field thus produces no average power at the control input for the same reason that it does not contribute to the average power at the disturbance location. Solving for the optimal control that minimizes the power input by the control force Π_u is therefore appropriate provided one also uses the dereverberated mobility to compute the feedback law.

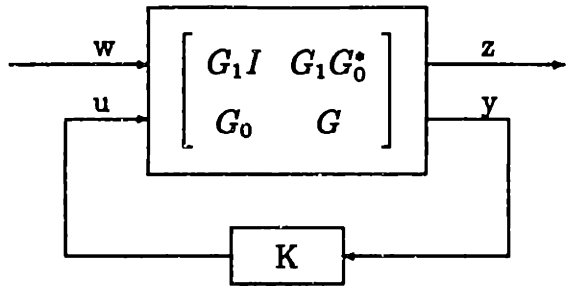

Figure 4.4: Power flow model

4.2.2 State Space Representation

Given the dereverberated driving point mobility, then the power properties of the driving point can be represented in state space for control design as in Section 2.1.2. (See Equations (2.4)–(2.8).)

The resulting control problem can now be formulated as a standard two-input two-output problem, as shown in Figure 4.4. The inputs are the control u and the normalized disturbance input w. The outputs are the sensor signal y and a cost variable z, defined so that z^*z is the power reflected back into the structure as a function of frequency. State space representations for the four elements in the system in Figure 4.4 can be obtained from the state space representation of G. These formulae are given in [61] for the case where $G(\infty) \neq 0$. Solutions for G_0 and $G_1 G_0^*$ when $G(\infty) = 0$ can be found as limits.

The transfer function from w to z is given by the lower linear fractional transformation,

$$H(s) \triangleq \frac{z(s)}{w(s)} = G_1 I + G_1 G_0^* K (I - G_a K)^{-1} G_0 \tag{4.24}$$

Note that $z^*z = w^*H^*Hw = \mathrm{tr}\{H^*HW\}$, where $W = ww^*$ is the incoming power, so H^*H is the relative power reflected back into the structure from the control system, and $(I - H^*H)$ is the relative power dissipated by the controller. That is, it is the power dissipated if the incoming waves at that point have unit power. The transfer function H is precisely the desired generalization of the reflection coefficient R in Section 4.1 to arbitrary structures.

4.3 Arbitrary Structures

The tools are now in place to develop a cost functional for an arbitrary structure that uses only local information to minimize the best estimate of the true $\mathcal{H}_2$ performance metric of the structure. The local knowledge is represented by the transfer function H obtained in the previous section, which generalizes the reflection coefficient R in Section 4.1. An expression similar to Equation (4.8) is desired that expresses the cost, averaged over uncertainty, in terms of H. There are three main steps to this derivation, and these rely on the properties of uncertain systems derived in Chapter 3. First, equipartition and incoherence are used to represent the average $\mathcal{H}_2$ performance in terms of the average modal energy. This energy can then be related to the power dissipated by the controller, using the local power flow information represented by H. Finally, conservation of energy relates this dissipated power to the power input by the disturbance.

The two basic assumptions underlying much of SEA theory are equipartition and incoherence. As noted earlier, incoherence implies that the amplitudes of different modes are uncorrelated. For a given structure, this will not occur unless the disturbances are spatially distributed. However, incoherence also results from averaging the covariance over an uncertainty distribution, as shown in Chapter 3. In SEA literature, the equipartition assumption typically requires that all modes within a given subsystem and within the same frequency band have the same energy. For the purposes of manipulating the average $\mathcal{H}_2$ cost, it is sufficient that equipartition be satisfied for each individual mode. The kinetic and potential energy of each mode must be equal, but the energy of one mode need not be equal to that of any other. This is precisely the result that was shown in Chapter 3 for structures with uncertain natural frequencies. From a wave perspective, there is a single assumption corresponding to equipartition and incoherence, which is that of a "diffuse" field. This means that at any point within the system, the waves coming from all directions are uncorrelated, and have equal intensities.

Any global $\mathcal{H}_2$ cost can be written as $\sqrt{\langle z^T z \rangle}$; the rms amplitude of a vector z.

Expanding this performance variable in terms of modes, with modal amplitudes $v_n(t)$, gives

$$z(t) = \sum_{n=0}^{\infty} c_n v_n(t) + \sum_{n=0}^{\infty} c'_n \dot{v}_n(t) \tag{4.25}$$

for appropriately defined modal coefficients c_n and c'_n. If equipartition holds, then the modes can be normalized such that the energy of mode n is $E_n = \left\langle v_n^T v_n \right\rangle = \frac{1}{\omega_n^2} \left\langle \dot{v}_n^T \dot{v}_n \right\rangle$. Since the modal incoherence assumption holds for the average covariance of the system over uncertainty, the average mean-square value of z is

$$\left\langle z^T z \right\rangle = \sum_{n=0}^{\infty} E_n (c_n^T c_n + \omega_n^2 {c'_n}^T c'_n) \tag{4.26}$$

Thus the average value over uncertainty of any quadratic cost can be related to the average modal energies. A similar relationship is observed in SEA literature, see for example [47].

For a modally dense structure the sum in Equation (4.26) can be approximated by an integral of the form

$$J = \left\langle z^T z \right\rangle = \int_{-\infty}^{\infty} C(\omega) E(\omega) \, \mathrm{d}\omega \tag{4.27}$$

The function $E(\omega)$ is the average energy in the structure as a function of frequency. The performance weighting function $C(\omega)$ in Equation (4.27) is obtained by averaging $c_n^T c_n + \omega_n^2 {c'_n}^T c'_n$ over the modes in each frequency region, and multiplying by the modal density. The approximation in Equation (4.27) is certainly valid above the Schroeder cutoff frequency, (see, for example, [75, 78]), where the modal spacing is comparable to or less than the half power bandwidth of each mode. The effect of an uncertain modal frequency is to smear the mode out over a broader frequency region. For an uncertain structure, the approximation in Equation (4.27) should be reasonable above the Schroeder cutoff frequency of the average system, which will be at a much lower frequency. Indeed, for the limiting case that yields the dereverberated mobility as the average transfer function, the result will hold at all frequencies.

The next step in the derivation is to relate the power dissipated by the controller, $\Pi_{diss}(\omega)$, to the structural energy $E(\omega)$. The dissipated power can be thought of equivalently in SEA terms as the coupling power flow between the structure and

the control system. This power can be determined using the results of Section 4.2. Recall that for a diffuse field, which is equivalent to making the equipartition and incoherence assumptions, all waves have equal intensity. This intensity is proportional to the average energy [47], and thus in the scalar case, the power flowing towards the actuator is proportional to the total energy in the structure.

Usually, only SISO low authority controllers will be used, since the sensors and actuators must all be collocated and dual. For there to be a MIMO LAC, there must be independent sensors and actuators which sense and act upon distinct structural motion at the same location. This would be the case, for instance, if one had both force and moment actuators, and both transverse and angular velocity sensors all mounted at the same location on a beam. In such a MIMO case, the concept of the modal energy can be generalized to a matrix representing the energy associated with the structural motion that can be sensed by each independent sensor. The dissipated power can also be considered to be a matrix of the dissipation associated with each direction of the vibration. The total energy and total dissipated power will then be the trace of the respective matrices.

Using the proportionality between incoming power flow and structural energy, the coupling power flow between the structure and the control system can be written as

$$\Pi_{\text{diss}}(\omega) = (I - H(j\omega)^* H(j\omega))E(\omega) \tag{4.28}$$

Equations (4.27) and (4.28) relate the average global cost to the average modal energy, and the dissipated power to the local structural properties and the modal energy. In order to obtain a cost functional, the unknown Π_{diss} in these equations must be determined. This is done by taking advantage of conservation of energy. This is one of the most fundamental properties of uncertain systems, yet many robust control approaches fail to take advantage of it. Applying conservation of energy to this system yields a power flow balance,

$$\mu E + \Pi_{\text{diss}} = \Pi_{\text{in}} \tag{4.29}$$

This equation is fundamental to Statistical Energy Analysis. The first term on the left hand side indicates power dissipation within the structure, which is proportional to

the average structural energy E. For a conservative system, the damping parameter μ is zero. The damping parameter μ is often poorly known, but is sufficiently small for many applications that it can be assumed negligible.

The power input from external disturbance sources $\Pi_{\text{in}}(\omega)$ in Equation (4.29) can be estimated or measured reasonably well for most systems. If the disturbances are specified by the power spectral density $V(\omega)$ of a force input, then the power input can be determined by again using the dereverberated mobility. Note that if the disturbance is narrowband (relative to the modal spacing) then the equipartition assumption fails. Otherwise, the disturbance will be uncorrelated with the reverberant field, and thus the reverberant field does not contribute to the mean input power [47]. The direct field is characterized by the dereverberated mobility at the disturbance source, denoted G_d, so that

$$\Pi_{\text{in}} = \text{tr}\left\{(G_d + G_d^*)V\right\} \tag{4.30}$$

The total power input is then just the sum of the input power from each disturbance source.

Equation (4.29) relates the remaining unknown Π_{diss} to a known quantity, Π_{in}. The resulting description of the average cost explicitly incorporates the knowledge that the structure approximately satisfies conservation of energy. Define $\gamma = \sqrt{1+\mu}$, then Equations (4.28) and (4.29) yield that the structural energy is given by

$$E(\omega) = \text{tr}\left\{\left(\gamma^2 I - H^* H\right)^{-1}\right\}\Pi_{\text{in}}(\omega) \tag{4.31}$$

provided that the required inverse exists, hence provided that H satisfies $\|H\|_\infty < \gamma$. If this is not the case, then the energy in the structure increases indefinitely, since the power added by the control exceeds that dissipated by the damping, and the cost is infinite. The reflection coefficient H in Equation (4.31) and throughout is a function of frequency, and is not indicated as such for clarity. The damping parameter γ is also, in general, a function of frequency.

From Equations (4.27) and (4.31), the cost at each frequency is

$$J(\omega) = C(\omega)\text{tr}\left\{\left(\gamma^2 I - H^* H\right)^{-1}\right\}\Pi_{\text{in}}(\omega) \tag{4.32}$$

and hence the total cost over all frequencies is

$$J = \int_{-\infty}^{\infty} \frac{1}{\gamma^2} C(\omega) \mathrm{tr}\left\{(I - \gamma^{-2} H^* H)^{-1}\right\} \Pi_{\mathrm{in}}(\omega)\, \mathrm{d}\omega \tag{4.33}$$

The maximum possible power is dissipated by a non-causal compensator, which yields $H = 0$ and

$$J_{min} = \int_{-\infty}^{\infty} \frac{1}{\gamma^2} C(\omega) \Pi_{\mathrm{in}}(\omega)\, \mathrm{d}\omega \tag{4.34}$$

Subtracting this quantity from the cost does not change the minimization problem, but yields a better conditioned optimization problem, and elucidates certain features of the cost. The parameter γ is related to the open loop damping, and is approximately unity for lightly damped systems. If this is not a function of frequency, or can be reasonably approximated as such, then the factor of $1/\gamma^2$ can also be dropped. Therefore, define the cost to be

$$J = \int_{-\infty}^{\infty} C(\omega) \mathrm{tr}\left\{(I - \gamma^{-2} H^* H)^{-1} H^* H\right\} \Pi_{\mathrm{in}}(\omega)\, \mathrm{d}\omega \tag{4.35}$$

The compensator that minimizes this cost also minimizes the average with respect to uncertainty of the global $\mathcal{H}_2$ performance metric. The knowledge that the structure approximately conserves energy is preserved.

For the SISO case, Equation (4.35) can be written more clearly as

$$J = \int_{-\infty}^{\infty} \frac{H^* H}{I - \gamma^{-2} H^* H} W^* W\, \mathrm{d}\omega \tag{4.36}$$

where the weighting function $W(j\omega)$ satisfies $W(j\omega)^* W(j\omega) = C(\omega)\Pi(\omega)$.

This cost can be compared with the $\mathcal{H}_2$ cost of Miller *et al.* [69], where

$$J_{\mathcal{H}_2} = \int_{-\infty}^{\infty} \mathrm{tr}\left\{\Phi_{dd}(\omega) H^* H\right\}\, \mathrm{d}\omega \tag{4.37}$$

and with the $\mathcal{H}_\infty$ approach of MacMartin and Hall [61], where

$$J_{\mathcal{H}_\infty} = \|H\|_\infty \tag{4.38}$$

The integrand of the cost in Equation (4.35) can be represented in block diagram form as shown in Figure 4.5. The $\mathcal{H}_2$ minimization of power flow in [69] is equivalent to the block diagram without the feedback loop. The main difficulty with the $\mathcal{H}_2$

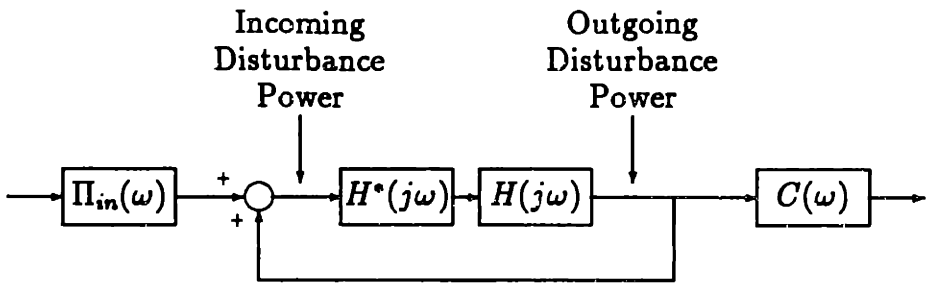

Figure 4.5: Block diagram representation of cost.

approach was that it gave no guarantee of stability, since the dereverberated model is not conservative. The presence of the feedback loop in the block diagram representation, or the inverse term in the cost functional, accounts for the fact that the structure is conservative; that is, that any energy imparted to the structure at some frequency will return to the actuator location eventually. Thus intuitively one can think of the disturbance power spectrum that reaches the actuator as being the sum of the external disturbance power and the outgoing disturbance power, as indicated in Figure 4.5.

An alternate approach for obtaining the integrand $(I-H^*H)^{-1}H^*H$ is to consider that if there is an incoming disturbance with unit energy, then the first reflected disturbance has energy H^*H, the second reflection has energy $(H^*H)^2$, and so forth. The total reflected energy in the structure is therefore

$$\sum_{i=1}^{\infty}(H^*H)^i = (I - H^*H)^{-1}H^*H \tag{4.39}$$

Once again, the minimum cost incurred before the disturbance reaches the actuator/sensor location has not been included in the cost functional. The ideal compensator that yields $H = 0$ therefore gives zero cost.

An analysis more directly comparable to that in Section 4.1 could be carried out as well. The cost in Equation (4.36) or (4.39) is similar to that obtained for the simple rod in Equation (4.8).

Both $\Pi_{in}(\omega)$ and $C(\omega)$ are purely real functions of frequency, and can thus be factored as $\Pi_{in}(\omega) = \Pi_+^*\Pi_+$ and $C(\omega) = C_+^*C_+$, where Π_+ and C_+ are both stable.

Defining $H_0 = C_+ H \Pi_+$, and $H_1 = H$ then

$$J = \int_{-\infty}^{\infty} \mathrm{tr}\left\{(I - \gamma^{-2} H_1^* H_1)^{-1} H_0^* H_0\right\} d\omega \tag{4.40}$$

This cost is only defined for $\|H_1\|_\infty < \gamma$. As $\|H_1\|_\infty \to \gamma$, the term $(I - \gamma^{-2} H_1^* H_1)^{-1}$ increases, penalizing the proximity to the constraint. Minimizing this cost functional will guarantee that $\|H_1\|_\infty < \gamma$, so that between the controller and the internal dissipation, power is dissipated at all frequencies, and thus the closed loop system is stable. If $\|H_1\|_\infty \ll \gamma$, then this cost approaches the $\mathcal{H}_2$ cost of H_0. Further properties on this cost functional can be found in [63], and in the following chapter.

4.4 Possible Extensions

There are several extensions to the cost functional just derived that are worth noting briefly.

4.4.1 Reverberant Information

First, Section 4.1 illustrated a possible means of including more information about the structure into the problem through the use of a probability distribution on the phase of the returning reverberant field. A similar analysis could be performed for more complicated structures. A transfer function G_R that contains information about the reverberant field can be defined. This is the transfer function from the outgoing disturbance z in Figure 4.4, through the structure, to the resulting incoming disturbance w. If the dereverberated transfer function G_D has been estimated from an experimental transfer function G, then the transfer function G_R can be estimated from

$$G_R = \frac{G - G_D}{G + G_D^*} \tag{4.41}$$

This transfer function has unit magnitude if the system is undamped (corresponding to conservation of energy), but varying phase. (Note that $|G_R| = 1$ iff $(G + G^*)(G_D + G_D^*) = 0$.) Following a similar analysis to that in Section 4.1, then G_R corresponds to the nominal value $e^{j\theta_0}$ for $e^{j\theta}$ in Equation (4.5). The approach

developed in the previous sections assumed that the phase of G_R was completely unknown. Some knowledge of the phase, and therefore of the modal frequencies can be retained by replacing the cost in Equation (4.35) with a cost similar in form to that of Equation (4.10). Increasing uncertainty in the phase can be accommodated by allowing α in Equations (4.9) and (4.10) to be an increasing function of frequency. Also note that state space evaluation of the resulting cost can be simplified by using the identity

$$\frac{1 - H_\alpha^* H_\alpha}{(1 - H_\alpha)(1 - H_\alpha^*)} = \frac{1}{1 - H_\alpha} + \frac{1}{1 - H_\alpha^*} - 1 \tag{4.42}$$

where $H_\alpha \triangleq \alpha G_R H$.

4.4.2 $\mathcal{H}_\infty$ Performance

Section 4.3 assumed that the true performance metric of interest on the structure was an $\mathcal{H}_2$ cost. While this is often the case, there are situations in which the real cost that should be minimized is an $\mathcal{H}_\infty$, or worst case cost. Due to the fact that the positivity constraint on the compensator for stability has been transformed into an $\mathcal{H}_\infty$ constraint as well, this case is actually easier to solve than the mixed $\mathcal{H}_2/\mathcal{H}_\infty$ problem. Solving for a compensator with two $\mathcal{H}_\infty$ constraints can be represented as a μ-synthesis problem [27,60]. With only two blocks, this problem can be solved using an iterative scheme. No examples are presented in Chapter 6, however, due to the lack of adequate software to solve realistic problems.

4.5 Summary

To conclude, therefore, the average value, over modal frequency uncertainty, of a global $\mathcal{H}_2$ performance metric can be expressed in terms of only local structural information. This result uses the equipartition and incoherence properties that were shown to hold in Chapter 3 for uncertain structures. The knowledge that the structure satisfies conservation of energy is explicitly preserved. The compensator that minimizes this cost must also be guaranteed to be stable, since the average global

cost is finite. Indeed, the compensator will be positive real, since it must satisfy the same $\mathcal{H}_\infty$ constraint that was used in [61] to guarantee positivity.

The local structural information is obtained from the dereverberated mobility model of the structure. This is the mobility obtained by considering only the direct field, and ignoring the contribution of the uncertain reverberant field. The ideal compensator that dissipates the most power possible is a non-causal impedance match. The compensator that minimizes the cost functional derived in this chapter is the best causal approximation to the impedance match. Note also that the impedance matching result is only valid for the dereverberated, and not the exact mobility. If the exact transfer function is used instead, the "ideal" compensator dissipates more power by destabilizing the structure, so that there is more power available to be dissipated.

Chapter 5

Optimization of Performance

Twixt the optimist and the pessimist, the difference is droll:
The optimist sees the doughnut, but the pessimist sees the hole.

–McLandburgh Wilson

The previous chapter demonstrates that the average $\mathcal{H}_2$ cost of an uncertain structure can be expressed in terms of local information. The average cost is expressed as a cost functional of the closed loop power reflection coefficient H, which can be obtained from a linear fractional transformation of the compensator. This chapter examines the properties, evaluation algorithm, and an optimization approach for this cost functional. For a state space representation of H, the cost can be evaluated from the solution to a Lyapunov and Riccati equation. The goal is to obtain the compensator that minimizes the cost. No closed-form expression for this compensator has been obtained, and a numerical algorithm for obtaining the optimization is given.

The cost functional derived in Chapter 4 is a combined $\mathcal{H}_2/\mathcal{H}_\infty$ cost. That is, it contains features of both $\mathcal{H}_2$ and $\mathcal{H}_\infty$ costs. It will be shown that the cost overbounds an $\mathcal{H}_2$ cost, and is only defined for systems that satisfy an $\mathcal{H}_\infty$ constraint. Combined $\mathcal{H}_2$ and $\mathcal{H}_\infty$ control problems are of interest in general, since they combine the problems of nominal performance and robust stability. Related work includes $\mathcal{H}_2$ optimization with an $\mathcal{H}_\infty$ constraint [12, 41, 73, 82, 83], minimum entropy $\mathcal{H}_\infty$ control [73, 74], and mixed $\mathcal{H}_2$ and $\mathcal{H}_\infty$ control [26, 101, 102]. The framework for mixed $\mathcal{H}_2/\mathcal{H}_\infty$ control problems considered in [101] will be of particular interest. There, the

cost functional is motivated in an input/output, induced norm sense. The system is subject to two inputs, one of bounded spectrum, and the other with bounded power. For the case where the first input signal is white and the second is causal, necessary and sufficient conditions are given for the existence of a controller which minimizes the cost. This case has also been shown [99,90] to be dual (for a full order controller) to the problem solved in [12]. The non-white and non-causal case in [101] is described but not solved (see Section 3.3 of the paper.) This case is, however, of particular interest as the cost is then precisely equal to the cost considered herein, revealing a close relationship between the present approach and the approach taken in [101]. In particular, for any system H, the cost defined below in Definition 5.1 can be bounded by $\sqrt{2}$ times the white and causal case.

The particular combined $\mathcal{H}_2/\mathcal{H}_\infty$ cost functional considered here, from Equation (4.40), can be defined more formally as follows.

Definition 5.1 *Consider a system* $H(s) = [H_0(s)\ H_1(s)]$ *and a positive number* $\gamma \in \mathbf{R}$, *with* $H_0 \in \mathcal{RH}_2$, $H_1 \in \mathcal{RH}_\infty$, *and* $\|H_1\|_\infty < \gamma$. *Then the cost* $L(H,\gamma)$ *is defined by*

$$L(H,\gamma) \triangleq \frac{1}{2\pi}\int_{-\infty}^{\infty} \mathrm{tr}\left\{(I-\gamma^{-2}H_1H_1^*)^{-1}H_0H_0^*\right\}\mathrm{d}\omega \tag{5.1}$$

If the power flow into the structure from external disturbance sources is given by $\Phi^*(j\omega)\Phi(j\omega)$, then a power balance yields that the total energy that can theoretically be dissipated in an undamped structure is given by $L([H\ H\Phi],1)$.

As noted in Section 4.1, in the SISO case with $H_0 = H_1$, $L(H,\gamma)$ can also be interpreted as the average $\mathcal{H}_2$ cost over a set of uncertainty of constant magnitude but unknown phase. This is analogous to the interpretation of the entropy cost of [74] as the average $\mathcal{H}_2$ cost over a set of uncertainty with bounded magnitude and unknown phase [18]. Finally, it is well known that the standard $\mathcal{H}_\infty$ problem is equivalent to posing a particular zero-sum differential game [81]. The final section of this chapter demonstrates that the cost $L(H,\gamma)$ is equivalent to a particular Stackelberg non-zero sum differential game.

It is unlikely that the current $\mathcal{H}_2/\mathcal{H}_\infty$ cost will be preferable to other $\mathcal{H}_2/\mathcal{H}_\infty$

approaches for the general problem of minimizing an $\mathcal{H}_2$ cost with an $\mathcal{H}_\infty$ constraint, since the overbound on the $\mathcal{H}_2$ cost obtained by $L(H,\gamma)$ is greater than that obtained by other approaches. The cost is, however, physically motivated, and represents the average value of an $\mathcal{H}_2$ cost over uncertainty. The relationship between this approach and others may eventually lead to closed-form solutions for the optimal compensators for this problem.

5.1 Properties

The following basic properties of $L(H,\gamma)$ can easily be shown to hold.

Proposition 5.2 *Let $H(s)$ and γ satisfy the conditions in Definition 5.1. Then*

(i) *$L(H,\gamma)$ is well defined.*

(ii) *$L(H,\gamma) \geq 0$, and $L(H,\gamma) = 0$ iff $H_0 = 0$*

(iii) *$L(UHV,\gamma) = L(H,\gamma)$ for any $U, V \in \mathcal{RL}_\infty$ with $U^*U = I$, $VV^* = I$.*

In the case where $H_1 = H_0$, further properties of the cost $L(H,\gamma)$ can be established by relating it to the entropy $I(H,\gamma)$ of a system defined, for example, in Reference [74].

Definition 5.3 *For $H \in \mathcal{RH}_2$, $\gamma \in \mathbf{R}$, and $\|H\|_\infty < \gamma$, the* entropy *at infinity is defined by*

$$I(H,\gamma) \triangleq -\frac{\gamma^2}{2\pi} \int_{-\infty}^{\infty} \ln \left| \det \left(I - \gamma^{-2} H^* H \right) \right| \mathrm{d}\omega \tag{5.2}$$

Also let $C(H)$ be the usual $\mathcal{H}_2$ cost associated with the system H:

$$C(H) \triangleq \frac{1}{2\pi} \int_{-\infty}^{\infty} \mathrm{tr} \{ H^* H \} \, \mathrm{d}\omega \tag{5.3}$$

Proposition 5.4 *For $H = [H_0 \; H_0]$, with H_0 and γ satisfying the conditions in Definition 5.3, consider the cost $L(H,\gamma)$, the entropy $I(H_0,\gamma)$, and the $\mathcal{H}_2$ cost $C(H_0)$. Define $\xi = \gamma^{-2}$, then*

(i) $L(H,\gamma) = \frac{\partial}{\partial \xi}(\xi I(H_0,\gamma))$

(ii) $L(H,\gamma) \geq I(H_0,\gamma) \geq C(H_0)$.

Proof: The first assertion follows directly from the proof of Proposition 2.3.2 in Reference [74]. The first inequality in (ii) follows from $L(H,\gamma) = I(H_0,\gamma) + \frac{\partial}{\partial \xi}(I(H_0,\gamma))$ and the result from Proposition 2.3.2 in [74] that $\frac{\partial}{\partial \xi}(I(H_0,\gamma)) \geq 0$. The final inequality is obtained from the result that $I(H_0,\gamma)$ itself bounds the $\mathcal{H}_2$ cost. □

That $L(H,\gamma)$ overbounds an $\mathcal{H}_2$ cost can also be shown to hold for the case $H_1 \neq H_0$.

Proposition 5.5 $L(H,\gamma) \geq C(H_0)$.

Proof: Since $\|H_1\|_\infty < \gamma$, $(I - \gamma^{-2} H_1 H_1^*) < 1 \ \forall \omega$ and $(I - \gamma^{-2} H_1 H_1^*)^{-1} > 1 \ \forall \omega$. The result then follows directly from the definition of $L(H,\gamma)$ in Equation (5.1). □

Finally, note that relaxing the $\mathcal{H}_\infty$-norm bound completely recovers the $\mathcal{H}_2$ cost.

Proposition 5.6 $\lim_{\gamma \to \infty} L(H,\gamma) = C(H_0)$.

Proof: This follows directly from the definition of $L(H,\gamma)$ in Equation (5.1) and the Dominated Convergence Theorem [84]. □

The relationship between $L(H,\gamma)$, the entropy, and the $\mathcal{H}_2$ cost can be clarified by comparing the respective integrands for a scalar argument. These functions are plotted in Figure 5.1. The current cost overbounds the entropy, which in turn overbounds the $\mathcal{H}_2$ cost.

5.2 Evaluation

A state space representation for the compensator that minimizes the cost $L(H,\gamma)$ is desired. In order to obtain this compensator, a state space algorithm for evaluating the cost is needed.

Consider a state space representation for a proper system $H = [H_0 \ H_1]$:

$$H = \left[\begin{array}{c|cc} A & B_0 & B_1 \\ \hline C & 0 & D \end{array}\right] = C(sI - A)^{-1} [B_0 \ B_1] + [0 \ D] \qquad (5.4)$$

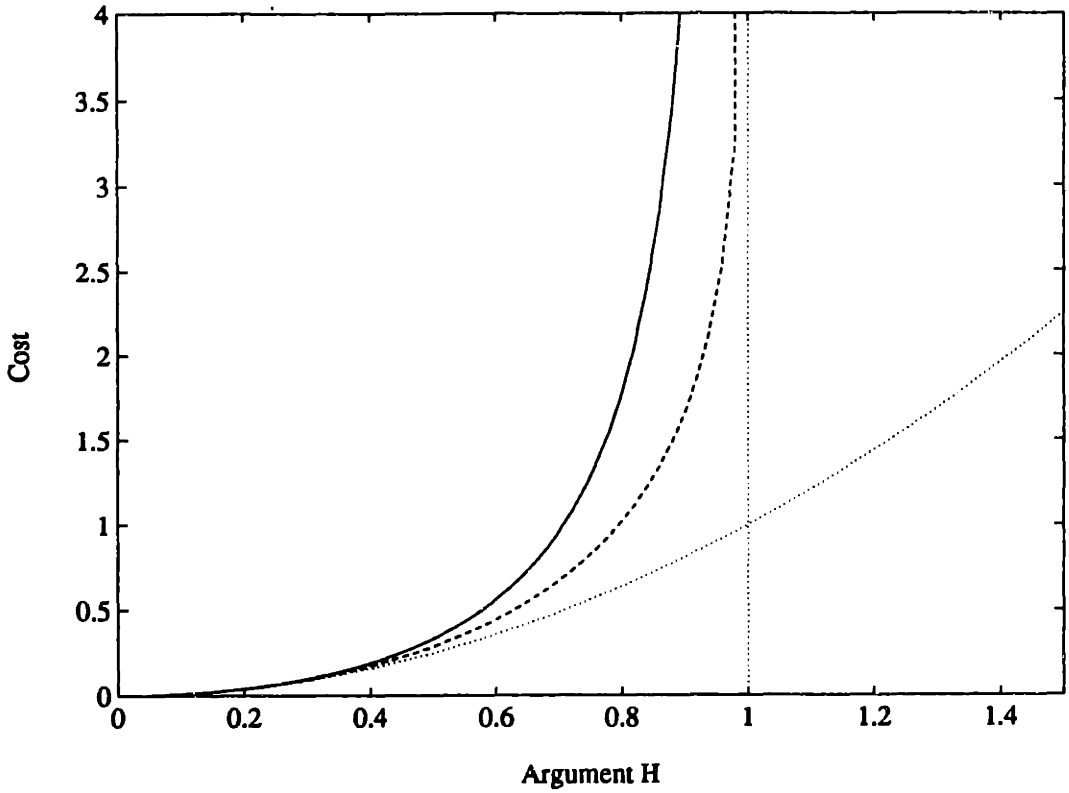

Figure 5.1: Comparison of $L(H,\gamma)$ (solid), entropy (dashed), and $\mathcal{H}_2$ cost (dotted) integrands for a scalar argument H. The constraint that the argument be bounded by one is also shown.

and define

$$Z = (I - \gamma^{-2} DD^T)^{-1} \tag{5.5a}$$

$$W = (I - \gamma^{-2} D^T D)^{-1} \tag{5.5b}$$

$$\bar{A} = A + \gamma^{-2} B_1 D^T Z C \tag{5.5c}$$

The aim is to evaluate $L(H,\gamma)$ in terms of the state space data. Note that if a non-zero term D_0 were included in Equation (5.4), then $H_0 \notin \mathcal{H}_2$ and hence $L(H,\gamma)$ would not exist.

Theorem 5.7 *Let* $H = [H_0 \; H_1]$ *be given by Equation (5.4),* Z, W *and* $\bar{A}$ *given by Equation (5.5),* $\gamma \in \mathbf{R}$, *and* $\|H_1\|_\infty < \gamma$. *Then*

$$L(H,\gamma) = \mathrm{tr}\left\{C^T Z C Q\right\} \tag{5.6}$$

where Y, Q satisfy $(\bar{A} + YC^TZC)$ stable and

$$\bar{A}Y + Y\bar{A}^T + YC^TZCY + \gamma^{-2}B_1WB_1^T = 0 \tag{5.7}$$

$$(\bar{A} + YC^TZC)Q + Q(\bar{A} + YC^TZC)^T + B_0B_0^T = 0 \tag{5.8}$$

Proof: Both Z and W exist since $\|H_1\|_\infty < \gamma$. Also since $H_1H_1^* < \gamma^2 I \ \ \forall\, \omega$, then $\exists M \in \mathcal{RH}_\infty$ given by

$$M^*M = H_0^*(I - \gamma^{-2}H_1H_1^*)^{-1}H_0 \tag{5.9}$$

A state space representation for M^*M is

$$M^*M = \left[\begin{array}{cccc|c} A & 0 & 0 & 0 & B_0 \\ -C^TZC & -A^T & -C^TZC & \gamma^{-2}C^TZDB_1^T & 0 \\ \gamma^{-2}B_1D^TZC & 0 & A+\gamma^{-2}B_1D^TZC & -\gamma^{-2}B_1WB_1^T & 0 \\ C^TZC & 0 & C^TZC & -(A+\gamma^{-2}B_1D^TZC)^T & 0 \\ \hline 0 & B_0^T & 0 & 0 & 0 \end{array}\right] \tag{5.10}$$

Define the transformation matrix

$$T = \begin{bmatrix} I & 0 & I & 0 \\ 0 & I & 0 & 0 \\ 0 & 0 & I & 0 \\ 0 & I & 0 & I \end{bmatrix} \tag{5.11}$$

and transform the system in Equation (5.10) via $(A, B, C) \rightarrow (TAT^{-1}, TB, CT^{-1})$. This yields that a minimal state space representation for M^*M is given by

$$M^*M = \left[\begin{array}{cc|c} \bar{A} & \gamma^{-2}B_1WB_1^T & B_0 \\ -C^TZC & -\bar{A}^T & 0 \\ \hline 0 & B_0^T & 0 \end{array}\right] \tag{5.12}$$

Using spectral factorization results from [31], the stable factor of M^*M is

$$M = \left[\begin{array}{c|c} \bar{A} + YC^TZC & B_0 \\ \hline Z^{1/2}C & 0 \end{array}\right] \tag{5.13}$$

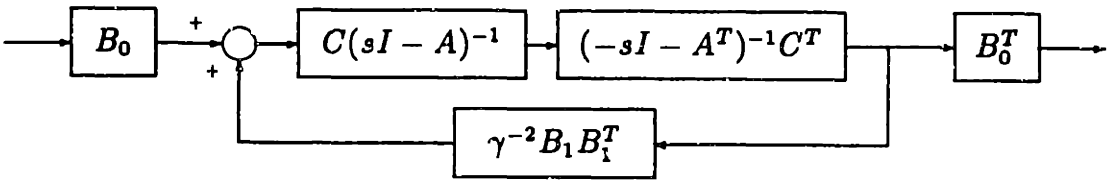

Figure 5.2: Block Diagram for M^*M

where Y is the stabilizing solution to the Riccati equation (5.7). Substituting Equation (5.9) into (5.1), it is clear from (5.3) that the cost $L(H,\gamma)$ is then given by $\|M\|_2$, where $\|M\|_2 = \mathrm{tr}\left\{C^TZCQ\right\}$ and Q satisfies the Lyapunov equation (5.8) [28]. □

In the case $D = 0$, these equations simplify considerably. The result can then be stated as follows.

Corollary 5.8 *Let* $H = [H_0\ H_1]$ *be given by Equation (5.4), with* $D = 0$, $\gamma \in \mathbf{R}$, *and* $\|H_1\|_\infty < \gamma$. *Then*

$$L(H,\gamma) = \mathrm{tr}\left\{CQC^T\right\} \tag{5.14}$$

where Y, Q *satisfy* $(A + YC^TC)$ *stable and*

$$AY + YA^T + YC^TCY + \gamma^{-2}B_1B_1^T = 0 \tag{5.15}$$

$$(A + YC^TC)Q + Q(A + YC^TC)^T + B_0B_0^T = 0 \tag{5.16}$$

In this case, a state space representation for M^*M can be found by noting that M^*M is the transfer function of the feedback system shown in Figure 5.2. So

$$M^*M = \left[\begin{array}{cc|c} A & \gamma^{-2}B_1B_1^T & B_0 \\ -C^TC & -A^T & 0 \\ \hline 0 & B_0^T & 0 \end{array}\right] \tag{5.17}$$

follows immediately.

In the case $H_0 = H_1$, the formulae in Corollary 5.8 can also be obtained from Proposition 5.4, wherein $L(H,\gamma)$ is related to the entropy. The differentiation indicated in the proposition yields these equations directly when applied to the equation for evaluating the entropy in [74, Lemma 5.3.2].

As in the $\mathcal{H}_2$ case, the equations in Theorem 5.7 and its corollary can be replaced by equivalent, or dual equations. Since there are now two equations required to evaluate the cost, one might expect a total of four possible sets of equations. Several of these are listed below.

Proposition 5.9 *Let the conditions of Theorem 5.7 hold. Then the cost may be evaluated from the following:*

(i)
$$L(H,\gamma) = \mathrm{tr}\left\{B_0^T P B_0\right\} \tag{5.18}$$

where Y satisfies Equation (5.7), and P satisfies

$$P(\bar{A} + YC^TZC) + (\bar{A} + YC^TZC)^T P + C^TZC = 0 \tag{5.19}$$

(ii)
$$L(H,\gamma) = \mathrm{tr}\left\{B_0^T (P + PQP) B_0\right\} \tag{5.20}$$

where P, Q satisfy $(A + \gamma^{-2} B_1 B_1^T P)$ stable and

$$P\bar{A} + \bar{A}^T P + \gamma^{-2} P B_1 W B_1^T P + C^TZC = 0 \tag{5.21}$$

$$(\bar{A} + \gamma^{-2} B_1 W B_1^T P)Q + Q(\bar{A} + \gamma^{-2} B_1 W B_1^T P)^T + B_1 W B_1^T = 0 \tag{5.22}$$

Proof:

(i) Equations (5.18) and (5.19) are the dual equations to (5.6) and (5.8) for evaluating the $\mathcal{H}_2$ norm of M.

(ii) With P and Q given by Equations (5.21) and (5.22), the transformation

$$T = \begin{bmatrix} I & Q \\ P & I + PQ \end{bmatrix}$$

diagonalizes the Hamiltonian matrix that is the system matrix of M^*M in Equation (5.12). The cost can then be evaluated by contour integration from the sum of the residues of the antistable part, which yields Equation (5.20).

□

Finally note that if $H_0 = H_1$ (that is, $B_0 = B_1$, and $D = 0$), then several additional, equivalent formulae for $L(H,\gamma)$ can be obtained by evaluating the cost associated with H^T; that is, the dual equations to those in Corollary 5.8 and Proposition 5.9.

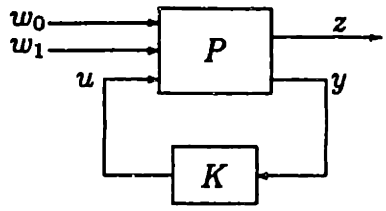

Figure 5.3: Feedback System

5.3 Optimization

The goal of this section is to present an approach for solving for the optimum controller that minimizes a cost functional of the form given in Definition 5.1. Linear time-invariant controllers will be assumed throughout, but this form is not proven to yield minimal cost. First, the necessary conditions that an optimal compensator must satisfy are presented. Conditions for the existence of such a controller are not discussed here. The necessary conditions are obtained by evaluating the cost of the closed loop system, and differentiating with respect to the compensator parameters. A closed-form solution for the optimum has not been found, and therefore a numerical optimization approach is also discussed.

5.3.1 Necessary Conditions

The system can be described by the block diagram in Figure 5.3, where the inputs are the disturbances corresponding to H_0 and H_1, and the control u, and the outputs are the performance, and the sensed output y. P can be realized in state space as

$$P = \left[\begin{array}{c|ccc} A & B_0 & B_1 & B_2 \\ \hline C_1 & D_{10} & D_{11} & D_{12} \\ C_2 & D_{20} & D_{21} & D_{22} \end{array}\right] \tag{5.23}$$

and H is then given by the lower linear fractional transformation,

$$H = \mathcal{F}(P,K) = \begin{bmatrix} P_{10} & P_{11} \end{bmatrix} + P_{12}K(I - P_{22}K)^{-1} \begin{bmatrix} P_{20} & P_{21} \end{bmatrix} \tag{5.24}$$

where P_{ij} are the partitions of P implied by the inputs and outputs.

The assumptions made are that:

(i) (A, B_2) is stabilizable and (A, C_2) is detectable.

(ii) D_{12} has full column rank and $D_{12}^T D_{12} > 0$.

(iii) D_{2i} has full row rank and $D_{2i} D_{2i}^T > 0$, $i = 0, 1$.

(iv) $D_{10} = 0$.

Admissible compensators K will be those which stabilize P, and satisfy $\|H_1\|_\infty < \gamma$. The problem statement is then

$$\min_K \{L(H, \gamma) : K \text{ admissible}\} \tag{5.25}$$

By a scaling of H, without loss of generality consider the case $\gamma = 1$.

The full state feedback problem is examined first, with normalized control weighting, so that $C_1^T = [C^T \; 0]$ and $D_{12}^T = [0 \; I]$. Also assume for simplicity that $D_{11} = 0$, and $B_0 = B_1$. This latter assumption allows the dual formulae to those of Proposition 5.9(i) to be used for evaluating the cost, which yields a much more symmetric form for the feedback gain matrix F. There is no technical difficulty in allowing $B_0 = B_1$ and using an alternate set of equations for evaluating the cost; the reason for choosing this particular set is to clarify the discussion of the time domain interpretation of $L(H, \gamma)$ given in Section 5.4.

Theorem 5.10 *Consider the problem statement (5.25), with the assumptions listed above, and* $A_{CL} \triangleq A + B_2 F$. *If* F *is a static feedback matrix that solves problem (5.25), then:*

$$F = -B_2^T (P\tilde{Q} + \tilde{P}Q)(Q + \tilde{Q})^{-1} \tag{5.26}$$

where P, Q, $\tilde{P}$, *and* $\tilde{Q}$ *satisfy* $A_{tmp} \triangleq (A_{CL} + B_1 B_1^T P)$ *stable and*

$$P A_{CL} + A_{CL}^T P + P B_1 B_1^T P + C^T C + F^T F = 0 \tag{5.27}$$

$$A_{tmp} Q + Q A_{tmp}^T + B_0 B_0^T = 0 \tag{5.28}$$

$$\tilde{P} A_{tmp} + A_{tmp}^T \tilde{P} + C^T C + F^T F = 0 \tag{5.29}$$

$$A_{tmp} \tilde{Q} + \tilde{Q} A_{tmp}^T + Q \tilde{P} B_1 B_1^T + B_1 B_1^T \tilde{P} Q = 0 \tag{5.30}$$

Proof: The closed loop system is

$$H = \left[\begin{array}{c|cc} A_{CL} & B_0 & B_1 \\ \hline C & 0 & 0 \\ F & 0 & 0 \end{array}\right]$$

From Theorem 5.7, the cost is $J = \mathrm{tr}\left\{CQC^T + FQF^T\right\}$, where Q solves the Lyapunov equation (5.28), and P satisfies the Riccati equation (5.27). Appending these two equations to the cost as constraints with Lagrange multipliers $\tilde{P}$ and $\tilde{Q}$ respectively yields the augmented cost as

$$\begin{aligned} J_{aug} = \mathrm{tr}\Big\{ & CQC^T + FQF^T \\ & + \tilde{P}(A_{tmp}Q + QA_{tmp}^T + B_0B_0^T) \\ & + \tilde{Q}(PA_{CL} + A_{CL}^TP + PB_1B_1^TP + C^TC + F^TF)\Big\} \end{aligned} \tag{5.31}$$

The equations for $\tilde{P}$, $\tilde{Q}$ and F are obtained immediately upon differentiating with respect to Q, P and F. □

An iterative approach to solving these equations appears to converge rapidly to the optimal feedback law F. Given an initial guess for F (say, from the minimum entropy control problem [74]), P, Q, $\tilde{P}$, and $\tilde{Q}$ can be computed sequentially as the solutions of Riccati and Lyapunov equations. Equation (5.26) can then be evaluated for F, and the process repeated.

For a system of order n and a fixed order compensator of order n_c, the necessary conditions for the optimum can be found, again using a Lagrange multiplier approach, in terms of four order $n + n_c$ matrix equations similar to Equations (5.27)–(5.30). A similar approach has been used before to solve a variety of control problems, e.g. [13], wherein the necessary conditions are simplified by identifying a projection operator. Here a similar projection operator has not been identified, due to the multiple constraint structure of the problem. Similar multiply-constrained fixed-order problems are investigated in [64]. It appears likely that for this problem, the "optimal" compensator with no constraint on the compensator state dimension does not have finite order; that is, unlike the standard $\mathcal{H}_2$ and $\mathcal{H}_\infty$ cost functionals, the cost continues

to decrease as the order of the compensator increases. Certainly, there is no *a priori* reason to expect that no improvement in the cost can be achieved for $n_c > n$.

5.3.2 Numerical Optimization

Optimal fixed-order compensators that satisfy the necessary conditions can be obtained numerically using a parameter optimization technique. Other similar approaches can be found in [55] and the references therein.

A quasi-Newton algorithm [85] was used in this thesis. The optimization problem can be reformulated as the minimization of a scalar function of a vector-valued argument. The quasi-Newton algorithm uses the function value, and gradients, and builds an estimate of the second derivative matrix; the Hessian. A faster optimization algorithm may be possible by using a Newton approach, and evaluating the Hessian exactly, once the estimate of the solution is close to the optimum [66]. If the function is quadratic, then knowledge of the Hessian matrix allows the minimum to be reached in one step. The code used to obtain the compensators in Chapters 6 and 7 used the BFGS (Broyden-Fletcher-Goldfarb-Shanno) [85] formula to update the Hessian.

The quasi-Newton algorithm used here requires that the function and gradient be calculated, and therefore an analytical expression for these is desired. If the (strictly proper) compensator with state space dimension n_c is represented as

$$K = \left[\begin{array}{c|c} A_c & B_c \\ \hline C_c & 0 \end{array}\right] \tag{5.32}$$

then the closed loop system $H_{cl} = \mathcal{F}(P, K)$ is

$$H_{cl} = \left[\begin{array}{cc|cc} A & B_2C_c & B_0 & B_1 \\ B_cC_2 & A_c + B_cD_{22}C_c & B_cD_{20} & B_cD_{21} \\ \hline C_1 & D_{12}C_c & 0 & D_{11} \end{array}\right] \tag{5.33}$$

The cost can be evaluated using Theorem 5.7.

The gradients are given by the following equations:

$$\frac{\partial J}{\partial A_c} = (PQ)_{22} + (XY)_{22} \tag{5.34}$$

$$\begin{aligned}\frac{\partial J}{\partial B_c} = {} & (P_{12}B_0 + P_{22}B_cD_{20})D_{20}^T + \gamma^{-1}(X_{12}B_1 + X_{22}B_cD_{21})WD_{21}^T \\ & +\gamma^{-1}\Big((PQ+XY)_{21}C_1^T + (PQ+XY)_{22}C_c^TD_{12}^T\Big)ZD_{11}D_{21}^T \\ & +(PQ+XY)_{21}C_2^T + (PQ+XY)_{22}C_c^TD_{22}^T\end{aligned} \tag{5.35}$$

$$\begin{aligned}\frac{\partial J}{\partial C_c} = {} & D_{12}^TZ\Big(C_1(Q+QPY+YPQ+YXY)_{12} \\ & +D_{12}C_c(Q+QPY+YPQ+YXY)_{22}\Big) \\ & +\gamma^{-2}D_{12}^TZD_{11}\Big(B_1^T(PQ+XY)_{12} + D_{21}^TB_c^T(PQ+XY)_{22}\Big) \\ & +B_2^T(PQ+XY)_{12} + D_{22}^TB_c^T(PQ+XY)_{22}\end{aligned} \tag{5.36}$$

where the implied partitions of the $(n+n_c)\times(n+n_c)$ matrices P, Q, X, and Y and their products is into $n\times n$, $n\times n_c$, $n_c\times n$ and $n_c\times n_c$ blocks. Making the appropriate definitions in comparing Equations (5.33) and (5.4), Y satisfies the Riccati equation (5.7), Q satisfies Equation (5.8), P satisfies the dual Lyapunov equation for evaluating $\|M\|_2$:

$$P(\bar{A}+YC^TZC) + (\bar{A}+YC^TZC)^TP + C^TZC = 0 \tag{5.37}$$

and X satisfies

$$X(\bar{A}+YC^TZC) + (\bar{A}+YC^TZC)^TX + PQC^TZC + C^TZCQP = 0 \tag{5.38}$$

The damping parameter γ is strictly less than one, and approximately one for lightly damped systems. The compensator will be guaranteed to be positive real only for $\gamma \geq 1$, since for $\gamma < 1$, the structure is dissipating energy, and the compensator is allowed to add power to the structure, provided that the damping dissipates greater power. Since the level of damping in the structure is usually highly uncertain, one does not want to rely on it; ideally, the compensator should dissipate power at all frequencies. However, since the compensator is strictly proper, there is no dissipation at $\omega \to \infty$. The cost is therefore only well defined for $\gamma < 1$. In the absence of damping information, the parameter should be set as close to one as possible.

An initial guess for the optimization that stabilizes the system and satisfies the $\mathcal{H}_\infty$ norm constraint can easily be found from the minimum entropy compensator [74]. For the structural control problem posed in Chapter 4, any positive real compensator is guaranteed to stabilize the structure and hence satisfy the $\mathcal{H}_\infty$-norm constraint. Thus any positive real compensator can be used as an initial guess. However, since the optimization problem is non-convex, local minima are likely to exist, and thus an initial guess which is close to the expected optimum is desirable. In practice, the $\mathcal{H}_\infty$ impedance matching solutions of [61] have been found to result in excellent convergence behavior.

Note that the representation of the compensator in Equation (5.32) contains extra degrees of freedom, since the state space representation is only unique to within a similarity transformation. Hence there are $n_c(n_c-1)$ extra variables in this representation. One could constrain the form of the compensator further and optimize over fewer variables. Each element in the gradient matrices in Equations (5.34)–(5.36) is the gradient with respect to the corresponding element of A_c, B_c, or C_c. Thus if some elements of the compensator matrices are fixed and some are free, the resulting gradient with respect to the free parameters is easily obtained by simply selecting the appropriate elements from the full gradient matrices.

However, constraining the form of the compensator does not necessarily lead to a faster optimization. Indeed, if a canonical form is chosen for the compensator, it may not even be possible to continuously vary the solution from the initial guess to the optimal solution [66]. If the A_c matrix consists of an arbitrary combination of 2×2 and scalar blocks on the diagonal, then any solution can be represented. However, a real pole in one block cannot coalesce with a real pole in a distinct block to form a complex pair of poles. Thus the constraint on the compensator representation may introduce additional local minima, and should not be used unless the current value of the solution is already close to the optimum. Without any constraint on the compensator form, though, the algorithm tends to be poorly conditioned near the minimum, because of the extra degrees of freedom. The minimum is not at a point, but on an $n_c(n_c-1)$ dimensional hyperplane. The increase in the number of variables

can also increase the solution time. The computations per step are approximately proportional to $(n + n_c)^3$, which is independent of the representation. However, the number of steps required to reach the minimum increases with the number of parameters.

The best approach appears to be to switch between different representations for the compensator depending on whether the solution is "close" to the optimum or not. The question of where one ought to make the switch between representations was not investigated thoroughly, although the intuition about the problems with the canonical representations would imply that the switch should be made as soon as one is certain that the correct pole-zero structure has been obtained. Unfortunately, this is a difficult property to test numerically. The second step of this two-step optimization procedure could be started with an estimate of the Hessian, computed from the final Hessian estimate of the first step, although this information was ignored in the numerical algorithm herein.

Far from the minimum, one should optimize over all of the extra degrees of freedom in the representation. Once a near-optimal solution is reached, convergence time is improved by constraining the compensator to be of some canonical form. Either of two approaches were used for this. The A_c matrix was constrained to have 2×2 or scalar blocks on the diagonal, where complex poles were represented as either of

$$\begin{bmatrix} 0 & 1 \\ -\omega^2 & -2\zeta\omega \end{bmatrix} \quad \text{or} \quad \begin{bmatrix} -\sigma & \omega \\ -\omega & -\sigma \end{bmatrix}$$

. The former allows real pole pairs to be represented in the same form, while the latter requires scalar blocks for every real pole. However, for high frequency poles, the first representation has poor conditioning properties, since $\omega^2 \gg 2\zeta\omega$. Even a few orders of magnitude between the parameters being optimized can lead to problems with termination due to the inverse scaling that results in the gradients.

Also note that for the cost derived in Chapter 3, $H_0 = WH_1$ for some weighting function W. Taking advantage of this form speeds up the algorithm, since the Riccati equation for Y only needs to be solved for a system with state dimension equal to that of H_1. Furthermore, since the states of the weighting function W are uncontrol-

lable from B_2, the system matrix in Equation (5.33) can be written in upper block triangular form, and the Lyapunov equations for Q, P, and X can be solved more efficiently by taking advantage of this structure.

5.4 Time Domain Interpretation

The form of the augmented cost for the linear control problem leads to an interesting differential games interpretation. It is well known that the central controller in the $\mathcal{H}_\infty$ problem can be found as the solution to a zero-sum differential game [81], where for minimizing $\|T_{zw}\|_\infty$, the control u and noise w solve the optimization problems:

$$u = \text{argmin} \int_0^\infty z^T z - \gamma^2 w^T w \, dt \tag{5.39}$$

$$w = \text{argmin} \int_0^\infty -z^T z + \gamma^2 w^T w \, dt \tag{5.40}$$

where u has information y about the state, and w has full information.

For the cost functional $L(H, \gamma)$, with $H_0 = H_1$, and under the assumption of linear feedback, the optimization problem is again equivalent to a differential game, but it is no longer a zero-sum game. Whether the problems are equivalent when both are allowed nonlinear feedback is unknown.

Proposition 5.11 *If an optimal linear compensator exists for problem (5.25), then it is the same as that of a Stackelberg differential game with u as leader, w_1 as follower and w_0 as unit intensity white noise, where u and w_1 solve the following optimization problems:*

$$u = \text{argmin} \lim_{t\to\infty} E\left\{z^T z\right\} \tag{5.41}$$

$$w_1 = \text{argmin} \lim_{t\to\infty} E\left\{-z^T z + \gamma^2 w_1^T w_1\right\} \tag{5.42}$$

where u has information y about the state, and w has full information.

Proof: Assuming a linear control law for u, the optimization problem for w_1 is easily solved with a single Riccati equation (which is Equation (5.27) for the state feedback case.) Appending this as a constraint for the optimization problem (5.41) results in an identical problem formulation to that of problem (5.25). □

This game seems to be a more natural problem to pose than the pure $\mathcal{H}_\infty$ differential game, since the control does not benefit from the use of noise, but instead optimizes an $\mathcal{H}_2$ cost functional, while the deterministic noise w_1 solves the same optimization problem as the noise in the $\mathcal{H}_\infty$ problem. In addition, the plant is now subject to a white noise input w_0. The resulting block diagram is again that of Figure 5.3. This problem looks similar to that considered in [26,101,102] since a single output is minimized in the presence of two disturbance inputs, one of which is associated with the $\mathcal{H}_2$ nature of the problem, while the other is associated with the $\mathcal{H}_\infty$ nature.

Note that for a non-zero sum differential game, the solution depends on how the optimality is defined. For the Stackelberg or leader-follower solution [87,65,7], one player (here the control u) acts as leader and announces a strategy. Knowing this strategy, the follower (here the noise w_1) solves its optimization problem. In general, the optimal control for the Stackelberg problem is known to be nonlinear [7]. Similar equations to (5.27)–(5.30) have been reported in [65], where the optimal linear state feedback law for a Stackelberg problem was found. The nonlinear, team optimal strategy obtained, for example, in [7] does not apply to this problem since the leader u cannot increase the follower w_1's cost indefinitely, and therefore cannot induce w_1 to follow a strategy desirable to u.

The differential games representation of problem (5.25) allows the matrices of Equations (5.27)–(5.30) to be given an interpretation. The matrices $-P$ and $+\tilde{P}$ correspond to the optimal cost-to-go for the costs associated with w_1 and u respectively, Q is the covariance of the state, and $\tilde{Q}$ is the sensitivity of the cost for u to changes in the cost for w_1.

5.5 Summary

The average value of the global $\mathcal{H}_2$ performance metric on the structure was shown in Chapter 4 to be equivalent to an $\mathcal{H}_2/\mathcal{H}_\infty$ cost functional of the power reflection properties at the actuator/sensor location. This cost can be evaluated for a state space

representation of the power properties, and the evaluation algorithm can then be used as the basis of an optimization algorithm for obtaining the state space representation of the compensator that minimizes the cost functional. No closed-form solution for this compensator was found; instead, a numerical approach was presented. The cost functional also bears a strong connection to other $\mathcal{H}_2/\mathcal{H}_\infty$ cost functionals, and to an interesting non-zero sum differential game.

Chapter 6

Examples

What we have to learn to do, we learn by doing.

–Aristotle, *Ethica Nicomachea* II (c. 325 B. C.)

This chapter demonstrates the approach developed in the previous chapters on several simple structural systems. The purpose of this is to understand how the approach works on simple systems where one has some physical intuition about the behavior of the structure. One of the goals of this chapter is to compare the compensators and performance obtained using the approach of this thesis with those obtained using a variety of existing control design techniques. The approach is demonstrated experimentally in Chapter 7 on a more complicated truss structure.

A two mass oscillator with a single flexible mode is considered first; for this simple system, much of the design can be done analytically. A low authority, parameter robust compensator is designed using the stochastic optimization approach of Chapter 4. The compensator and resulting performance are compared with those obtained using LQG (or $\mathcal{H}_2$) optimization, rate feedback, the "maximum entropy" approach of Hyland [52], and a multiple model approach (e.g. [4].)

Since this thesis builds on previous impedance matching approaches, the design method should be compared not only with other parameter-robust control design techniques, but with previous impedance matching methods. These have been based on both dereverberated models [61], and wave based models [69]. The simplest structure that illustrates wave propagation problems is a free-free Bernoulli-Euler beam. Com-

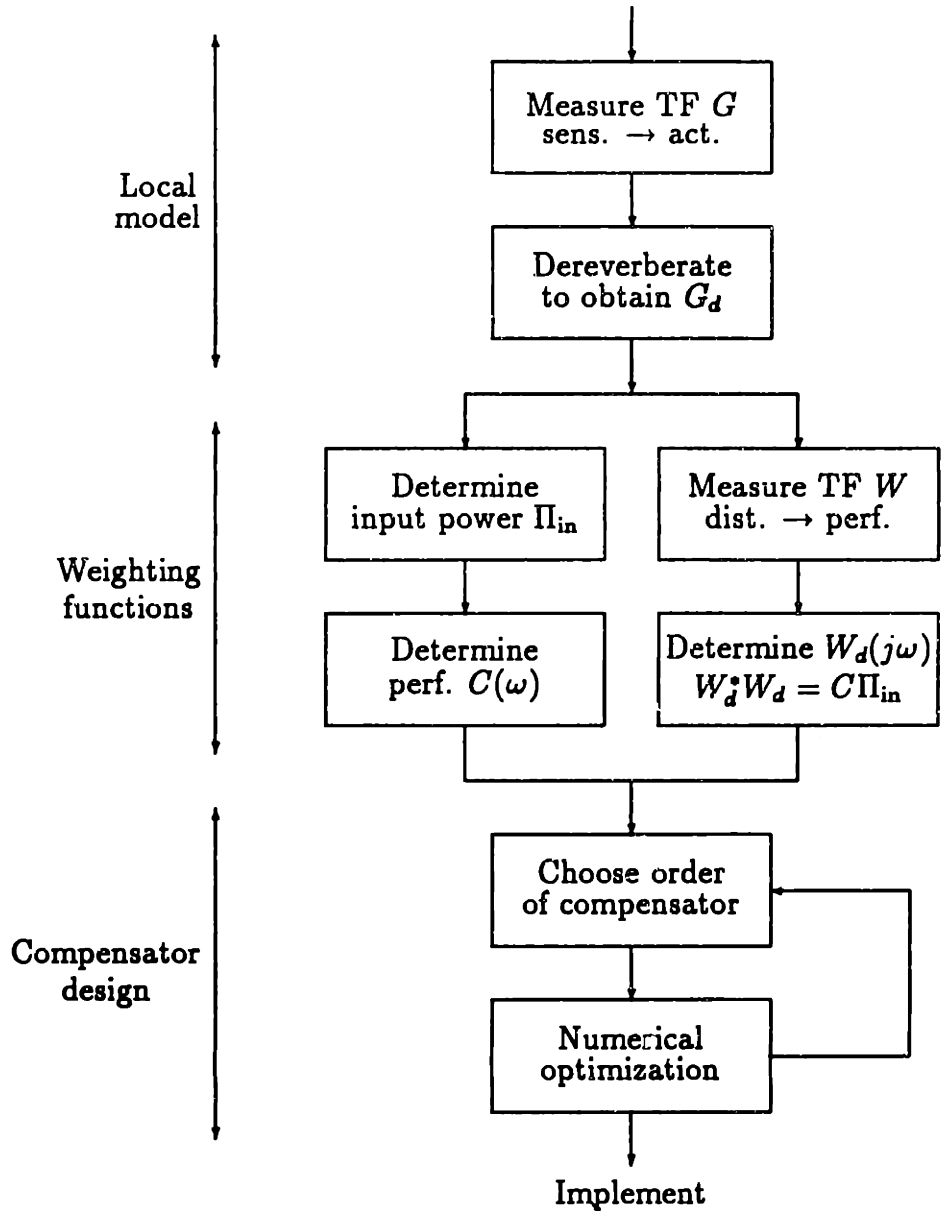

Figure 6.1: Compensator design procedure

pensators designed with the stochastic optimization approach are compared with the non-causal, ideal compensator of Equation (2.3), a constant gain impedance match, or "rate feedback", and the $\mathcal{H}_\infty$ impedance matching approach of [61].

The "stochastic optimization" compensator design approach developed in the previous chapters is summarized in Figure 6.1. The first step is to obtain the reverberant transfer function, from experimentally measured data, a finite element model, or an analytical model. The impedance matching results require a local model, so the next step is to obtain the dereverberated transfer function. This can be calculated using

a logarithmic averaging procedure, as described in Section 7.2.3, or obtained directly from an analytical model. The next step is to determine the weighting function to use. Chapter 4 discussed two weighting functions, the input power $\Pi_{in}(\omega)$ that relates disturbances to the average energy, and the performance weighting $C(\omega)$ that relates the average energy to the performance variable. An alternative approach that is discussed in Section 7.2.5 is to measure the transfer function between disturbance and performance, and "dereverberate" that transfer function. The optimal compensator that minimizes the cost in Equation (4.35), and therefore the average value of the global cost, can be obtained using a numerical optimization procedure. The order of the compensator is fixed, and optimization performed. The compensator order can then be increased, until no significant reduction in performance is achieved.

6.1 Two Mass Oscillator

First, consider the simple example of a single mode oscillator, such as the spring-mass system in Figure 6.2. The inputs are disturbance and control forces w and u acting on different masses, and the output y is the velocity of the mass on which the control input acts. The structure is similar to that of the ACC Benchmark problem [97,98], but the sensor output has been changed to permit collocated control.

Note that if the disturbance and control forces act at the same location, then the assumptions that result in an impedance matching solution are not valid. The optimal control in that case is high gain, so that the disturbance input location is effectively clamped. Rather than maximizing dissipation, this solution minimizes

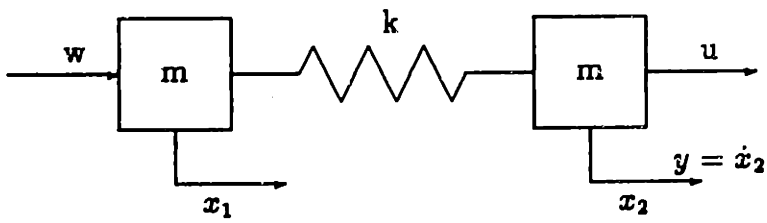

Figure 6.2: Two mass oscillator.

the power input by the disturbance. While this solution is preferable if possible, there are many structural control problems where one may be unable to place control inputs which are collocated and of like type, corresponding to every disturbance that impinges upon the system. Thus, a representative example to demonstrate structural control should include noncollocated disturbance and control inputs. However, the control engineer often has greater control over sensor and actuator placement, and hence requiring these to be collocated is not as significant a restriction. Subject to this requirement, the two mass system shown in Figure 6.2 is the simplest structure that exhibits properties representative of general structural control problems.

The state space representation of the system in Figure 6.2 is given by

$$\begin{aligned} \dot{x} &= Ax + B_1 w + B_2 u \\ y &= Cx \end{aligned} \tag{6.1}$$

where

$$A = \begin{bmatrix} 0 & 0 & 0 \\ 0 & 0 & \omega_n \\ 0 & -\omega_n & 0 \end{bmatrix} \quad B_1 = \mu \begin{bmatrix} 1 \\ 0 \\ 1 \end{bmatrix} \quad B_2 = \mu \begin{bmatrix} 1 \\ 0 \\ -1 \end{bmatrix} \tag{6.2}$$

$$C = \mu \begin{bmatrix} 1 & 0 & -1 \end{bmatrix} \tag{6.3}$$

and where $\omega_n = \sqrt{\frac{2k}{m}}$ and $\mu = \sqrt{\frac{1}{2m}}$. The system has been transformed into energy coordinates, so that half the square of the first state is the rigid body mode kinetic energy, and the remaining states correspond to the flexible mode potential and kinetic energy. The displacement state of the rigid body mode is unobservable and uncontrollable, and has been eliminated. As noted in Chapter 3, the last two states do not correspond exactly to the energy coordinates for a damped structure, since in a real structure, only kinetic energy is dissipated, and not potential energy. However, for light damping, the difference is small.

Choosing $\omega_n = 1$ and $\mu = 1$, the transfer function from control signal to sensor is

$$G_{22}(s) = \frac{1}{s} + \frac{s}{s^2 + 1} \tag{6.4}$$

The ideal compensator is the impedance match of the dereverberated mobility, not of the exact mobility. The dereverberated mobility can be approximated by shifting

the poles and zeroes of the original system to the real axis; that is, by adding enough damping so that the resulting system is no longer resonant. The original poles are at 0 and $\pm j$, and the original zeroes are at $\pm 0.7071j$. The dereverberated system therefore has a pair of poles at -1, a pair of zeroes at $-.7071$, and a pole at the origin. A simpler approximation to the dereverberated transfer function can be obtained by replacing the part of the system matrix A in Equation (6.2) corresponding to the flexible modes:

$$A_{\text{flex}} = \begin{bmatrix} 0 & \omega_n \\ -\omega_n & 0 \end{bmatrix}$$

with the critically damped system matrix:

$$A_{\text{derev}} = \begin{bmatrix} -\omega_n & 0 \\ 0 & -\omega_n \end{bmatrix}$$

The resulting "dereverberated" transfer function is

$$G_d(s) = \frac{1}{s} + \frac{1}{s+1} \tag{6.5}$$

The dereverberated transfer functions obtained by either approach are approximately the same. The second form, given in Equation (6.5), will be used for simplicity. The reverberant and dereverberated transfer functions are plotted in Figure 6.3. Some damping has been added to the reverberant transfer function so that the peak is finite. The dereverberated transfer function at the disturbance input is also given by Equation (6.5).

In order to compute the power reflection coefficient H in Equation (4.24), the stable spectral factor G_0 of $G_d + G_d^*$ must be determined, as in Equation (2.5). This computation is most easily done in the frequency domain. The result is

$$G_0(s) = \frac{\sqrt{2}}{s+1} \tag{6.6}$$

The state space approach of [61] yields the same solution, but requires solving two Lyapunov equations, and taking the limit as the feedthrough term D is reduced to zero.

Assume, for simplicity, a white spectrum for the disturbance force w. Then from Equation (4.30), the input power is determined by the dereverberated input mobility

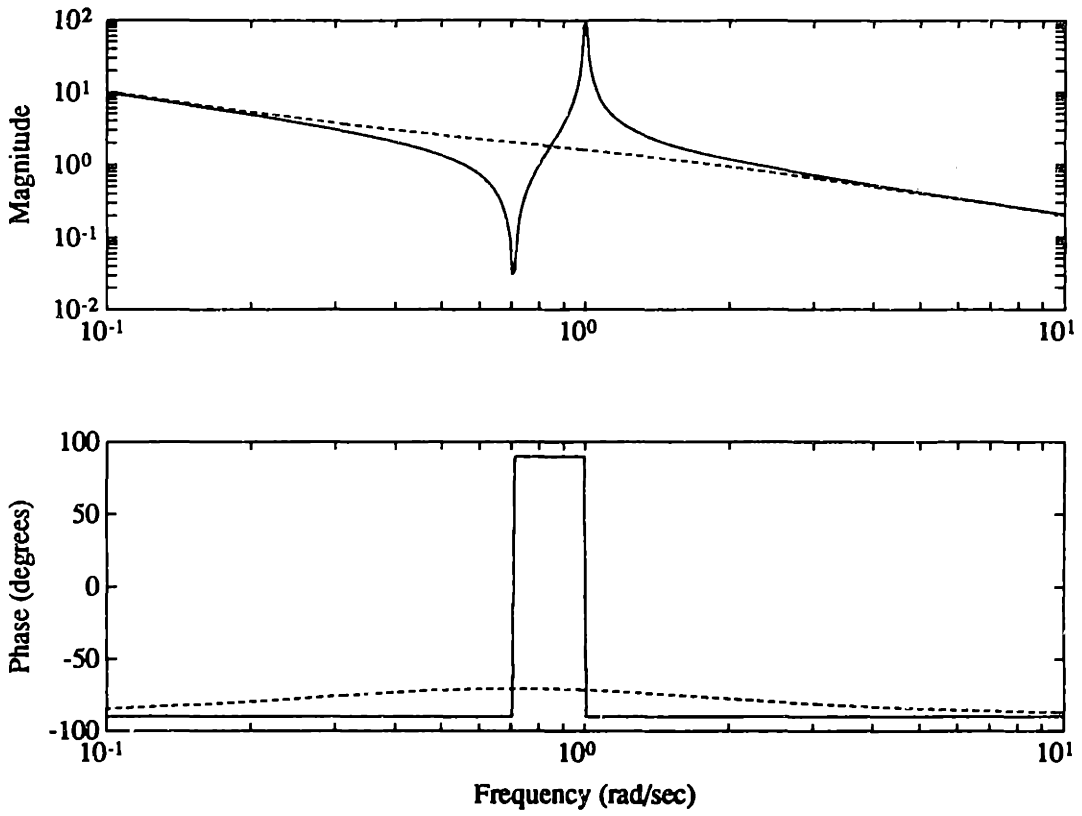

Figure 6.3: Reverberant (solid) and dereverberated (dashed) mobility for two mass oscillator example.

at the disturbance source. Also, for simplicity, let the cost functional be the total energy in the system. The weighting function W in Equation (4.36) is therefore G_0 given in Equation (6.6).

For the limiting case of large uncertainty in the natural frequency of the system, the average energy is minimized by a compensator that minimizes the cost in Equation (4.35). This compensator is most easily obtained by solving a numerical optimization problem, as discussed in Chapter 5. The resulting compensator is shown in Figure 6.4, compared with an LQG compensator designed for the nominal system. The LQG compensator is both unstable and non-minimum phase, and destabilizes the system for sufficiently large variations in the spring stiffness. The total cost, evaluated as a function of the spring constant k for these two compensators is shown in Figure 6.5.

Figures 6.4 and 6.5 also compare these compensators with those designed using

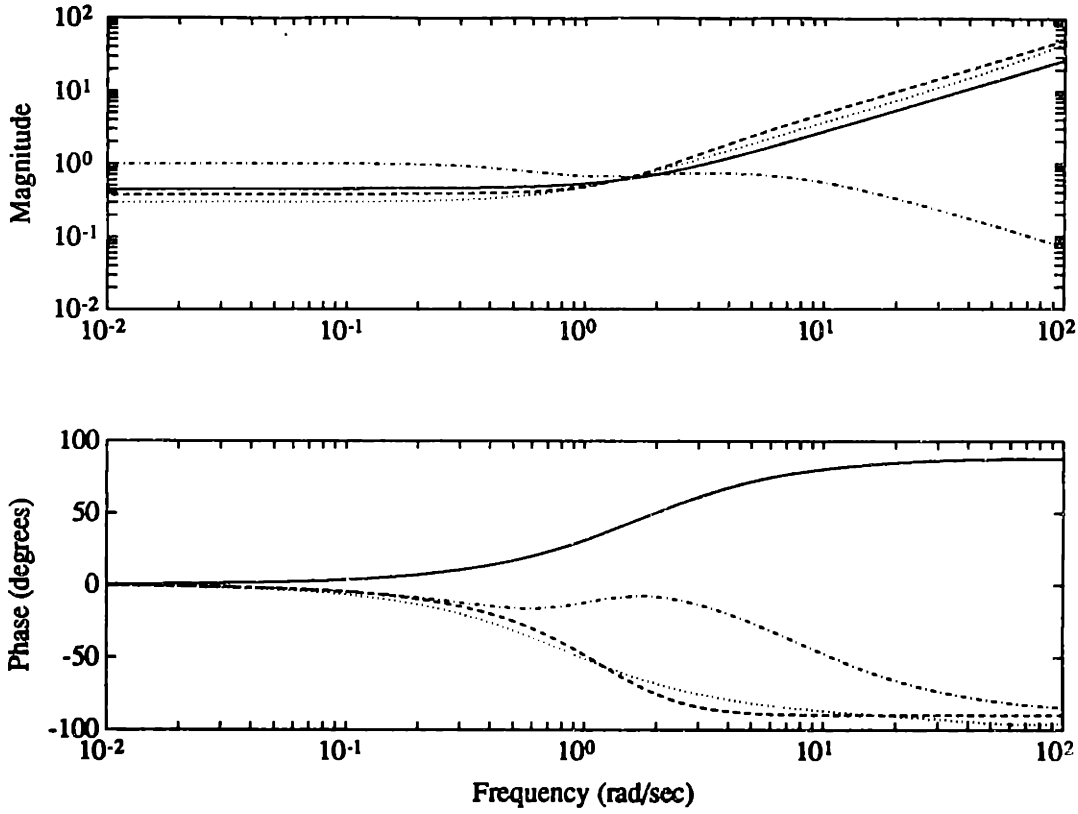

Figure 6.4: Compensators for two mass oscillator example. Stochastic optimum (solid), LQG (dashed), multiple model (dotted), and maximum entropy compensator (dash-dot).

two other parameter-robust techniques; a multiple model approach, and the maximum entropy approach of Hyland [52]. For the multiple model case, the cost is averaged over the nominal, and plants with poles and zeroes differing from the nominal by ± 0.75 of their nominal values. The LQG compensator is used as the initial guess, and the optimal compensator is obtained through a numerical optimization, similar to that discussed in Section 5.3.2. The resulting compensator has the same system order as the plant, although this is not required by the approach.

For the maximum entropy compensator, uncertainty in the natural frequencies is assumed, with A_1 in Equation (2.9) given by $A_1 = 0.1A_0$. The optimal compensator that minimizes a cost based on Equation (2.11) is given by Equations (219)–(227) in [13]. This solution requires that four modified Lyapunov and Riccati equations be solved. An iterative approach was used to these equations, similar to that presented

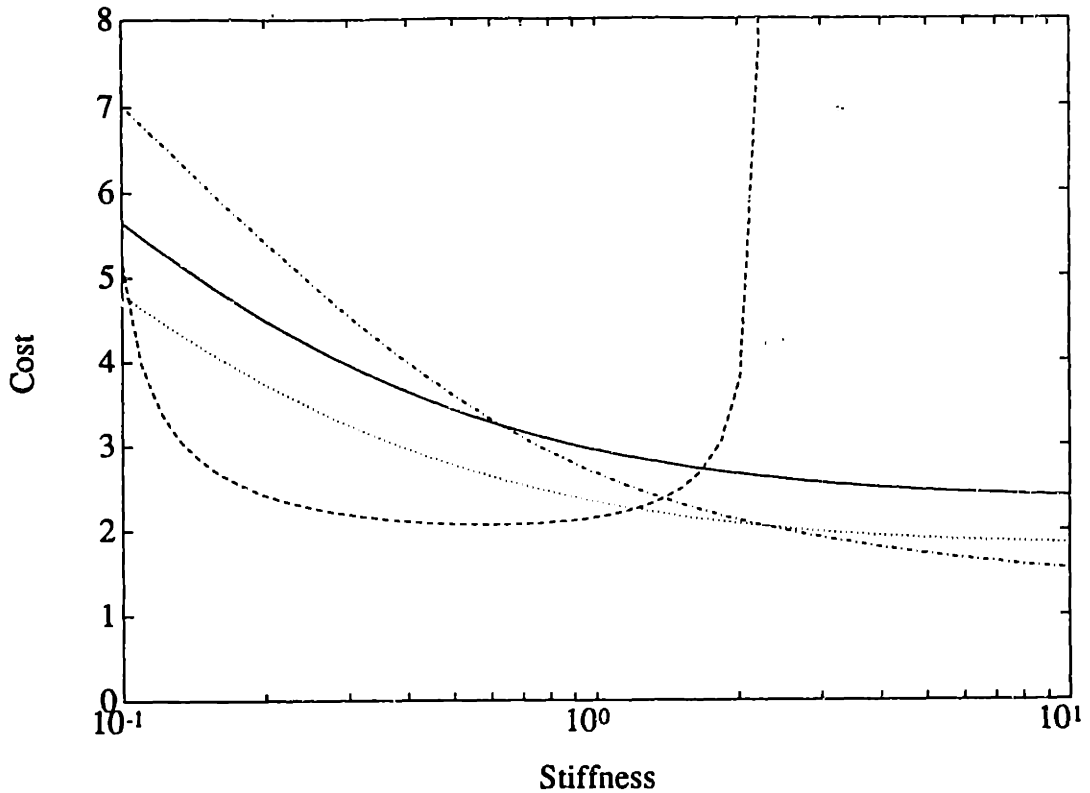

Figure 6.5: Cost as a function of uncertain stiffness for two mass oscillator example. Stochastic optimum (solid), LQG (dashed), multiple model (dotted), and maximum entropy compensator (dash-dot).

in [51]. The LQG Riccati solution matrices were used for initial estimates. At each step in the iteration, the additional terms in the modified Lyapunov and Riccati equations were evaluated based on the previous estimates, and treated as additional driving noise terms. New estimates for the solution of these matrix equations could then be obtained by solving ordinary Lyapunov and Riccati equations. This approach is simple to program, and has adequate convergence properties for relatively small uncertainties, and low order systems.

The stochastic optimum is more robust than LQG, although it does sacrifice some performance at the nominal stiffness value in order to achieve this robustness. Both the maximum entropy and multiple model approaches also achieve better robustness than the LQG approach. For this example, the multiple model solution is superior to the stochastic optimum for an uncertain stiffness in the range plotted. This is

because the stochastic approach averages over all values of the natural frequency, and thus guarantees stability for any value of the uncertain frequency. However, at higher values of the stiffness, the multiple model solution is unstable. The comparison between the two is also slightly misleading, since for this system there is only a single uncertain parameter, and hence the uncertainties can easily be described by several distinct models. In a complex structure, the stochastic optimization implicitly averages over all parametric uncertainties, while the computation required in the multiple model approach may become too cumbersome.

For this simple example, the LQG controller is robust to a 50% variation in the uncertain parameter, but as the next example demonstrates, this conclusion may not be true in more complex structural systems.

6.2 Bernoulli-Euler Beam

The single mode oscillator example demonstrates the stochastic optimization approach for a simple structural system for which several parameter-robust control design techniques can easily be used. The dereverberated mobility model, however, holds more intuitive appeal for a continuous structure that exhibits wave behavior. As this is the case for many structural systems, such an example should also be considered. The simplest structure that exhibits dispersive wave behavior is the transverse vibration of a uniform undamped free-free Bernoulli-Euler beam. Note that the dynamics of compression waves in a uniform rod satisfy a simpler wave equation; however, since this system is non-dispersive, it is not representative of realistic structures. There are many results that hold for the rod, but for no other structure.

Consider a uniform undamped free-free Bernoulli-Euler beam, with a collocated force actuator and velocity sensor at one end, and a disturbance force acting at the other end. This system is shown in Figure 6.6. With $v(x,t)$ as the transverse displacement of the beam, the partial differential equation describing the beam vibration is

$$\rho A \frac{\partial^2 v}{\partial t^2} + EI \frac{\partial^4 v}{\partial x^4} = 0 \tag{6.7}$$

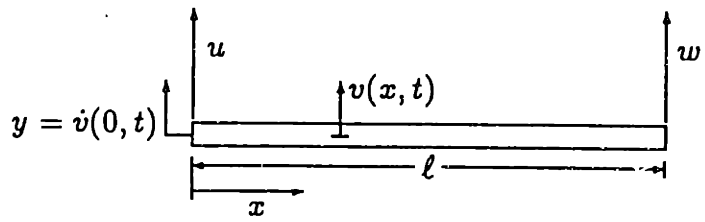

Figure 6.6: Beam example with collocated force actuation and rate sensing at left end, and a disturbance force acting at the opposite end.

with boundary conditions

$$EI \left.\frac{\partial^3 v}{\partial x^3}\right|_{x=0} = u \qquad EI \left.\frac{\partial^3 v}{\partial x^3}\right|_{x=\ell} = w \tag{6.8}$$

$$EI \left.\frac{\partial^2 v}{\partial x^2}\right|_{x=0} = 0 \qquad EI \left.\frac{\partial^2 v}{\partial x^2}\right|_{x=\ell} = 0 \tag{6.9}$$

where EI is the bending stiffness, and ρA is the mass per unit length. A complete description of the dynamics of this system in terms of travelling and evanescent wave modes can be found, for example, in [67]. The dereverberated mobility may be calculated from the wave information [61] as

$$G(s) = \frac{\sqrt{2}}{(\rho A)^{3/4}(EI)^{1/4}} \cdot \frac{1}{\sqrt{s}} \tag{6.10}$$

The dereverberated input mobility G_d at the other end of the beam where the disturbance enters is also given by Equation (6.10). The exact and dereverberated transfer functions are plotted in Figure 6.7. The dereverberated transfer function could also be obtained from the logarithmic average of the exact transfer function, or by critically damping all of the poles in the model of the exact beam. This last approach would, however, require a large number of poles to be kept in order to obtain a reasonable approximation to the dereverberated mobility, and the resulting approximation would have the same large number of poles. The smooth function in Equation (6.10) can instead be approximated by many fewer poles.

With no causality constraint, the compensator that best matches the input impedance and thus dissipates the maximum possible power at all frequencies is, from

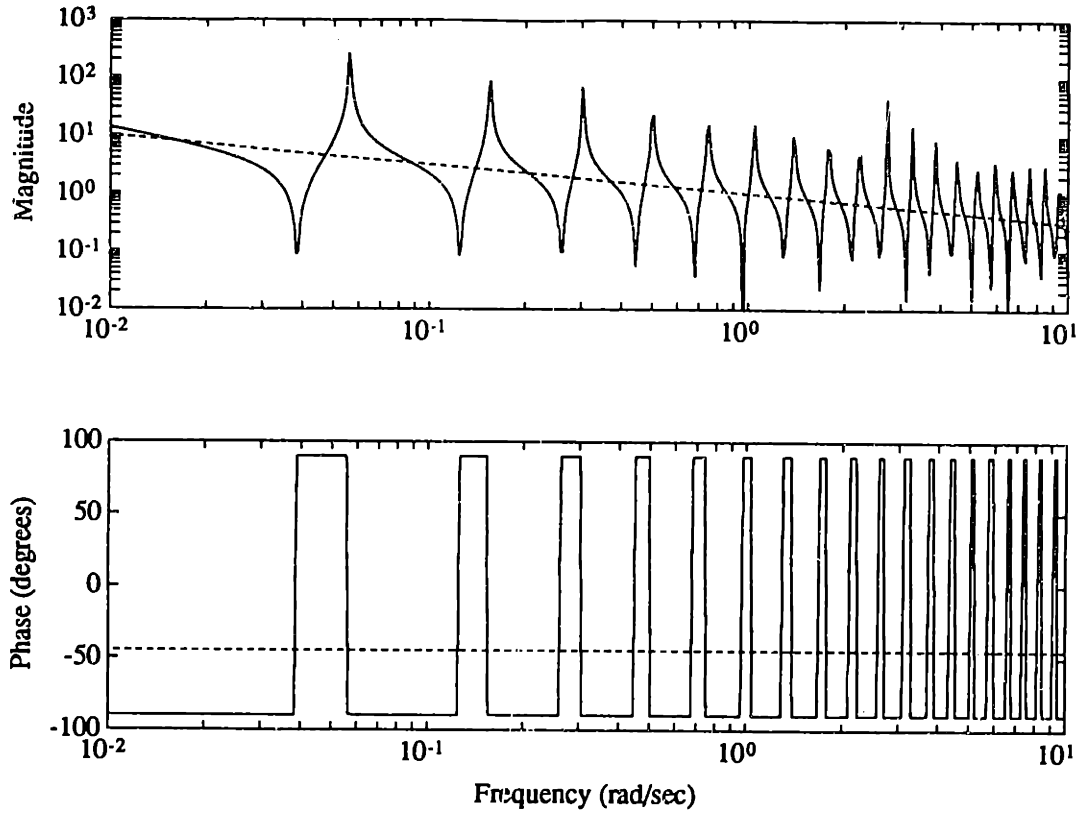

Figure 6.7: Reverberant (solid) and dereverberated (dashed) mobility for beam example.

Equation (2.3):

$$K(s) = \frac{(\rho A)^{3/4}(EI)^{1/4}}{\sqrt{2}} \cdot \sqrt{-s} \tag{6.11}$$

Note that this is the same compensator as that obtained by the unconstrained optimization in [69], though the derivation differs, and in Flotow and Schäfer [96], by setting the reflection coefficient to zero. This is the ideal compensator for the structure, but it cannot be implemented, because $\sqrt{-s}$ is not analytic in the right half plane. As noted in Section 2.1.2, if the compensator transfer function were unstable, then the closed loop system would be unstable. The right half plane dynamics must therefore correspond to a non-causal compensator, with non-zero impulse response for $t \leq 0$.

The $\mathcal{H}_\infty$-optimal compensator with unity weighting has the same magnitude as

the non-causal optimum, but a 90° phase shift at all frequencies [61]:

$$K(s) = \frac{(\rho A)^{3/4}(EI)^{1/4}}{\sqrt{2}} \cdot \sqrt{s} \tag{6.12}$$

This compensator is causal, but irrational. It can be approximated to an arbitrary degree of accuracy over a finite frequency region by a rational compensator. The fixed-form optimization in [69] also yields the same controller.

With velocity feedback, a low gain at the frequency of a lightly damped pole will not add significant damping. A gain that is too high will move the pole to a nearby open loop zero, which will also be lightly damped. An appropriate choice of gain will add significant damping to a given mode, and those nearby, but it is not possible to add significant damping to all of the modes at the same time. Thus the gain in velocity feedback must be optimized to provide damping at a certain frequency. Far enough away from this frequency, the gain is either too low, or too high. The optimal gain can be computed as the inverse of the magnitude of the dereverberated mobility at the chosen center frequency.

Now consider the design of a stochastically optimal compensator for this system. The disturbance spectrum is chosen to be

$$V(\omega) = \left(\frac{\omega}{(\omega + a)^2}\right)^2 \tag{6.13}$$

This spectrum has more energy near $\omega = 1$, rolling off at both higher and lower frequencies. From Equation (4.30) the input power is

$$\Pi_{\text{in}} = (G_d + G_d^*) \cdot \left(\frac{\omega}{(\omega + a)^2}\right)^2 \tag{6.14}$$

The performance is the relative displacement between two interior points:

$$J = \|v(0.8\ell, t) - v(0.1\ell, t)\|_2 \tag{6.15}$$

With this cost, none of the low frequency modes are unobservable. The relative displacement error performance metric is motivated by a space-based interferometric problem, to be discussed in Chapter 7. This cost is plotted by mode number in Figure 6.8. Also shown is a smoothed average cost, which is proportional to $1/\omega^2$ at high

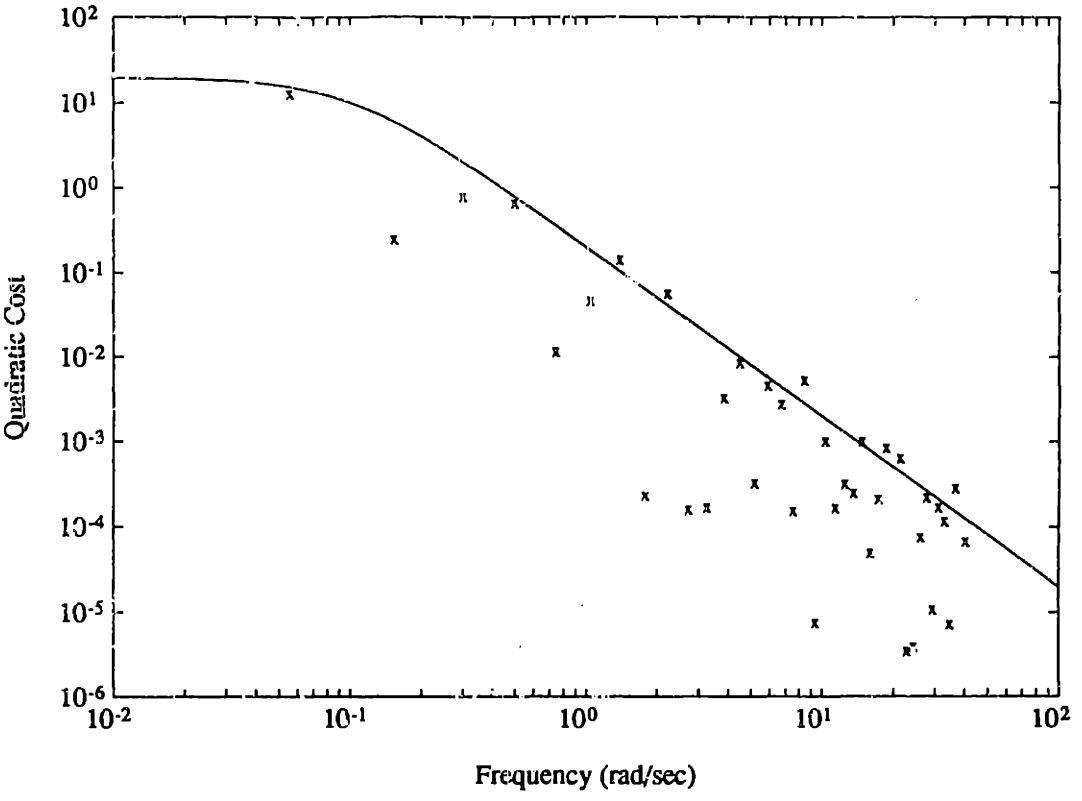

Figure 6.8: Modal costs, and average modal cost for beam example

frequencies. The performance weighting $C(\omega)$ in Equation (4.27) is the average modal cost, multiplied by the modal density. The modal density for a beam is proportional to $1/\sqrt{\omega}$ [57].

The dereverberated input mobility is irrational, but can be approximated adequately in the frequency range of interest by a rational function with logarithmically spaced alternating poles and zeroes on the negative real axis. A seventh order approximation was used. The transfer function of this approximation matches the exact dereverberated mobility to within 2 degrees of phase and 0.25 dB magnitude for 2 decades above and below the center frequency of the weighting function. A fifth order optimal compensator was designed. While increasing the order of the compensator always yields a decrease in the cost, no significant decrease was obtained for order higher than fifth. This compensator is plotted in Figure 6.9. Also plotted is the LQG compensator designed for the nominal system, the $\mathcal{H}_\infty$ optimal impedance match

compensator [61], and a rate feedback compensator for comparison. The Rayleigh-Ritz model used to derive the LQG compensator contains the first 40 modes of the system, up to a frequency of 40 rad/sec. Since negligible sensor noise and control cost were assumed for the impedance matching compensators, this was also assumed for the LQG compensator. As a result, this compensator destabilizes the system for small errors in the length of the beam. The LQG compensator could be made more robust, at the expense of nominal performance, by adding sensor noise and a control weighting. This *ad hoc* approach to adding robustness was used to design an LQG compensator that was robust to a 1% change in the length of the beam. The performance of this compensator is also shown in Figure 6.10. The nominal performance is almost the same as that of the stochastic optimum, while the robustness properties are very different. Figure 6.10 shows the total cost achieved by the various compensators as a function of the uncertain length of the beam. Also shown, for comparison, is the locus obtained by computing the optimal compensator and corresponding cost at each length. This curve represents a lower bound on the achievable cost. These costs were computed using a 40 mode Rayleigh-Ritz model.

Another method of comparing the performance of the compensators is to look at the power dissipated by them. The fraction of the incoming power that is reflected back into the structure is given by the transfer function H in Equation (4.24). The magnitude of this transfer function is shown for the stochastic, rate, and $\mathcal{H}_\infty$-optimal compensators in Figure 6.11. This is precisely the quantity whose infinity-norm is minimized by the approach in [61], and hence the $\mathcal{H}_\infty$-optimal compensator yields equal dissipation at all frequencies. The rate feedback compensator provides good dissipation at the most important frequency, and less dissipation at both higher and lower frequencies. The stochastic optimal compensator does a comparable job at the most important frequency; however, the design technique is also provided with information regarding the relative importance of higher and lower frequencies. Since the cost functional in the problem is based on displacements, there is a greater contribution to the cost from energy in lower frequency modes than from energy at higher frequencies. Therefore, the stochastically optimal compensator does a better

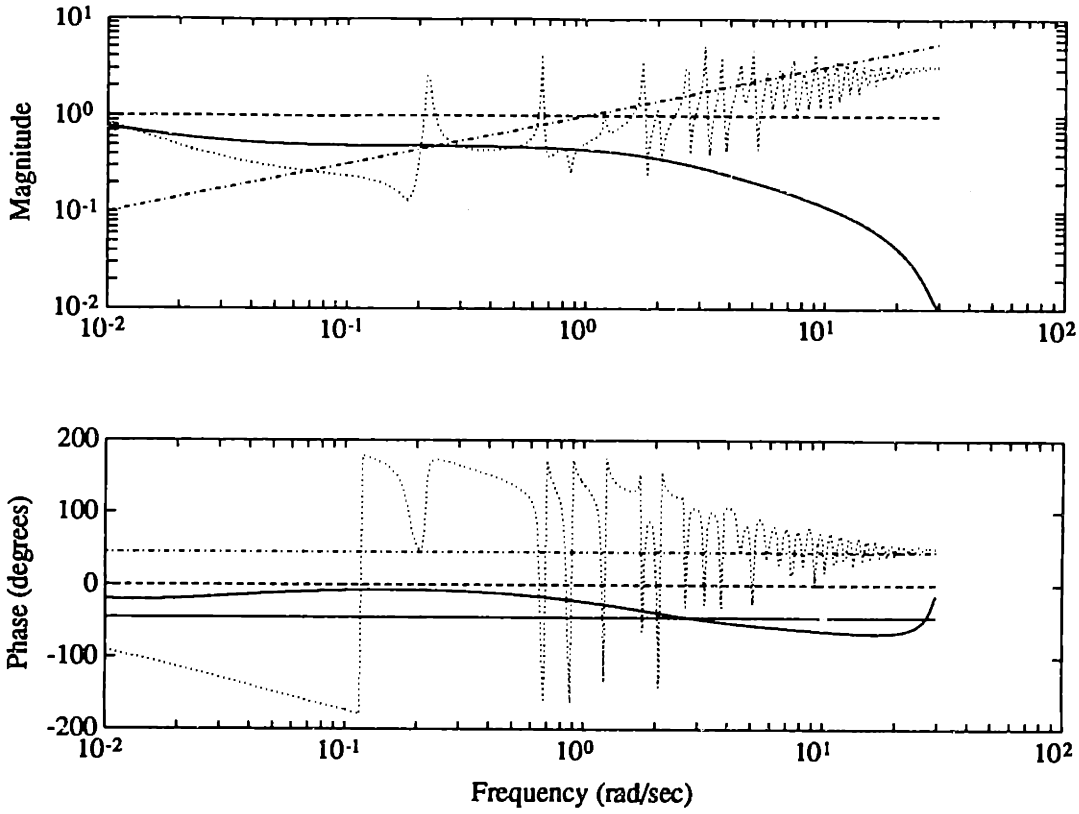

Figure 6.9: Compensators for beam example. Stochastic optimum (solid), rate feedback (dashed), nominal LQG (dotted) and $\mathcal{H}_\infty$-optimal (dot-dash). The optimal impedance match has the same magnitude as the $\mathcal{H}_\infty$ compensator, but a phase of $-45°$ (solid).

job than rate feedback at lower frequencies. This is the source of the improvement in performance shown in Figure 6.10.

6.3 Summary

The stochastic optimization approach developed in Chapter 4 yields compensators with good performance and robustness properties for systems with collocated and dual sensors and actuators. An approach which does not include any information about uncertainty in the model, such as LQG, can have arbitrarily poor robustness properties. The technique of this thesis can also be compared with other parameter-robust control design techniques, such as the maximum entropy and multiple model approaches. For simple systems, these approaches yield good robustness properties,

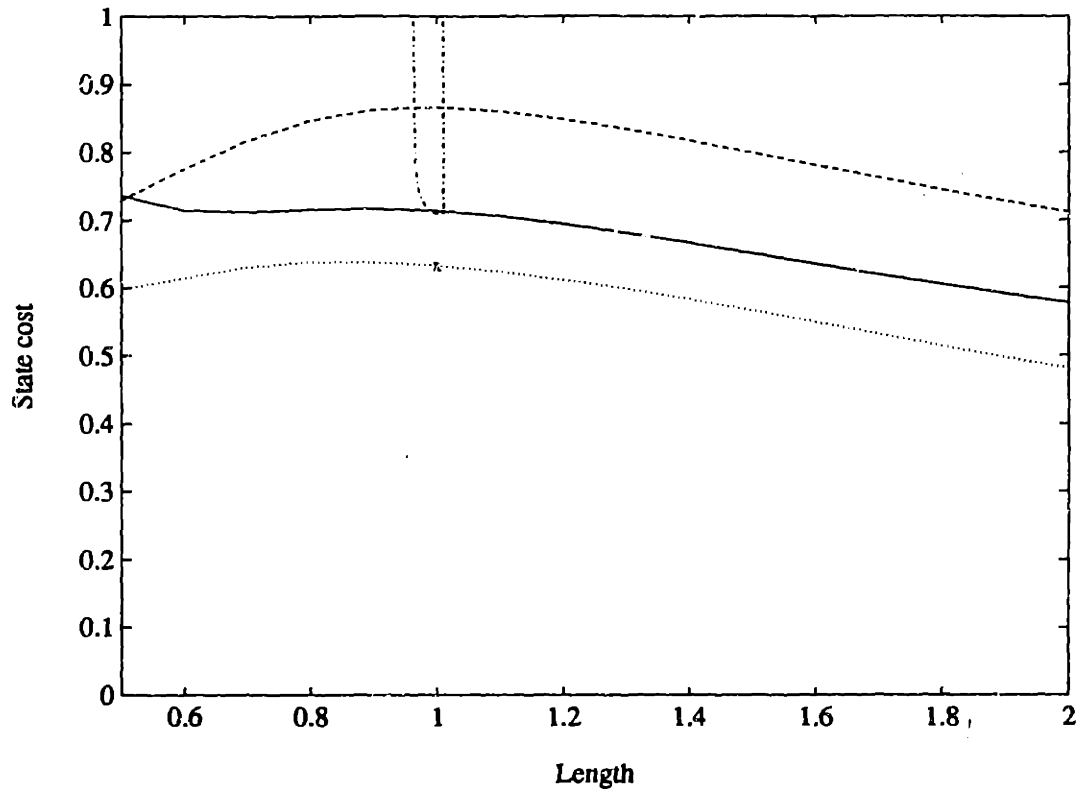

Figure 6.10: Cost as a function of uncertain length for beam example. Stochastic optimum (solid), rate feedback (dashed), LQG (x) and the locus of $\mathcal{H}_2$-optimal compensators designed at each length (dotted). Also shown is the LQG compensator with fictitious control weight and sensor noise (dash-dot).

although there is no guarantee of closed-loop stability for all possible values of the uncertainties.

A simple low authority control impedance matching approach such as rate feedback is guaranteed to be stabilizing. However, better performance can be achieved by using the optimal approach developed in this thesis, while still guaranteeing closed-loop stability.

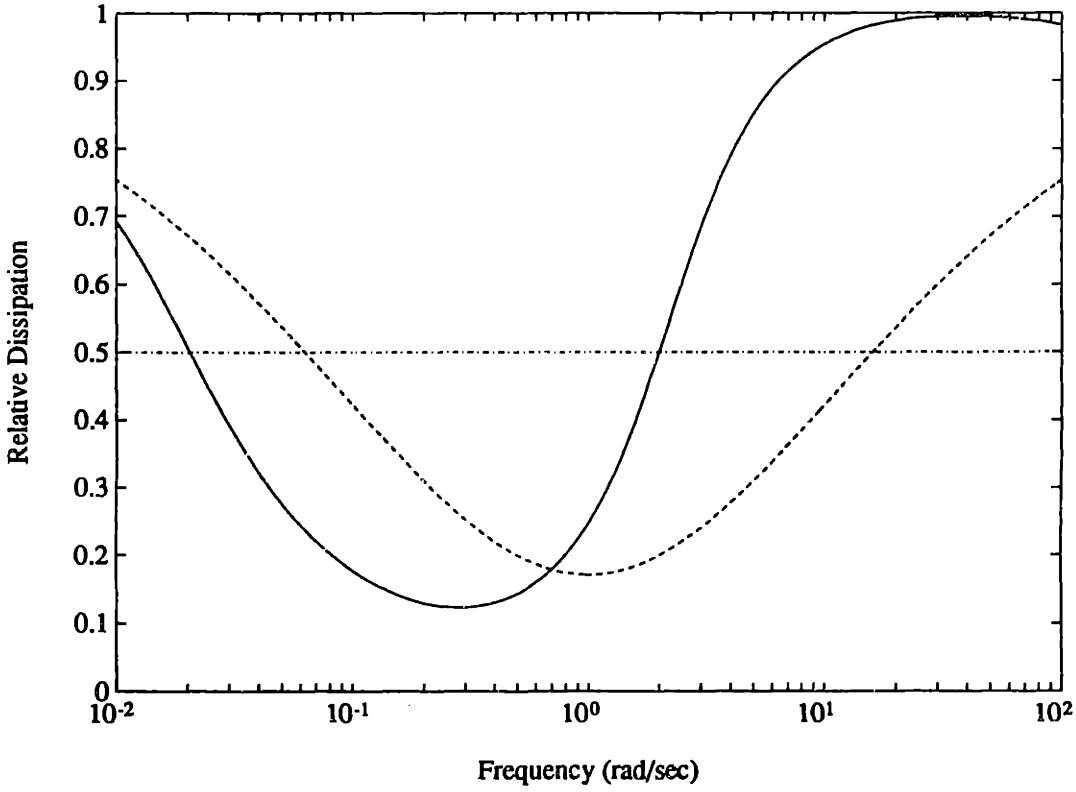

Figure 6.11: Fraction of power reflected for beam example. Stochastic optimum (solid), rate feedback (dashed), and $\mathcal{H}_\infty$-optimal (dot-dash).

Chapter 7

Experimental Verification

Observation, not age, brings wisdom.

–Hippocrates

While theoretical results are valuable, they must ultimately be tested in an experiment. In addition to verifying the validity and usefulness of the theoretical results, the experiment indicates difficulties or limitations in their application, and appropriate directions for further research.

The approach described in the previous chapters was tested on the multipoint alignment testbed in the Space Engineering Research Center laboratory at M.I.T. This testbed and the associated research program are intended to evaluate the benefits of the application of Controlled Structures Technology to a space-based astronomical interferometer requiring large baselines and precision alignment. A detailed description of the testbed, its scientific motivation, performance metric, disturbances, sensors, and actuators can be found in Reference [17]. The following section gives a brief synopsis of the relevant details.

The results of this chapter demonstrate that the approach taken in this thesis yields better performance on a complex laboratory structure than a constant gain feedback approach such as rate feedback. The results are also compared with a passive damping scheme. In addition, a number of implementation issues are discussed, such as the choice of dual sensors, and the computation of the dereverberated transfer function from experimental data.

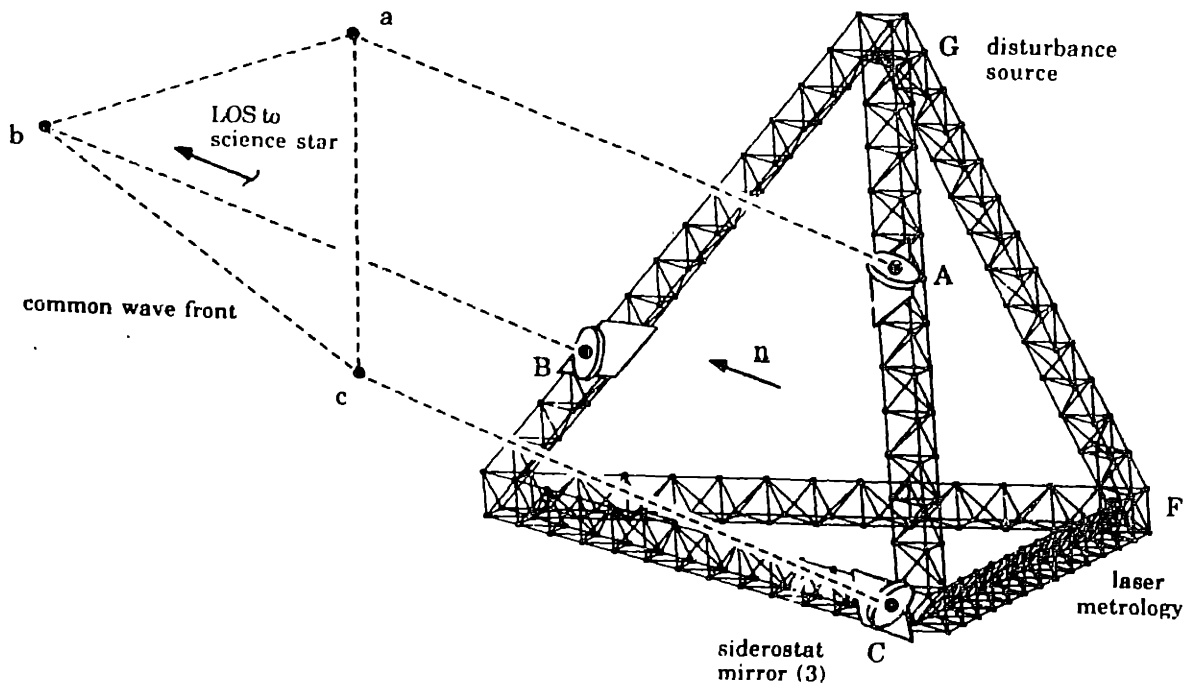

Figure 7.1: Definition of geometry for testbed performance metric

7.1 Interferometer Testbed Description

The interferometer testbed is a $1/10^{th}$ scale model of the reference space-based mission. Six 3.5 meter long triangular truss legs form a tetrahedron, as shown in the schematic in Figure 7.1 (from [17].) A picture of the interferometer is also included as Figure 7.2. Three mock siderostats, labelled A, B, and C in the schematic, are located on three of the legs of the truss. Light from the science star would be collected by these siderostats, and combined at the vertex labelled F, out of the plane of the three siderostats. A laser is mounted at this vertex in order to provide an optical measurement of the pathlength between this vertex and each of the three siderostat locations. The absolute pathlengths between each of the siderostats and the collecting optics will be denoted AF, BF, and CF. For the sake of brevity, the difference between any two of these pathlengths will be denoted A–B, B–C, and C–A, rather than AF–BF, BF–CF, and CF–AF.

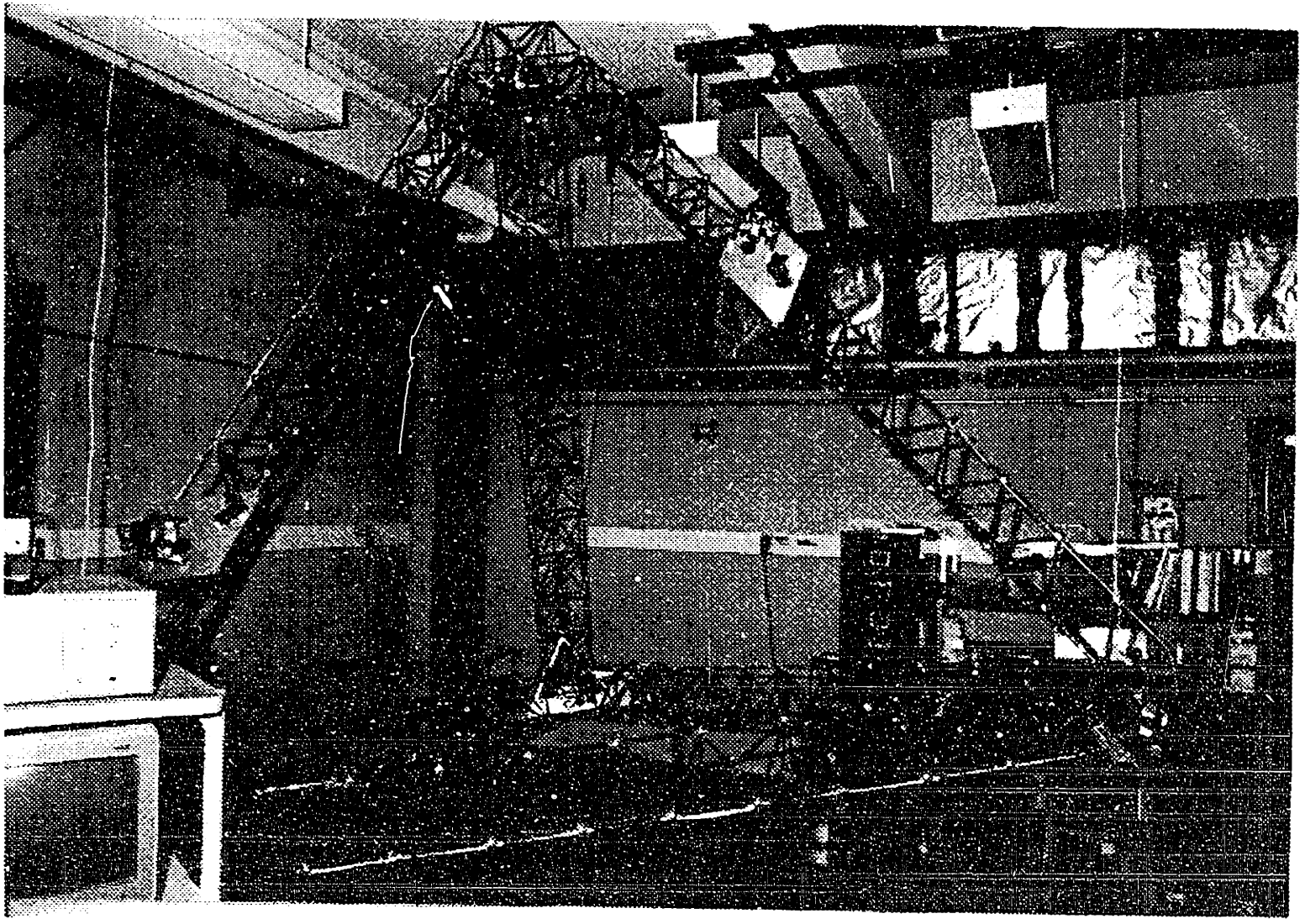

Figure 7.2: The SERC Interferometer Testbed

7.1.1 Performance Metric

The full-scale interferometer combines light received from a pair of siderostat locations, and determines information about the science star by measuring the phase difference between the two light waves. A number of these measurements taken at different baseline lengths and orientations builds up an image of the star. The image quality is primarily dependent on the accuracy of the differential phase measurement. Thus, it is essential that the difference between any two pathlengths from siderostats to collecting optics be maintained to within a fraction of the wavelength of the light. On the testbed, therefore, the performance goal for structural control is to maintain each of the three possible differential pathlength (DPL) measurements to below 50 nm rms displacement between 10 and 500 Hz. The laser signals are sampled by a real-time computer at 1800 Hz.

The full description of the performance problem includes information about the disturbances impinging upon the structure. Three piezoelectric disturbance sources are mounted at the vertex labeled G in Figure 7.1. The force spectrum for these actuators is not that specified in [17]. Instead, a simpler spectrum has been implemented, which is flat at low frequencies, with a two-pole roll-off at 70 Hz. Additional disturbances from the ambient laboratory environment are also averaged into the rms performance measurements, although the contributions from these are minor.

The majority of the differential pathlength signal energy is below the maximum frequency considered of 500 Hz. The open-loop performance of a particular differential pathlength, A-B, is shown in Figure 7.3, taken with no active or passive damping struts in the structure. The contribution to the DPL in different frequency regimes is shown in the results section for comparison with the closed loop data, in Figure 7.20. On average, for the three different differential pathlengths, over 85% of the mean-square displacement occurs above 80 Hz. The current finite element model of the structure does not accurately predict the modal frequencies or mode shapes above 80 Hz. Thus any active control for this frequency region must either be based on a measurement model, or use an approach that does not rely on precise knowledge of the modal frequencies.

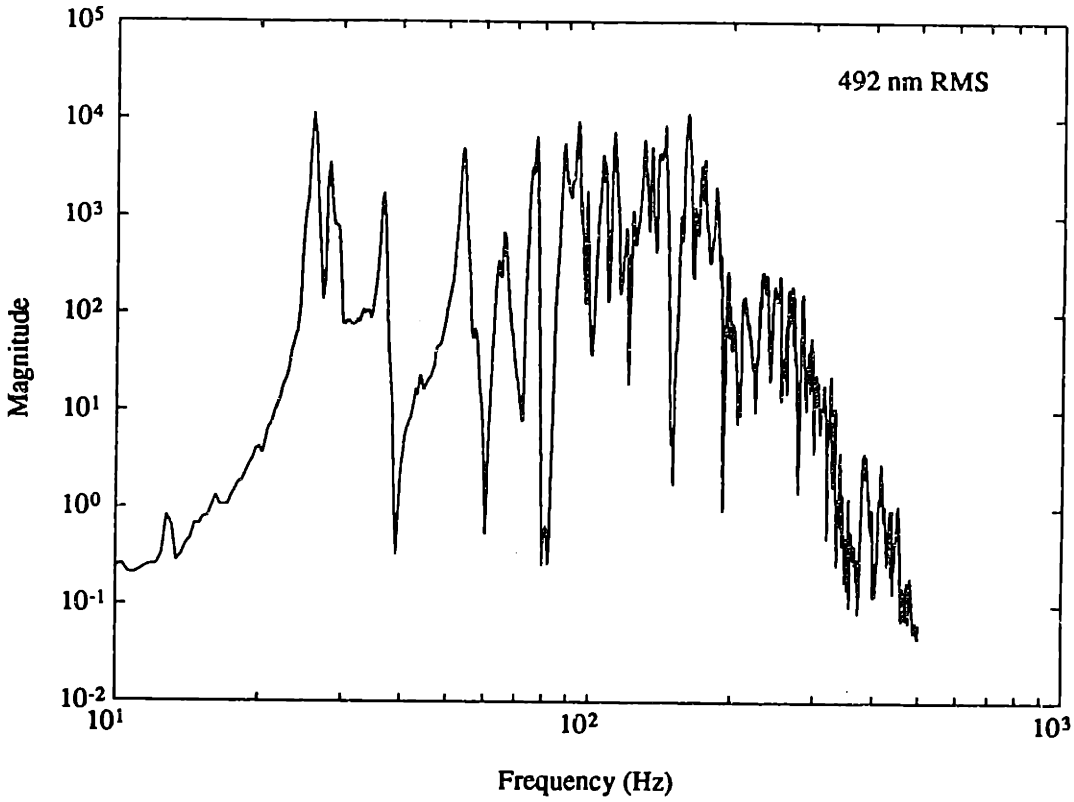

Figure 7.3: Autospectrum of open-loop differential pathlength A–B, in nm^2/Hz.

7.1.2 Control and Damping Hardware

There are a variety of sensors and actuators available for feedback on the interferometer testbed. For the low authority control experiments, the actuators used were active struts. These struts can replace any single strut on the interferometer truss, giving the control designer a great deal of flexibility in placement. Each active strut contains a pre-loaded piezoceramic strut made by Physik Instrumente. A strain gauge is mounted on the piezo stack, and a load cell is mounted in the load path of the strut. An active strut, mounted in the testbed, is shown in Figure 7.4. The picture shows the strut with two accelerometers mounted to sense axial motion. These were not present during the experiment. In addition to the piezoceramic strut and the load cell, the active strut shown includes a spacer, and a steel flexure to prevent out of plane forces and moments from being transmitted to the strut. Properties of the

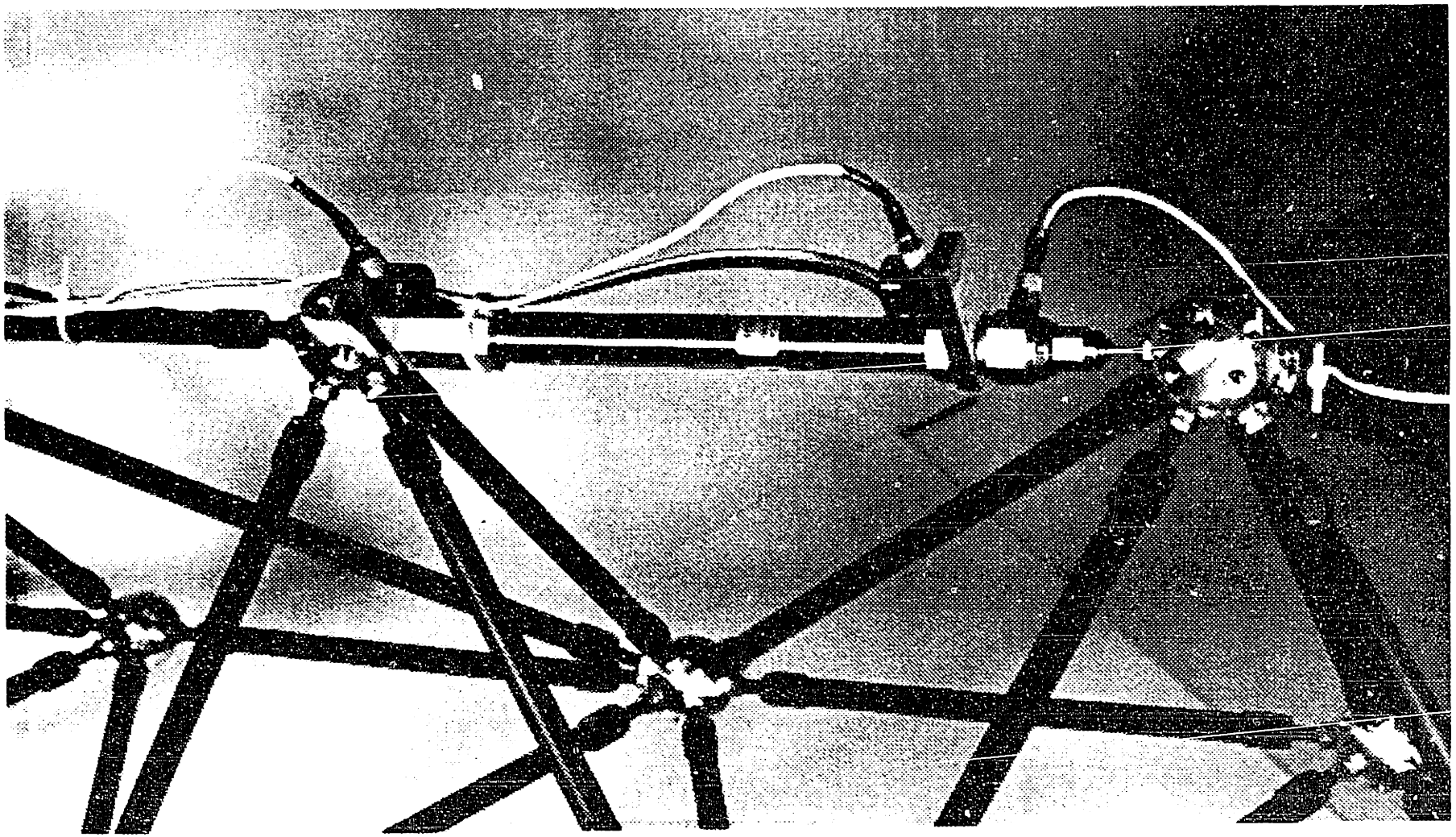

Figure 7.4: Active strut for the SERC interferometer testbed

Description	Value
Load cell gain	11.24 mV/N
Strain gauge gain	0.115 V/μm
Piezo gain	0.9 μm/V

Table 7.1: Active strut sensor and actuator properties

actuators and sensors in an active strut are given in Table 7.1. The piezoelectric actuator induces a strain under an applied voltage, and this results in a net elongation of the active strut. The gain between these is not exactly linear, and it is the low amplitude asymptote that is given in Table 7.1.

High authority control of the interferometer testbed will use a real-time digital computer for implementation. However, the maximum sample rate of the currently available computer in SERC is about 3000 Hz. With a full sample delay for computation, and another half sample delay for the zero order hold, there is a 36° phase lag at 200 Hz due to the time delay. The low authority control scheme should provide a performance improvement at frequencies up to about 200 Hz. The contribution to the rms pathlength above this frequency is small. Because a low authority controller relies on phase stabilization, the compensator must remain positive real at frequencies much higher than that at which performance is desired. Thus the time delay of the digital computer is unacceptable. Instead, the low authority control should be implemented using analog circuits. This is not difficult, since each controller is relatively low order, and all of the compensators are SISO. To simplify the implementation, an analog computer was used. In a realistic application, significantly smaller, lightweight components would be used instead.

Since the goal of low authority control is generally to add active damping, the active approach can also be compared with a passive damping approach. There are several passive damping augmentation devices available for the testbed. A high loss factor viscous strut was used, that can be interchanged with any strut on the structure. These "D-struts" are manufactured by Honeywell, and have been employed in several

CST (Controlled Structures Technology) projects [1,2,76]. Each strut has a stiffness comparable to the dynamic stiffness of the structure at 50 Hz, and a peak loss factor between $\eta = 1$ and $\eta = 1.5$ which occurs between 55 and 70 Hz. These struts are designed to add significant damping in a relatively narrow frequency range, similar to the goal of low authority control.

7.2 Control System Design

7.2.1 Actuator Placement

Two active struts were sufficient to demonstrate the effectiveness of the control design techniques. Using a second strut demonstrates that the two low authority control laws can be designed and implemented independently without difficulty. Since only a relatively small performance improvement can be achieved by actively damping a single strut out of the 641 struts that make up the testbed, each additional active strut used also makes the differences between control design methods more visible. Thus, more struts would have been preferable, but not essential for comparing control design approaches.

In order to get sufficient control authority over those modes that strongly influence the performance metric, the active struts were placed close to two of the siderostat plates, denoted A and B in Figure 7.1. Placement schemes based on maximum residue locations of the finite element model are inconsistent with the assumptions of poor modal information that require low authority control; much of the benefit of low authority control is provided in a frequency region above that in which the finite element model is valid. Using engineering intuition, however, is essential. The strut locations that were selected are on the truss longeron that is behind, but not attached to the siderostat plates. (Strut numbers 6207 and 3304.) These locations, shown schematically in Figure 7.5, should be capable of significant authority over the absolute pathlengths A and B. An extension/compression of these struts results in a pistoning motion of the siderostat plates. (Using the current finite element model,

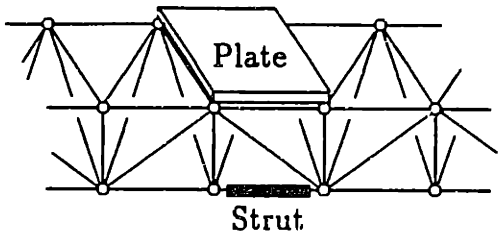

Figure 7.5: Active strut placement in truss

these locations are not optimal; indeed they are the 45^{th} and 31^{st} best locations, respectively. It is unclear how much of an increase in performance reduction could be achieved with the struts in the best possible location, and whether these locations can be better predicted.)

7.2.2 Sensor Selection

The active strut, as described earlier, has a piezoelectric stack as an actuator, and both a strain gauge and a load cell available for feedback. Both of these sensors can be considered to be collocated, since the frequency at which non-collocation becomes important is much higher than required. However, for impedance matching control, the actuated and sensed variable should also be dual, in the sense that their product should be the power flow into the structure. The dual variable to the actuator variable must be obtained from some combination of the two sensors available.

The effect of the active strut actuator depends on the structure in which it is placed. The piezoelectric is a transformer, where the across and through variables on one port are the electrical voltage and the current, and the variables on the other port are the mechanical strain and stress. Applying a voltage to the piezo stack induces a strain. If the strut is mechanically free, this applied voltage results in an extension of the strut, and the strut therefore acts as a displacement actuator. If the strut is mechanically clamped, then the induced strain results in a force being applied. In a real structure, the actuator provides neither pure force, nor pure displacement. The relationship between strut displacement δ, compressive force F and an applied

voltage V is given, from [16], by

$$\frac{d_{33}V}{h} = \frac{\delta}{\ell} + \frac{F}{EA} \tag{7.1}$$

where d_{33} is a material constant, h is the stack thickness, ℓ is the length of the strut, and EA is its axial stiffness.

For passive damping applications, it is probably desirable to have a strut that is impedance matched to the structure. For active control, this is less relevant, since the strut properties can be modified actively. Indeed, it is easier to use a strut that is at one of the extremes; either a pure force, or a pure displacement actuator. The best control law for an active strut that is at neither extreme is to first apply a feedback law that converts the strut into one of the two pure forms. This can be shown by the following argument.

The goal of the impedance matching approach is to dissipate maximum power by constraining the relationship between the power dual variables at the actuator/sensor location to be some frequency dependent compensator $K(s)$. Provided that this constraint is satisfied, the feedback architecture used to achieve it is irrelevant. Since force and displacement rate are power dual, this goal can be stated as $F = K(s)\cdot(s\delta)$. If the strut satisfies Equation (7.1), then either of the following control laws would enforce the desired impedance:

$$V = \frac{h}{d_{33}\ell}\left(\frac{1}{K(s)} + s\frac{\ell}{EA}\right)\frac{F}{s} \tag{7.2}$$

or

$$V = \frac{h}{d_{33}EA}\left(K(s) + \frac{1}{s}\frac{EA}{\ell}\right)s\delta \tag{7.3}$$

In each of Equations (7.2) and (7.3), the second term within the brackets is the feedback that is required to convert the strut to a pure displacement, or a pure force actuator, respectively. Both forms are equivalent, and will dissipate exactly the same power from the structure. Furthermore, once a feedback loop has been used to convert the actuator into either a pure displacement, or a pure force actuator, the required feedback law (either $K(s)$ or $1/K(s)$) can be obtained by impedance matching arguments, since the dual sensor is available.

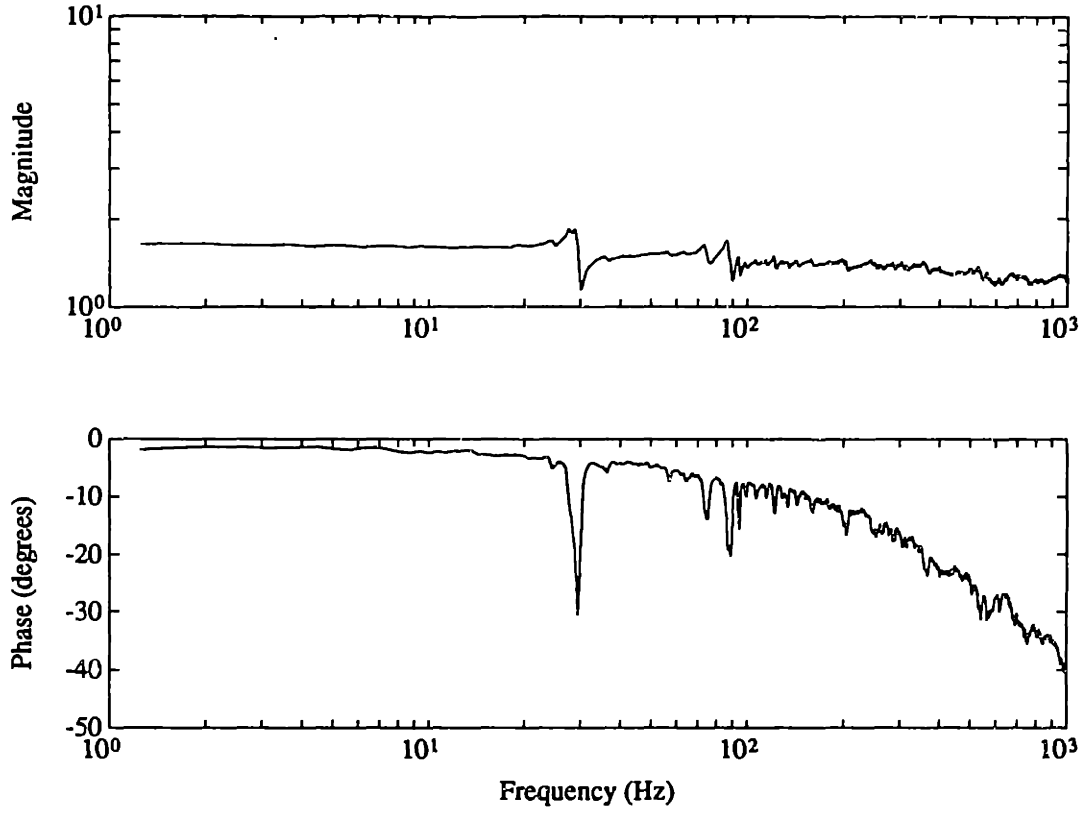

Figure 7.6: Transfer function between active strut voltage and strain, plate B

Ideally, one would like to write Equations (7.2) and (7.3) as a feedback using the optimal impedance matching compensator from a single sensor signal that includes contributions from both the force and the displacement. This sensor would therefore be the "dual" sensor to the mixed force/displacement actuator. However, even if the new sensor is allowed to be a frequency dependent mix of the dual sensor for the extreme cases, it is not clear that a dual sensor to the mixed actuator exists that does not depend explicitly on the desired impedance match $K(s)$.

In the interferometer testbed, the procedure described in the previous paragraphs is unnecessary. The active strut is significantly stiffer than the dynamic stiffness of the rest of the structure in the frequency range of interest, and therefore commands displacement. This is illustrated by the transfer function between the applied voltage and the strain signal, shown in Figure 7.6 for the active strut behind siderostat plate B (referred to as strut B.) The transfer function is almost flat, indicating that the sensed

strain is almost exactly a gain times the applied voltage. The transfer function between voltage and strain at siderostat plate A illustrates a similar conclusion for strut A. For comparison, the voltage to force transfer functions for the two active struts are shown in Figures 7.7 and 7.8.

Since the actuator commands displacement, it also effectively commands the extension rate of the strut. The dual variable to extension rate is force, and thus the impedance matching solution requires that the extension rate and force be related through a compensator. Equivalently, the transfer function between the extension and the integral of force can be constrained. Thus, the integral of force should be fed back to the voltage signal. This yields a form similar to that in Equation (7.2), where now the second term within the brackets is negligible. Integral of force feedback has been used elsewhere for stiff actuators (see for example [79].)

7.2.3 Dereverberated Transfer Function

In order to design impedance matching compensators between the integral of force and the stack voltage, the dereverberated driving point transfer function must be identified. In this case, the transfer function of interest is the impedance (velocity to force), rather than the mobility (or force to velocity). As noted in Chapter 2, the dereverberated transfer function can be determined by averaging the log magnitude of the experimental transfer function.

The dereverberated impedance includes only the effect of the direct field, and not the reverberant field. Since complex poles are associated with oscillation, or reverberation, it should be possible to describe the dereverberated transfer function using only real poles and zeroes. Hence, write that

$$G(s) = k\frac{\prod_{i=1}^{n_z}(s+b_i)}{\prod_{i=1}^{n_p}(s+a_i)} \tag{7.4}$$

where $b_i \geq 0, i = 1,\ldots,n_z$, and $a_i \geq 0, i = 1,\ldots,n_p$. The number of poles is n_p, and the number of zeroes n_z is either n_p or $n_p - 1$. Fitting the log magnitude of the

measured reverberant transfer function $G_{exp}(s)$ with $G(s)$ constrained to be of this form should give the dereverberated transfer function.

The cost functional for the fit is given by

$$J = \int_0^\infty (\log|G_{exp}| - \log|G|)^2 \, d(\log\omega) \tag{7.5}$$

$$= \int_0^\infty \left(2\log|G_{exp}| - 2\log k - \sum_{i=1}^{n_z} \log\left(\omega^2 + b_i^2\right) + \sum_{i=1}^{n_p} \log\left(\omega^2 + a_i^2\right)\right) d(\log\omega) \tag{7.6}$$

The gradients were computed analytically, and the minimization performed using a BFGS quasi-Newton search routine similar to that described in Section 5.3.2 that was used to minimize the stochastic cost functional of Chapter 4. The number of poles used to describe the dereverberated impedance was increased until there was no significant decrease in the cost J. For both of the active strut transfer functions, three poles were found to be adequate to describe the dereverberated transfer function between applied voltage and the integral of the force sensor output, in the frequency range of interest. These transfer functions are plotted, together with the corresponding measured transfer functions, in Figures 7.7 and 7.8.

The transfer functions plotted are positive real up to 622 Hz, and are within 10° of positivity up to 1500 Hz, where the dynamics of the actuator and sensor, or the non-collocation becomes important. These transfer functions also assume perfect integration. In reality, the integrator low frequency roll-off determines a low frequency limit to positivity as well.

7.2.4 Impedance Matching

The compensator that dissipates the maximum power from a structure is the impedance match given by Equation (2.3). Since both dereverberated transfer functions are frequency dependent, this optimization yields a non-causal transfer function, which cannot be implemented, and must be approximated. In the beam example of Section 6.2, the dereverberated mobility was calculated exactly from the wave model for the beam. As a result, the computed non-causal compensator would, if implemented, dissipate all of the vibrational energy that arrives at the controlled end. Also, since

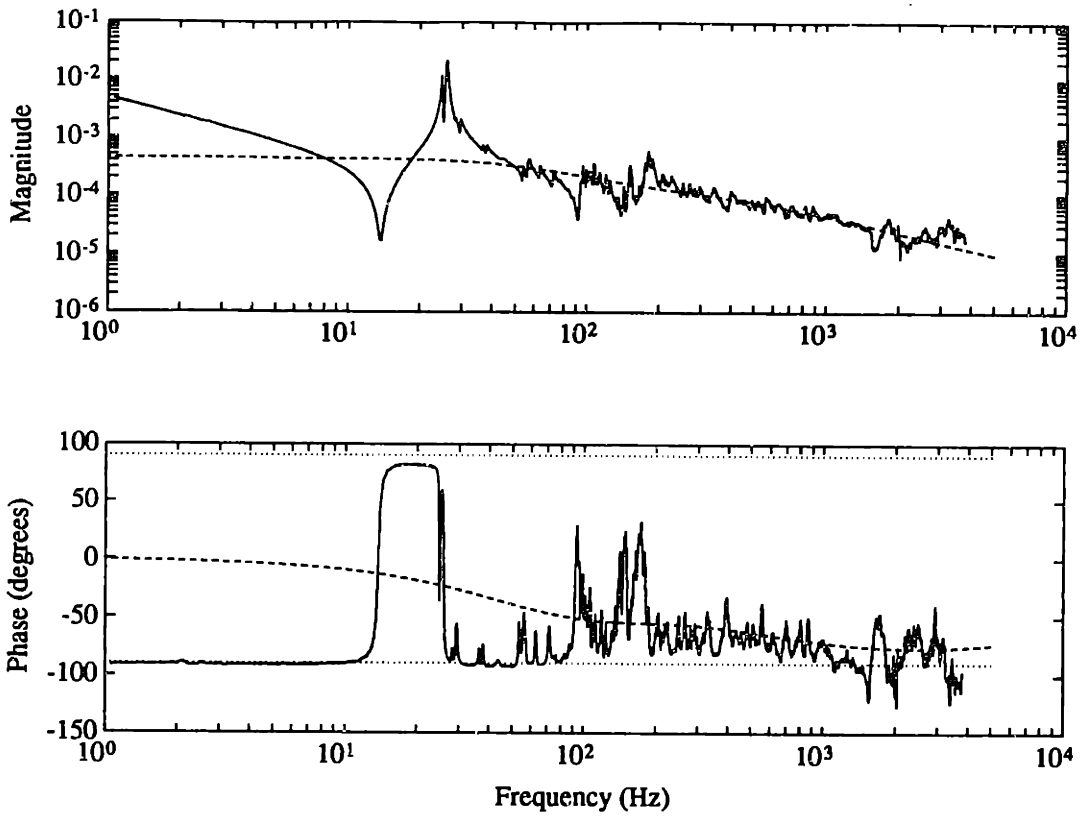

Figure 7.7: Measured (solid) and dereverberated (dashed) transfer function between active strut voltage and integrated force near plate A. (In Volts/Volt.)

all vibration on the beam involves reflections off of the controlled end, the beam could be critically damped with such a controller. On the experimental structure, the dereverberated impedance is at best an approximation of the real dereverberated transfer function, so perfect matching cannot be attained even with a non-causal compensator. Furthermore, if the perfect non-causal impedance match could be implemented, there would still be vibrational energy in the structure associated with reflections off of other locations.

The simplest approximation to the desired impedance match that can be made is to constrain the compensator to be simply a constant gain. The optimal gain at a given frequency ω_0 can easily be shown to be the magnitude of the non-causal solution at that frequency, so

$$K_C = \frac{1}{G(j\omega_0)} \tag{7.7}$$

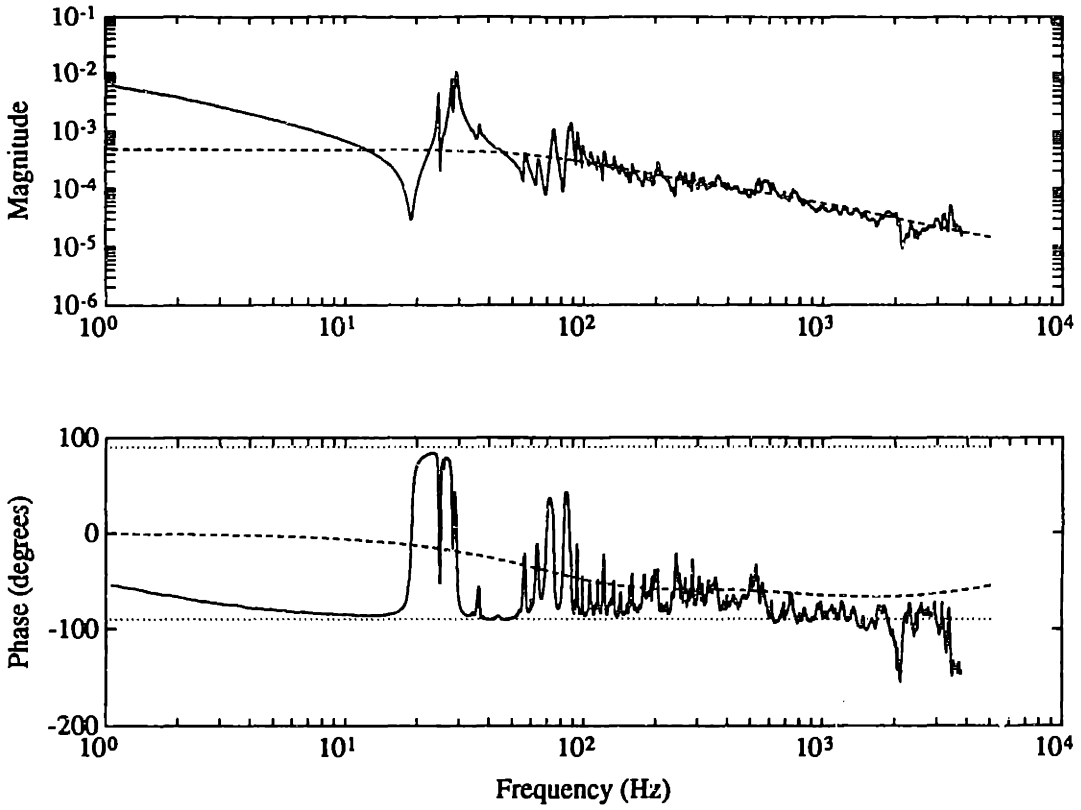

Figure 7.8: Measured (solid) and dereverberated (dashed) transfer function between active strut voltage and integrated force near plate B. (In Volts/Volt.)

This is the "rate feedback" solution. (The constant gain solution only corresponds to feedback of rate for a force actuator. For any other actuator, constant gain impedance matching generalizes the concept of rate feedback.) This solution will be compared in the experiment to the stochastic optimal solution.

7.2.5 Stochastic Optimum

Now consider the design of compensators using the technique developed in Chapter 4. As noted in the introduction, there are several different reasons for using low authority control. In most structural control problems, a high authority compensator can probably be designed with a sufficiently high bandwidth to meet performance specifications, provided that a low authority controller adds some damping to a few modes in the roll-off region of the HAC. This requires that damping be added to the

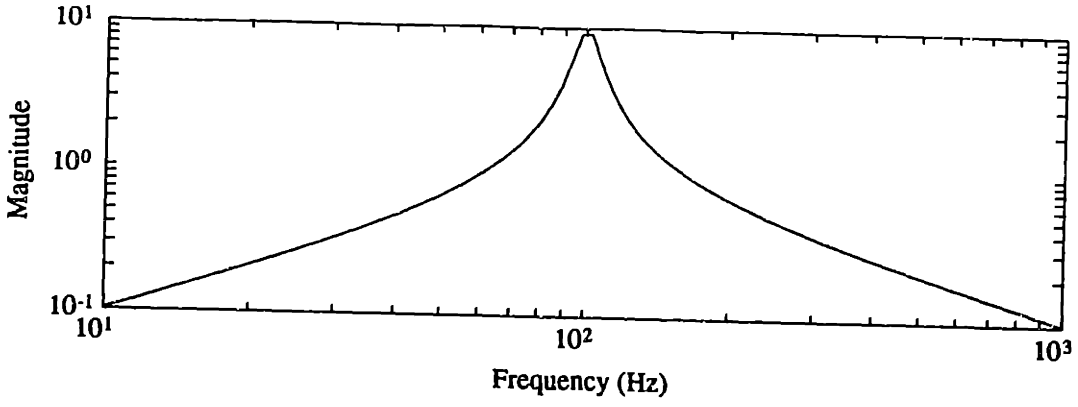

Figure 7.9: Narrowband weighting function used in control design

structure in a narrowband frequency region that is specified by the demands of the HAC, and not by the disturbance input power or performance metric. While this may be the more common purpose of a LAC, in the case of the interferometer testbed, the bandwidth of the disturbance and performance specification, combined with the errors in the model, require that the low authority controller provide a more direct performance benefit. The frequency distribution of the active damping requirements for such a case are dictated by the disturbance input power, and the performance, as described in Chapter 4.

In order to meet a narrowband requirement, the product $C(\omega)\Pi_{in}(\omega)$ in Equation (4.35) can be viewed simply as a weighting function that describes the relative important of different frequency regions. A weighting function was chosen to result in the most dissipation possible near a single frequency, ω_0. With $W^*(j\omega)W(j\omega) = C(\omega)\Pi_{in}(\omega)$, the chosen weighting function $W(j\omega)$ is given by

$$W(s) = \frac{\omega_0 s}{s^2 + 2\zeta_0\omega_0 s + \omega_0^2} \tag{7.8}$$

This function is plotted in Figure 7.9 for a central frequency $\omega_0 = 100$ Hz, and $\zeta_0 = .05$. Using the three-pole fit of the dereverberated impedance, and the numerical optimization approach described in Section 5.3.2, optimal compensators were designed to minimize the expected cost using this weighting function. For both strut locations, compensators with a single pole-zero pair were sufficient; increasing the compensator order did not appreciably change the cost. Since the dereverberated

impedance is represented with only real poles and zeroes, it does not have a strong frequency dependence near the center frequency ω_0, and hence neither does that of the desired, non-causal compensator. The causal compensator is also unlikely to have a strong frequency dependence near ω_0. Thus, although the weighting function chosen is narrowband, one should expect that the achieved damping will not be as strongly frequency dependent.

In order to meet the more broadband requirements of the actual disturbance and performance environment of the testbed, the appropriate weighting function must be determined. The spectrum of the input power could be determined from Equation (4.30) by measuring the dereverberated transfer functions at the disturbance input location, since the spectrum of the disturbance is known. Similarly, the effect of modal energy in each frequency region upon the differential pathlengths could be determined. Rather than attempting to describe each of these functions independently, however, their product can be determined directly from the experimentally measured transfer function from disturbance to performance.

The cost in Equation (4.35) is obtained by adding a frequency dependent function to the original cost. From Equation (4.33), the expected value of the performance, without this addition, is

$$J = \int_{-\infty}^{\infty} \frac{C(\omega)\Pi_{in}(\omega)}{(I - \gamma^{-2}H^*H)}\, d\omega \tag{7.9}$$

If the perfect impedance match were implemented, then the closed loop power reflection coefficient H would be zero, and the structure would be completely damped. Thus the weighting $W(j\omega)^*W(j\omega) = C(\omega)\Pi_{in}(\omega)$ is the performance at each frequency if the structure were completely damped. But as noted before when discussing the computation of the dereverberated impedance, the damped transfer function can be computed from experimental data by fitting the log magnitude with a function constrained to have only real poles and zeroes. The same fitting software can be used as before. The resulting seven pole weighting function $W(j\omega)$ obtained by fitting the transfer function between the disturbance and the absolute pathlength from siderostat B to vertex F is shown in Figure 7.10, along with this transfer function. The filter that shapes the spectrum of the disturbance is included in the transfer

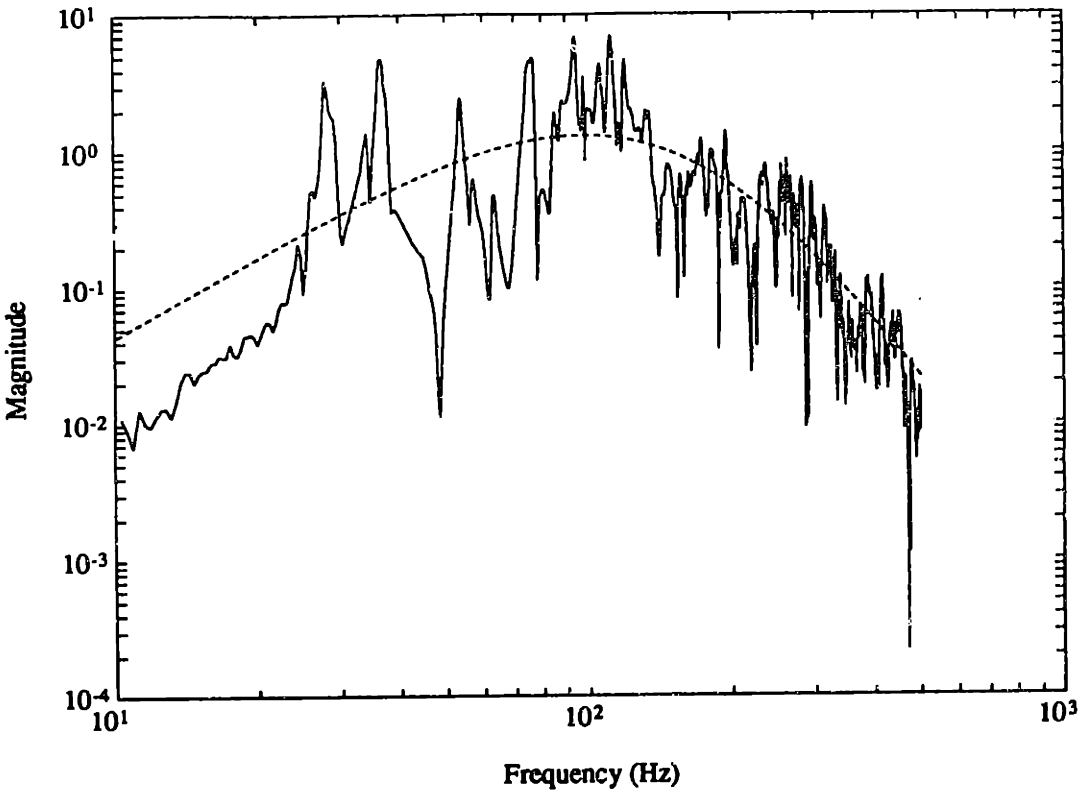

Figure 7.10: Broadband weighting function used in control design (dashed), and transfer function from disturbance to siderostat B absolute pathlength (solid).

function. The absolute pathlength was used rather than a single differential pathlength, because all three DPL's contribute to the performance. Since strut B can be expected to minimize the performance primarily through minimizing the absolute pathlength of siderostat B, this transfer function provides a reasonable estimate of the influence of the disturbance on the total performance, as seen by strut B. The weighting function resulting from the fit to any absolute or differential pathlength is similar, and using a different pathlength does not appreciably change the resulting "optimal" compensator. Again, the optimal compensators obtained required only a single pole/zero pair.

The weighting function obtained by this method has a maximum at about 100 Hz. The central frequency ω_0 in both the constant gain feedback, Equation (7.7), and in the narrowband solution, Equation (7.8), was also chosen to be 100 Hz, for compar-

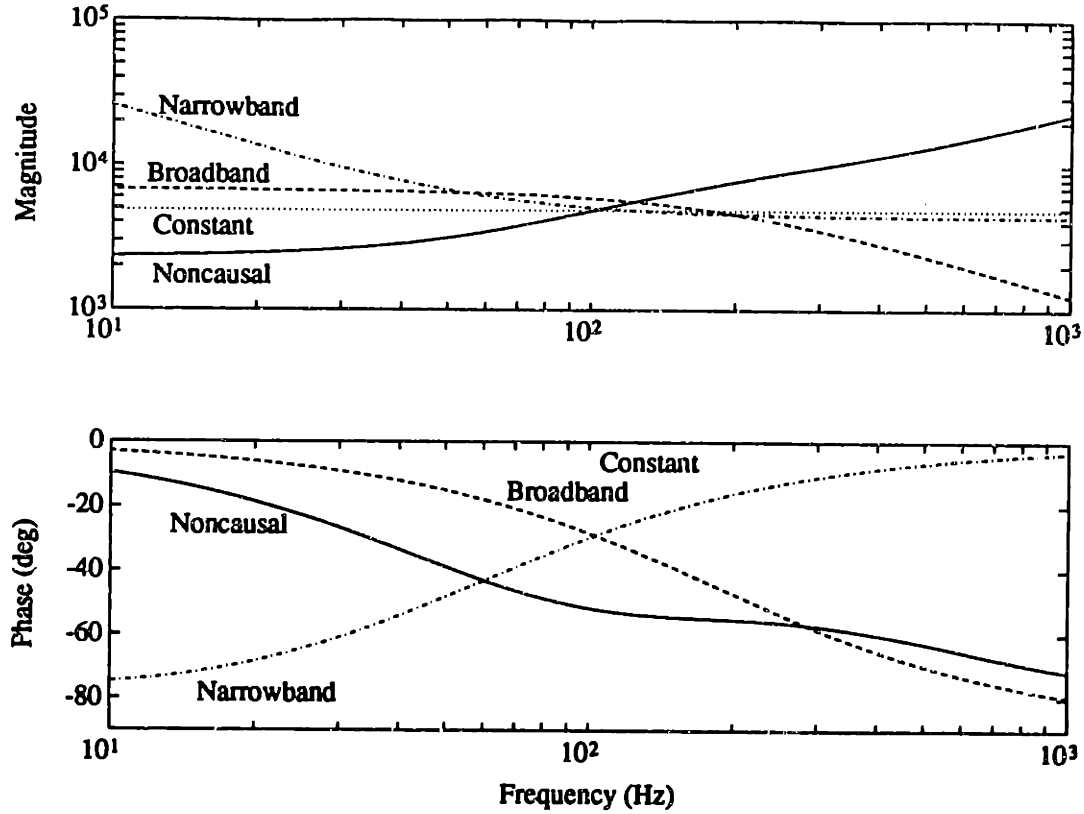

Figure 7.11: Compensators for active strut at plate A. Non-causal optimum (solid), constant gain solution (dotted), broadband stochastic optimum (dashed) and narrowband solution (dash-dot).

ison. Without a high authority compensator to drive the narrowband requirement, the decision as to the frequency at which to center the performance is somewhat arbitrary. A frequency of 100 Hz is perhaps high, but not unrealistic. The choice of center frequency for the constant gain compensator follows since it was implemented only to provide a comparison with the stochastically optimal compensators.

The resulting compensators are shown in Figure 7.11 for the strut at siderostat plate A, and in Figure 7.12 for the strut at plate B. Greater damping is obtained by the frequency dependent compensators by more closely matching both the magnitude and phase of the non-causal optimum at the center frequency of the weighting function. The closed-loop power reflection coefficient H for each of the compensators is plotted in Figures 7.13 and 7.14. A value of unity indicates that all of the incoming

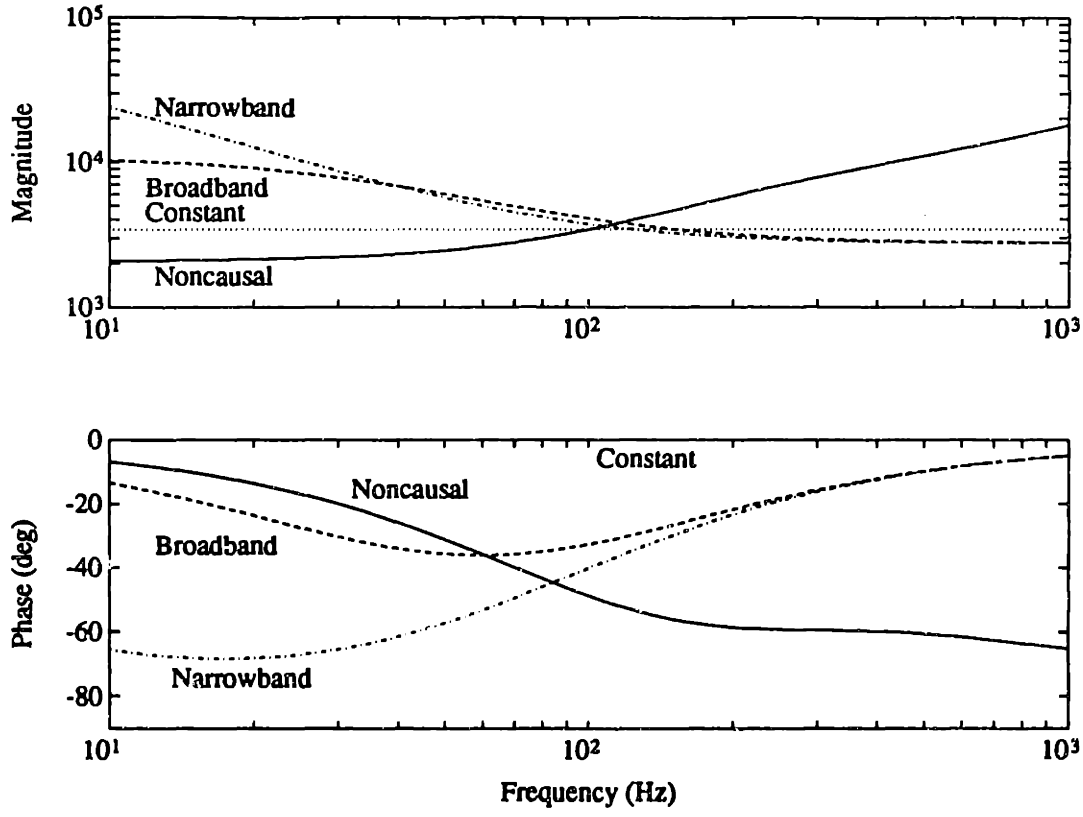

Figure 7.12: Compensators for active strut at plate B. Non-causal optimum (solid), constant gain solution (dotted), broadband stochastic optimum (dashed) and narrowband solution (dash-dot).

power is being reflected, and there is no dissipation, while a value of zero indicates the "complete" dissipation attained by the ideal non-causal impedance match at that frequency. While the constant gain compensator was chosen to maximize dissipation at $\omega_0 = 100$ Hz, it achieves its best damping at lower frequencies due to the fact that the experimentally determined dereverberated impedance is almost constant at low frequencies, and thus any constant gain feedback has the correct phase in this frequency region.

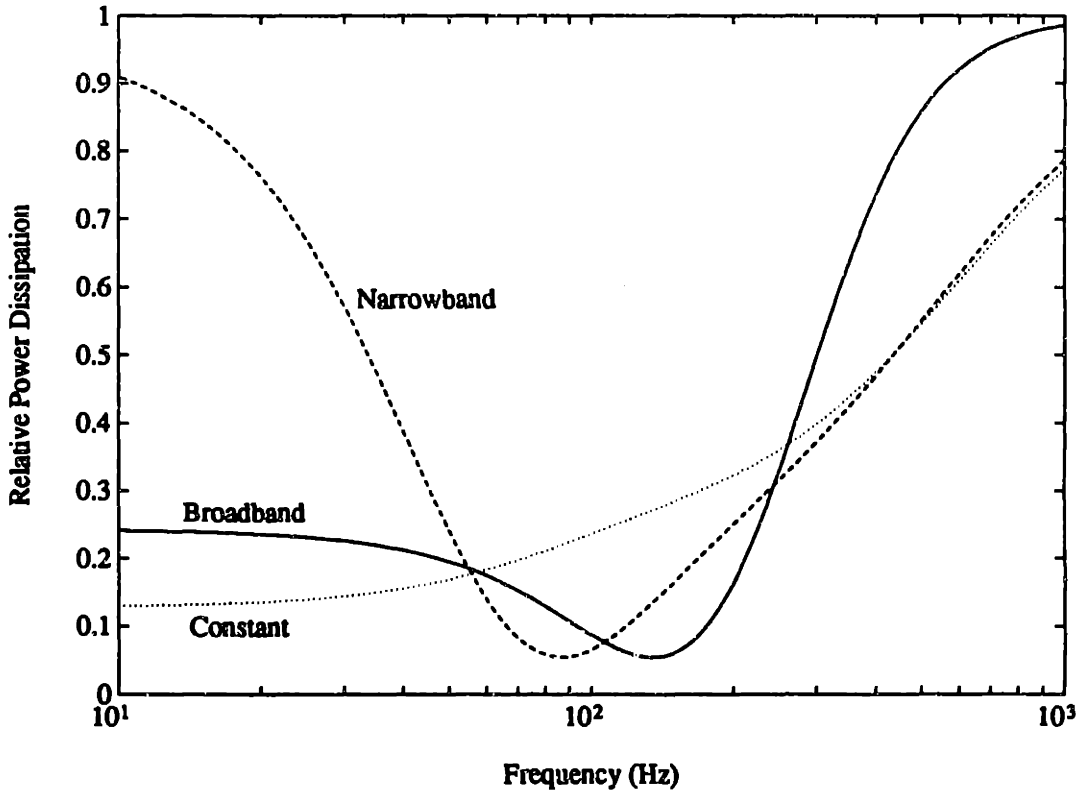

Figure 7.13: Relative power dissipation for compensators at plate A. Constant gain solution (dotted), broadband stochastic optimum (solid) and narrowband solution (dashed).

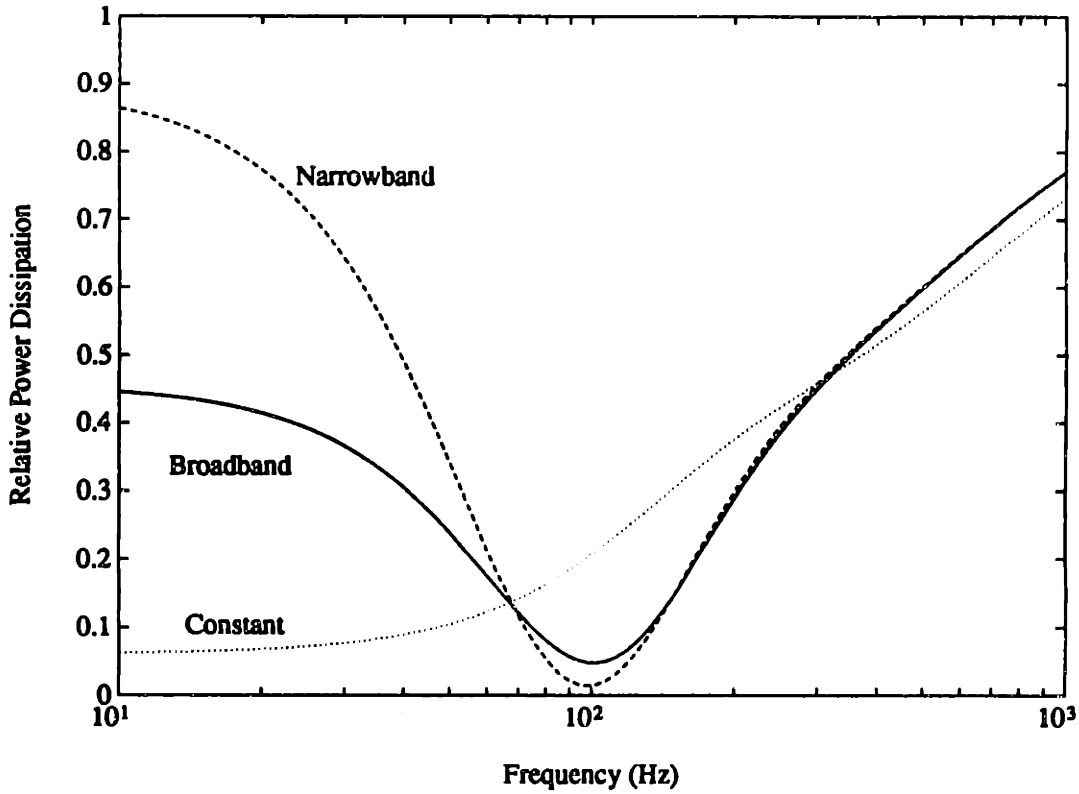

Figure 7.14: Relative power dissipation for compensators at plate B. Constant gain solution (dotted), broadband stochastic optimum (solid) and narrowband solution (dashed).

7.3 Implementation

As noted earlier, the compensators were implemented on an analog computer. These compensators were designed for the power dual variables of integrated force to displacement. Thus all of them required an integration of the load cell output. This integrator was rolled off at low frequencies to prevent saturation. The integrator transfer function was

$$K_{\text{int}} = \frac{s}{s^2 + 2\zeta_i\omega_i s + \omega_i^2} \tag{7.10}$$

The dereverberated model of the structure is not valid below the first mode, which is at about 20 Hz, and thus no control authority is desired below this frequency. High gain at low frequency results in destiffening the structure, which is likely to increase (worsen) the performance, rather than decrease (improve) it. Thus a relatively high value for ω_i is desired. However, the design gain and phase of the compensators should be maintained as close to the first mode as possible, and particularly above about 50 Hz where more low authority control performance is desired. A further constraint on the integrator poles results from the requirement of closed-loop stability. While the true collocated and dual transfer function is positive real, the phase contribution of the integrator at low frequencies results in a deviation from positivity. This places a lower bound on the integrator pole frequency in order to allow sufficient roll-off of the compensator. This bound varies between about 1 Hz for the constant gain compensators, up to almost 10 Hz for the narrowband solution, depending on the low frequency gain of the desired compensator. The final values of $\omega_i = 11.25$ Hz and $\zeta_i = .7071$ were chosen as a compromise between the various requirements, and kept constant for all implemented compensators.

The implemented transfer functions were:

$$K_{CA} = 4834\frac{s}{s^2 + 100s + 5000} \tag{7.11}$$

$$K_{CB} = 3418\frac{s}{s^2 + 100s + 5000} \tag{7.12}$$

$$K_{NA} = 4400\frac{s}{s^2 + 100s + 5000} \cdot \left(1 + \frac{361}{s + 6.09}\right) \tag{7.13}$$

$$K_{NB} = 2759\frac{s}{s^2 + 100s + 5000} \cdot \left(1 + \frac{548}{s + 20.7}\right) \tag{7.14}$$

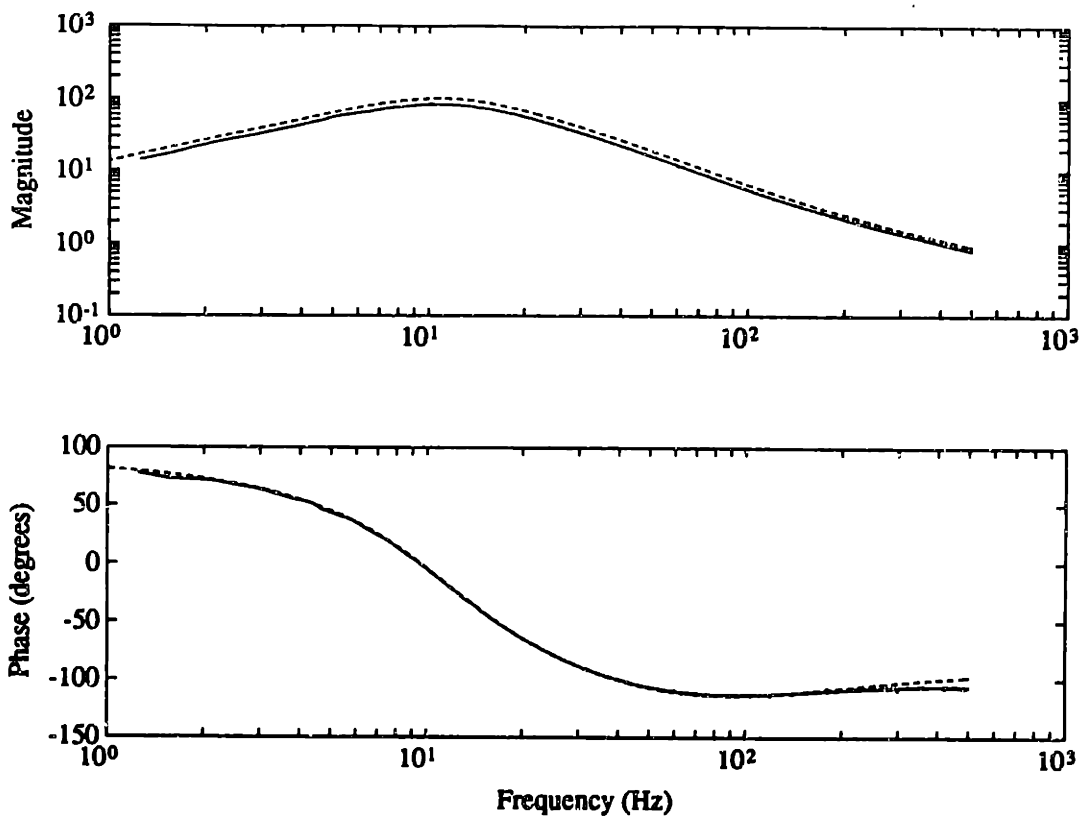

Figure 7.15: Comparison of implemented (solid) and desired (dashed) broadband, stochastically optimal compensators at plate B.

$$K_{BA} = 7840 \frac{s}{s^2 + 100s + 5000} \cdot \left(\frac{1000}{s + 1164} \right) \tag{7.15}$$

$$K_{BB} = 2759 \frac{s}{s^2 + 100s + 5000} \cdot \left(1 + \frac{548}{s + 191} \right) \tag{7.16}$$

The first subscript on the compensator refers to whether it is the constant gain (C), narrowband stochastic solution (N), or broadband stochastic solution (B). The second refers to the strut location, A or B, for which the compensator was designed. A typical comparison between the implemented and desired compensators is shown in Figure 7.15, for the broadband compensator at siderostat plate B (K_{BB}).

A typical loop transfer function is shown in Figure 7.16, again for the broadband compensator at siderostat B. This transfer function indicates that the closed loop system will be stable. The loop tranfer function also indicates that the correct gain (approximately) has been implemented; the magnitude of the loop transfer function should be unity at the frequency where the most damping is to occur.

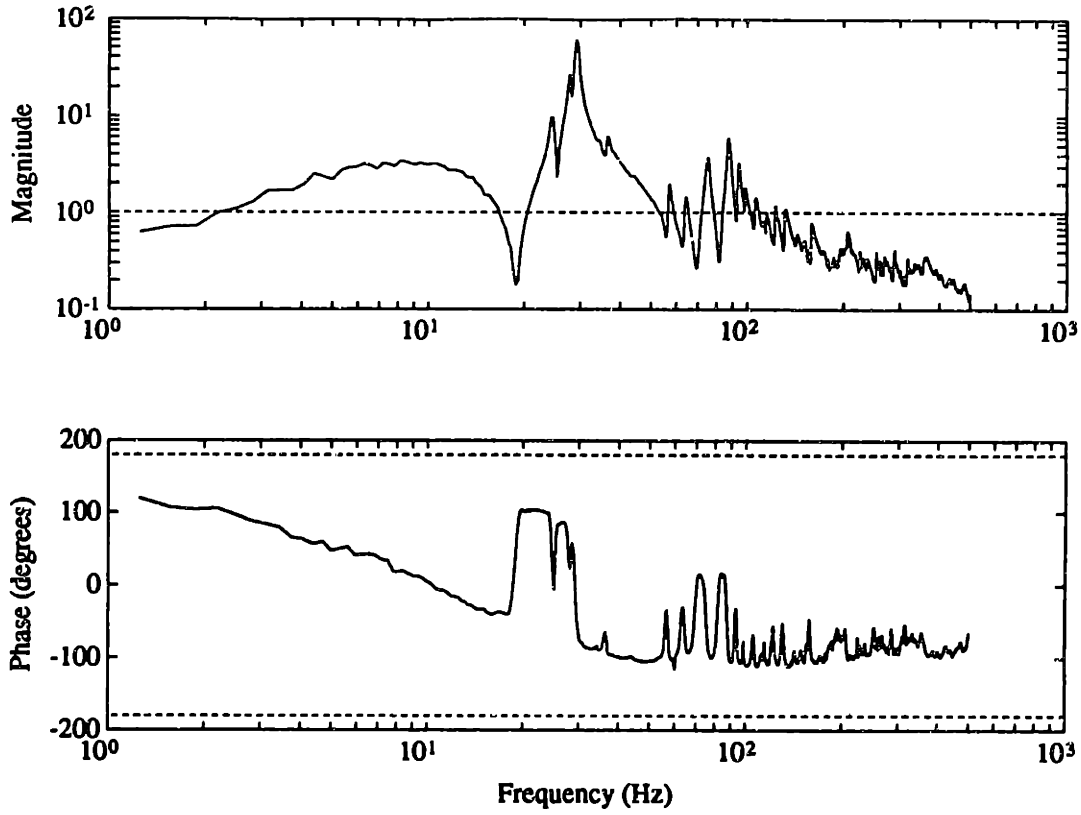

Figure 7.16: Measured loop transfer function for broadband, stochastically optimal compensators at plate B.

7.4 Results

The difference in performance between the implemented narrowband and broadband stochastic solutions was small. One possible reason for this is that the errors in computing the dereverberated impedance may be sufficiently large such that the narrowband impedance match is no better at the central frequency than the broadband compensator, and hence both compensators should provide similar performance. Another possibility is that two active struts may not be sufficient to illustrate the performance difference between the two compensators. With more active struts, the difference between the two stochastic solutions, particularly near $\omega_0 = 100$ Hz, might be more noticeable. Even with more struts, and the correct dereverberated impedance, there should not be a large difference between the two compensators' performance, because the broadband compensator that minimizes the desired performance metric over the

	rms DPL			% Reduction		
	A–B	B–C	C–A	A–B	B–C	C–A
Baseline truss	495	417	602	0	0	0
With active struts	492	424	594	-0.7	1.8	-1.2
With D-struts	469	403	564	-5.4	-3.3	-6.2
Constant Gain (B)	465	412	590	-6.1	-1.2	-2.0
Constant Gain (A&B)	443	378	557	-10.5	-9.4	-7.4
Stochastic (A&B)	444	355	549	-10.4	-14.9	-8.8

Table 7.2: Achieved performance, and relative improvement, for 10–500 Hz

entire frequency range is still relatively narrowband in its goals, when compared with the performance achieved by the constant gain solution. Therefore, results are only presented for the open-loop, constant gain feedback, and the broadband stochastic optimization solution.

After implementing the active damping compensators using active struts, the results were compared with passive damping augmentation. The viscous D-struts described in Section 7.1.2 were used for the passive damping. These high loss factor struts are designed to add significant damping in a relatively narrow frequency range, similar to the goal of low authority control. Both active struts used in the LAC tests were replaced by D-struts at the same locations, in order to compare the two.

The performance is composed of the rms differential pathlength error for the three different combinations of pathlengths. This data is shown in Table 7.2 for several different cases. The baseline testbed configuration has no active or passive damping struts in place. Simply adding the active struts to the structure, with no control, results in a change in the performance metric due to the different stiffness and damping characteristics of the active strut as compared with a nominal strut. The performance with each active strut replaced by a D-strut is included to illustrate the possible improvement in damping achieved per strut by an active technique over passive. The difference between closing a single constant gain feedback loop on strut B and clos-

	10–80 Hz			80–150 Hz			150–500 Hz		
	A–B	B–C	C–A	A–B	B–C	C–A	A–B	B–C	C–A
Baseline truss	193	197	166	357	333	468	284	155	340
With active struts	189	200	167	373	337	489	259	164	294
With D-struts	162	190	139	360	322	463	252	151	291
Constant Gain (B)	167	175	170	349	338	482	258	159	295
Constant Gain (A&B)	145	181	143	335	299	457	251	145	284
Stochastic (A&B)	140	168	148	340	278	445	249	143	286

Table 7.3: Achieved performance in frequency bands

	10–80 Hz			80–150 Hz			150–500 Hz		
	A–B	B–C	C–A	A–B	B–C	C–A	A–B	B–C	C–A
Baseline truss	0	0	0	0	0	0	0	0	0
With active struts	-1.8	1.6	0.8	4.4	1.1	4.4	-8.8	5.3	-13.3
With D-struts	-16.0	-3.3	-16.4	0.9	-3.5	-1.0	-11.2	-2.6	-14.4
Constant Gain (B)	-13.6	-11.0	2.3	-2.3	1.3	2.9	-8.9	2.1	-13.1
Constant Gain (A&B)	-24.9	-8.1	-13.5	-6.2	-10.5	-2.4	-11.4	-6.8	-16.3
Stochastic (A&B)	-27.5	-14.5	-11.0	-4.9	-16.6	-5.0	-12.1	-8.0	-15.9

Table 7.4: Percentage reduction in performance, in frequency bands

ing both loops is also shown. There is a diminishing return associated with closing more loops; the greatest decrease in performance is achieved with the first amount of damping added. Finally, active control using the broadband, stochastically optimal approach of this thesis yields about a 30% increase in the performance achieved per strut over the constant gain solution.

The performance for the various cases is shown in Table 7.3 for each of several frequency regions. Table 7.4 shows the corresponding relative improvement over the baseline performance. The same information is presented graphically in Figures 7.17, 7.18, and 7.19. The rms differential pathlength errors in each of several frequency

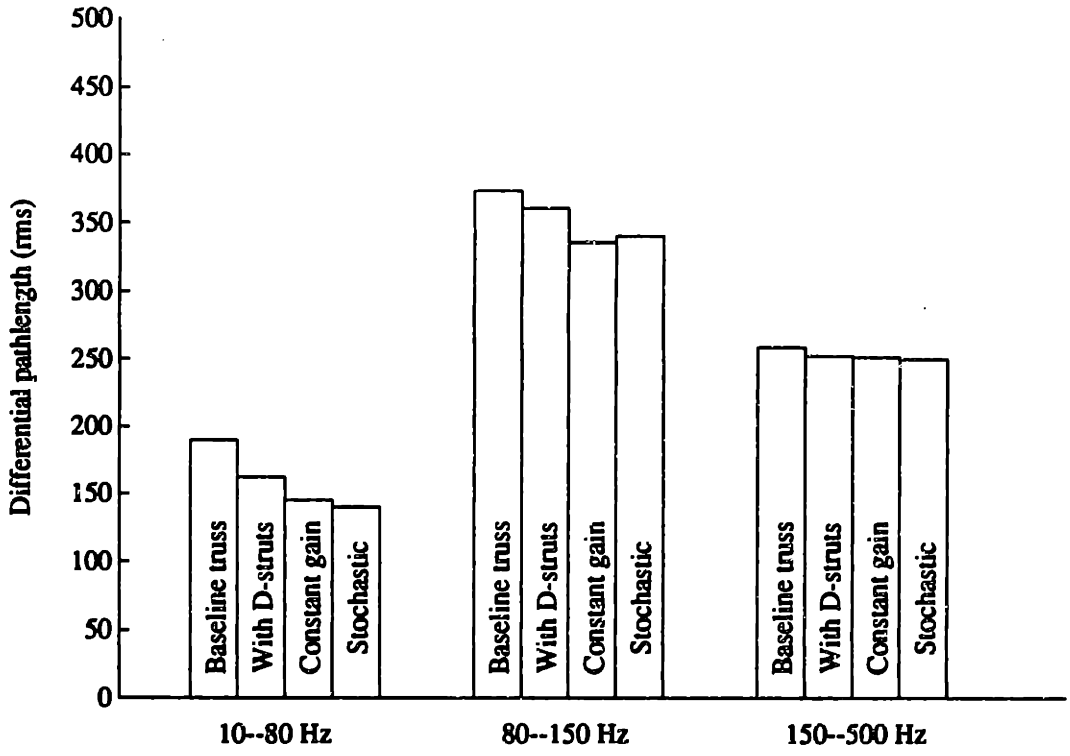

Figure 7.17: Differential pathlength error A–B, for baseline, with two D-struts, with constant gain feedback, and stochastic optimum feedback. (rms in nm^2/Hz).

regions is shown, comparing the baseline configuration with the passive D-struts, constant gain feedback, and the stochastic case.

The open and closed loop autospectra are compared in Figure 7.20 for pathlength B–C, where the broadband stochastic solution obtained the best performance. Below the first mode of the structure, at about 20 Hz, the compensator increased the rms displacement, rather than decreasing it. This is due to the fact that the dereverberated model is not valid in this frequency region. The feedback effectively destiffens the active strut, resulting in an increase in rms displacement. This increase is, of course, more than offset by the decreases at higher frequencies.

A more detailed comparison between the constant gain and stochastic optimum compensators can be made by comparing the performance over a narrow frequency range, as shown in Figure 7.21. The transfer function from the disturbance to the

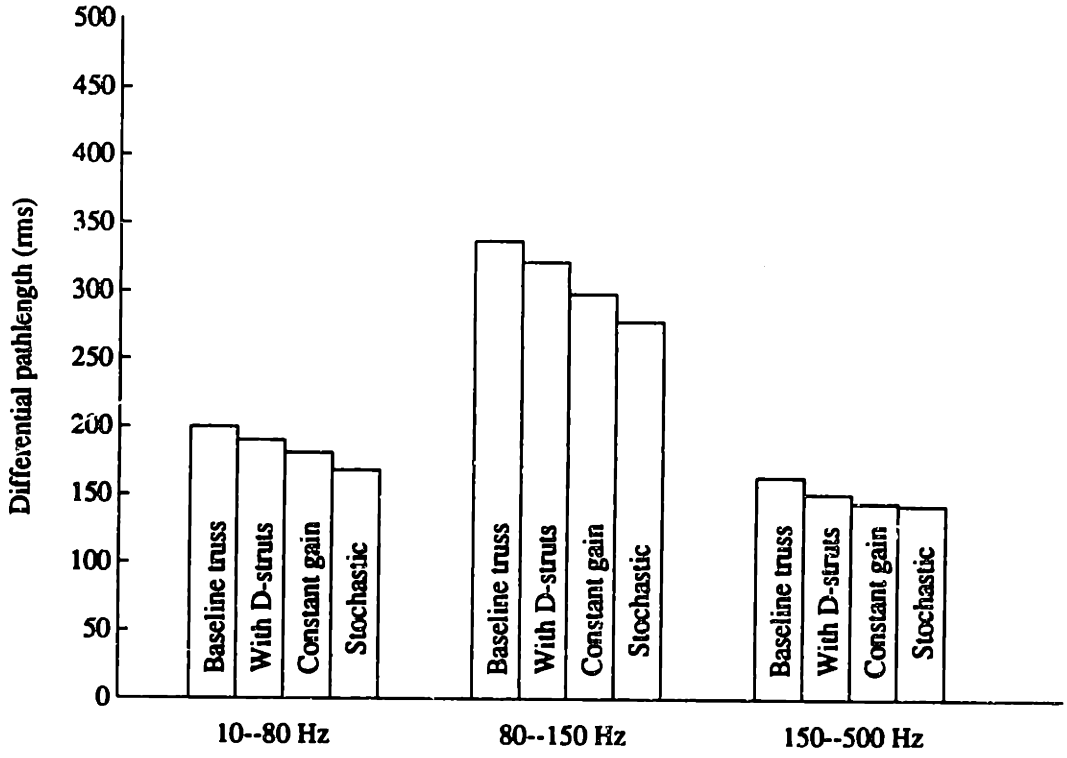

Figure 7.18: Differential pathlength error B–C, for baseline, with two D-struts, with constant gain feedback, and stochastic optimum feedback. (rms in nm^2/Hz).

differential pathlength is shown, with the filter that shapes the disturbance spectrum included. As predicted by the power flow analysis, shown in Figures 7.13 and 7.14, the stochastic optimum achieves greater damping in this frequency region. Indeed, this is the source of the overall decrease in performance between the two compensators. The difference in damping is shown more explicitly in Table 7.5. The damping ratios were obtained by fitting transfer functions between 50 and 150 Hz. In addition to indicating the amount of damping added by the various schemes, and the increase in damping of the stochastic approach over constant gain feedback, this table illustrates the large number of modes within the bandwidth of the controller. Modes below 50 Hz and those above 150 Hz are not included. Note that the damping values quoted are highly uncertain for some of the modes that are not particularly visible in the transfer function data.

Frequency (Hz)	Open-loop Damping	with D-struts	Constant Gain Fdbk	Stochastic Optimum	
52.5	-	0.18	0.24	0.29	
53.6	0.79	0.77	0.98	1.03	⋆
57.1	0.48	0.55	1.34	1.70	
59.2	0.48	0.17	0.67	1.55	
63.4	0.75	0.37	0.55	0.37	
74.8	1.28	1.44	3.63	1.61	
77.0	0.47	0.44	0.49	0.49	⋆
81.1	1.02	2.46	1.67	2.26	
84.4	0.82	1.05	1.01	0.69	⋆
87.0	1.04	0.86	1.58	2.01	⋆
93.8	0.81	1.51	1.56	1.98	⋆
96.0	0.10	0.16	0.13	0.12	
98.3	0.13	0.14	0.15	0.24	⋆
98.9	0.97	1.93	1.68	0.96	
106.0	0.56	0.56	0.90	1.19	⋆
111.5	1.01	1.08	0.93	0.94	⋆
117.3	-	0.90	0.69	1.50	
119.4	0.57	0.62	0.77	1.16	⋆
121.6	0.42	0.39	0.49	0.28	
124.7	0.48	0.46	0.88	0.99	
134.8	1.11	1.12	1.39	1.50	⋆
135.5	2.63	2.31	1.62	1.32	
138.4	0.35	0.81	0.39	0.32	
141.8	0.84	0.98	0.83	0.90	
145.8	-	0.46	1.70	1.45	
149.8	1.28	1.08	2.79	2.41	

Table 7.5: Modal damping (%) on interferometer with active and passive damping. The modes with the greatest residues in the open loop transfer function are indicated with a "⋆." Modes for which the damping in a particular transfer function could not be obtained are indicated with a "-".

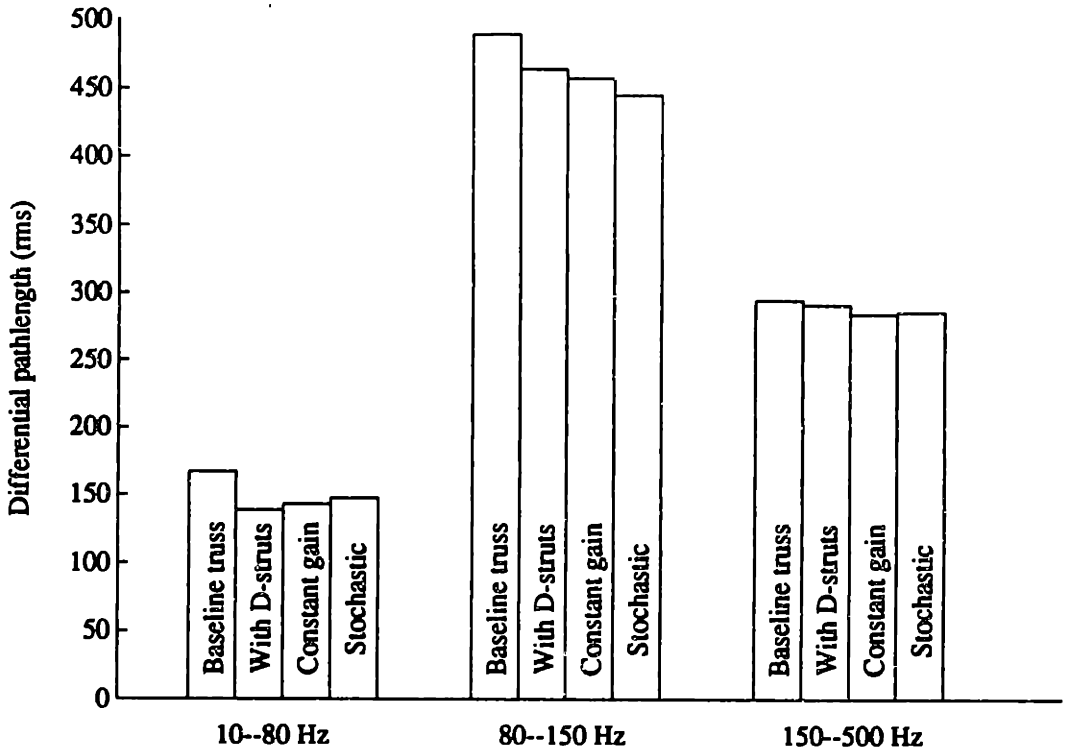

Figure 7.19: Differential pathlength error C–A, for baseline, with two D-struts, with constant gain feedback, and stochastic optimum feedback. (rms in nm^2/Hz).

The data presented above gives the improvement in performance obtained by using low authority control alone. A realistic attempt to improve the performance using this approach would probably use about 10 active struts, with a corresponding improvement in overall performance achieved. However, while this is a valid use for LAC, it is not the only, nor the usual justification for implementing these controllers. For broadband damping, it is likely that a passive damping scheme would be more reliable, and incur a smaller weight penalty. For the narrowband application of adding damping in the roll-off region of a high authority controller, however, an active approach has advantages over passive damping augmentation. This is due to the greater peak damping capability of an active approach, together with its flexibility in tuning the target frequency, and the potential elimination of any weight penalty by using the same hardware as the HAC. For this application, the relevant performance

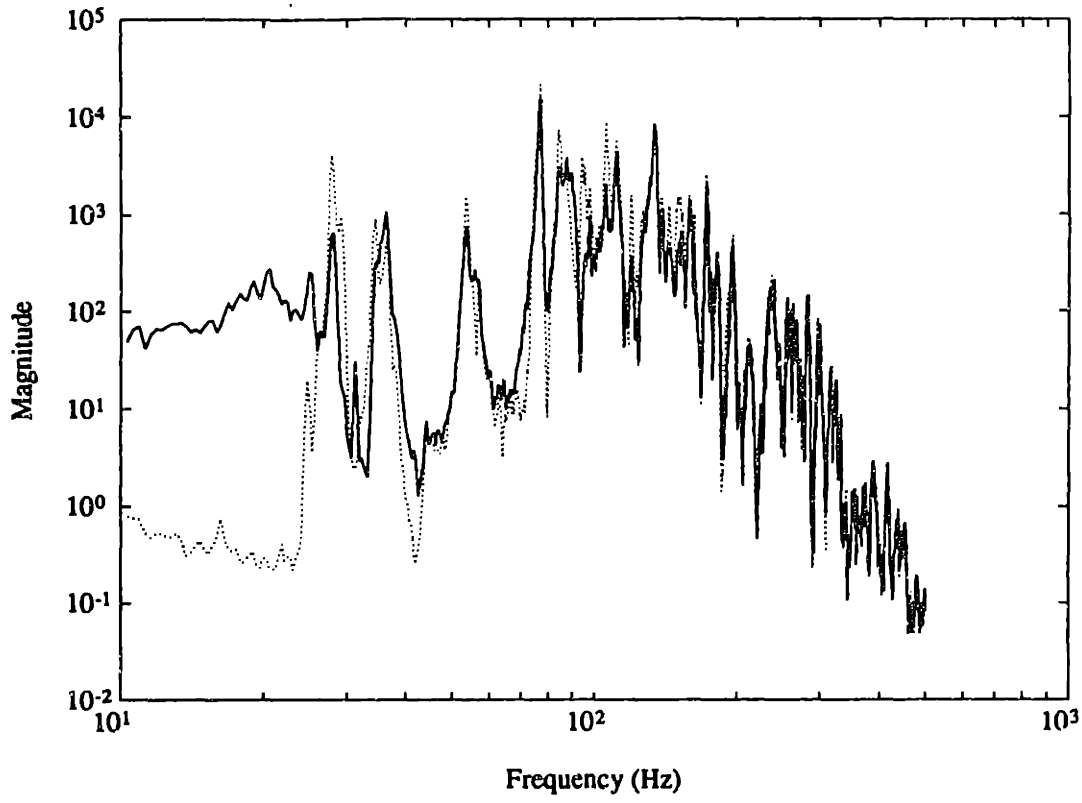

Figure 7.20: Differential pathlength error B–C, for open-loop (dotted), and stochastic optimum feedback (solid). (rms in nm^2/Hz).

improvement that ought to be attributed to low authority control is the difference between the achievable performance of a high authority controller before and after implementation of the LAC. Thus, the true test of the relative merits of constant gain feedback, the stochastic optimization approach, and passive viscous damping awaits a high authority control experiment on the testbed.

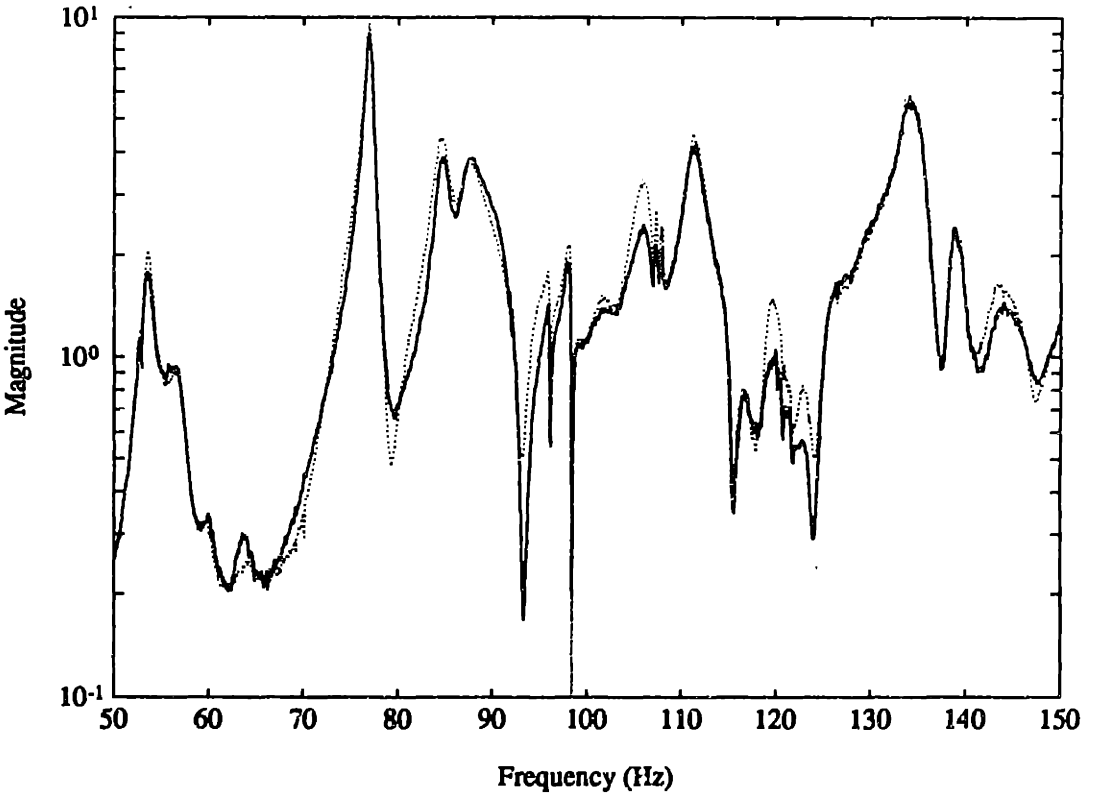

Figure 7.21: Differential pathlength error transfer function B–C, for rate feedback (dotted), and stochastic optimum feedback (solid).

Chapter 8

Conclusions and Recommendations

Holds promise for the future.
Needs more work.
Send money.

--Alou Macalou and E. F. Crawley

8.1 Summary

This thesis investigates an approach to structural modelling and optimal control design for low authority control. The parametric uncertainty that is inherent in any model of the structure is represented by treating the uncertain parameters as stochastic variables. This is similar to the approach taken in Statistical Energy Analysis [58, 47]. In order to describe the statistical aspects of the structure's response, SEA assumes that equipartition and incoherence hold. These properties have been shown in this thesis to result from averaging the state covariance over a stochastic description of the parametric uncertainty. SEA predicts mean energy levels based on input power flows determined through an average, or dereverberated mobility. It was shown in earlier research that this model describes the local dynamics of the structure. Using this model, and the equipartition and incoherence properties for uncertain systems, the expected value of a global $\mathcal{H}_2$ performance metric is shown to

be equivalent to an $\mathcal{H}_2/\mathcal{H}_\infty$ cost functional that depends only on the local information. This cost can be evaluated in state space by solving a Lyapunov and a Riccati equation. The compensator that minimizes this cost must be found numerically, as no closed-form solution has been found. The performance of compensators designed with this stochastic optimization approach has been demonstrated on several simple examples, and experimentally verified on the M.I.T. SERC interferometer testbed.

8.2 Contributions and Conclusions

1. A stochastic modelling approach has been investigated for treating parametrically uncertain structures. Statistical Energy Analysis assumes that equipartition and incoherence hold; that is, that modes in the same frequency band have the same energy, and that different modal amplitudes are uncorrelated. Similar properties have been shown herein to result from a stochastic description of parametric uncertainty. For a large class of uncertainty distributions, the steady state average covariance of a system with large uncertainty in the modal frequencies is of a form where there is equal kinetic and potential energy for each mode, and there is no correlation between kinetic and potential energy states, or between modes. These conclusions have previously been shown for time-averaged covariance, or for particular assumptions on the nature of the forcing.

2. For collocated and dual sensors and actuators, the optimal compensator that maximizes power dissipation is known to be given by an impedance match [61], which is generally non-causal. Previous causal approximations have used $\mathcal{H}_2$ optimizations [68, 69], which did not guarantee stability, and $\mathcal{H}_\infty$ optimizations [61,62], which guaranteed stability by constraining the compensator to be positive real, but did not minimize the true performance metric. Minimizing the global mean-square performance metric, subject to the constraint that only local information is available, is shown herein to yield a mixed $\mathcal{H}_2/\mathcal{H}_\infty$ optimization problem. The resulting optimal compensators both guarantee closed

loop stability, and minimize the quantity of interest. This cost functional can be interpreted as the average value of the global performance metric over large uncertainty in the modal frequencies of the structure.

3. The $\mathcal{H}_2/\mathcal{H}_\infty$ cost that describes the best estimate of the global $\mathcal{H}_2$ cost is related to another unsolved $\mathcal{H}_2/\mathcal{H}_\infty$ cost functional [26, 101, 102], and to a Stackelberg non-zero sum dynamic differential game. The same cost also arises by averaging an $\mathcal{H}_2$ cost over a complex parameter uncertainty of known magnitude but unknown phase. The entropy cost functional of [74] has been shown elsewhere [18, p. 114] to be the average $\mathcal{H}_2$ cost over a complex parameter uncertainty of bounded magnitude, and unknown phase.

4. An optimally designed low authority compensator achieves better performance than the usual "rate feedback," or constant gain approach. Improvements of approximately 30% in performance reduction over rate feedback were obtained on a complex laboratory structure. The optimal approach will always give superior performance over constant gain feedback. Whether the additional effort required to design the compensator is worthwhile depends on the specific problem.

5. The maximum entropy approach [52] to parameter-robust control design was originally justified using a Stratonovich multiplicative white noise model. The resulting covariance equation used for maximum entropy control design is the same as the average covariance of a system which has an uncertain modal frequency with a Cauchy probability distribution. The result has not been shown for damping or mode shape uncertainty. Since the maximum entropy approach can be considered to be a cost averaging approach, it takes advantage of equipartition, incoherence, and conservation of energy. This last property is particularly important for structural control, since many existing robust control design techniques rely on unstructured uncertainty models that do not take this property into account [27, 28]. The results illustrate some of the reasons for the success of the maximum entropy design technique, and also point out a limitation,

since the cost averaging assumed only eigenvalue uncertainty. There is clearly a connection between the maximum entropy approach and the approach of this thesis, since both incorporate cost averaging over uncertain modal frequencies, and take advantage of the properties of parametrically uncertain structures.

8.3 Recommendations

1. The usual purpose in implementing a low authority controller is to add damping to the structure in the roll-off region of a high authority controller. The experimental results in Chapter 7 quote performance data based on implementing only the LAC. While this performance improvement can certainly be attributed to low authority control, it is not entirely fair to consider only this contribution. The total benefit of LAC includes the difference in achievable performance of a high authority controller, with and without the LAC implemented. An experiment should therefore be performed wherein the various possible LAC schemes are implemented simultaneously with a high authority controller. In addition to giving a better indication of the benefits of active damping, such an experiment would provide the correct comparison between constant gain feedback, the stochastic optimal control, and passive damping augmentation.

2. Throughout the thesis, it was assumed that the transfer function between the sensor and actuator was positive real, and hence that a positive real compensator would guarantee stability (or equivalently, that the product of the input and output variables had the same sign as the power flow.) In real structures, this will never be the case, due to actuator and sensor dynamics, time delays and non-collocated actuators and sensors. The simultaneous sensing and actuation approach of [3,24] could be used to eliminate the last problem, while using analog circuits rather than digital control can eliminate the time delay problem. These solutions will increase the frequency at which the transfer function deviates from positivity, but they will not eliminate the problem completely. The control design technique could be modified to allow for perturbations from the

positive real condition, based on a modified small gain test [89]. An unstructured uncertainty could describe the additional phase lag without introducing much conservatism, since the model error is known to be in approximately the worst possible direction. Stability can therefore be guaranteed by including an appropriate $\mathcal{H}_\infty$ norm constraint. Since this constraint can be posed in state space, the numerical optimization could be modified in a relatively straightforward way to incorporate it. If $\mathcal{H}_\infty$ performance is desired, rather than $\mathcal{H}_2$ performance, then the combination of the performance and the positive realness constraint leads to a two block μ problem, as discussed in Section 4.4.2. For this problem, including an additional constraint due to the deviation of the real structure from positivity would simply result in a three block μ problem. It may also be possible in both the $\mathcal{H}_2$ and $\mathcal{H}_\infty$ performance problems to modify the existing positive real constraint to include the additional requirement, without adding an additional constraint.

3. In general, the first few modes of a structure are relatively well known, and the uncertainty in modal frequency increases with mode number. A compensator which discards low frequency information is too conservative. The assumption in this thesis has been that the control design is split into low authority, and high authority controllers, which are designed somewhat independently. Ideally, a single compensator would be designed which takes advantage of the information available in any frequency band, and performs both tasks. Thus an additional modification to the approach could be to incorporate some knowledge of the lowest structural modes. One possible approach to this problem would be to continue with the development given in Section 4.4.1. However, this approach seems excessively complicated. Note that the maximum entropy robust control design technique [13,52] does yield high authority control where there is sufficient modelling accuracy, and collocated positive real control at higher frequencies where the model is inaccurate.

Furthermore, it is apparent from the experimental data that the impedance matching approach presented herein actually increases the performance metric below the frequency of the first flexible mode. This results from the compensator destiffening the structure at low frequencies. Even if the explicit distinction between high and low authority control is made, the design procedure should be capable of identifying different frequency regions above and below the first mode, and acting accordingly. Such an approach may be related to an active isolation approach, which requires that forces be transmitted at low frequencies, but not at high frequencies.

4. The cost averaging approach in Chapter 3 only applies to commuting uncertainty, and therefore only treats eigenvalue uncertainty. This assumption could be relaxed, in order to better justify the maximum entropy approach. While it is unlikely that a useful solution could be obtained for the non-commuting case, it may be possible to obtain bounds on the error in terms of uncertainty limits that would help in obtaining compensator synthesis results.

5. The narrowband stochastically optimal compensator on the interferometer experiment did not achieve a noticeable improvement in dissipation over the broadband compensator at the center frequency. The reasons for this might be worth investigating. One possible reason is that the errors in computing the dereverberated mobility, or indeed the error of assuming such a local model to be applicable at all, may be too large to allow almost-perfect impedance matching at a single frequency. Another possible reason is that since not all of the vibrational energy in the truss passes through one or two active struts, the approximate impedance match of the broadband compensator at the center frequency is sufficient to get almost all of the possible performance improvement at that frequency. If the latter reason is true, then more struts would be required to demonstrate the difference between compensators; if the former reason holds, then no number of struts would ever demonstrate a noticeable improvement with the narrowband compensator.

On the brass beam experiment studied in [62,68], where neither of these reasons were applicable, narrowband compensators were capable of achieving extremely high damping in one or two modes. If this were possible on more general structures, then it would allow a small number of actuators to target damping to a single mode that destabilizes a high authority controller, while a more broadband passive damping approach may need significantly more elements to achieve the same result. Furthermore, many realistic structural vibration or noise control problems have extremely narrowband disturbance spectra, with a center frequency which may change slowly as a function of time. This is the case, for example, on many spacecraft where the primary source of structural vibration is from reaction wheel imbalances, and occurs at harmonics of the reaction wheel speed. If excellent narrowband performance can be achieved through an impedance matching approach, then the center frequency could be tuned to the disturbance frequency. The guaranteed stability properties of a local controller could make this approach preferable to more general active control methods, while the narrowband capability could result in a lower weight penalty than passive damping augmentation.

References

[1] Anderson, E., M. Trubert, J. Fanson, and L. Davis, "Testing and Application of a Viscous Passive Damper for Use in Precision Truss Structures," *Proceedings, AIAA Structures, Structural Dynamics, and Materials Conference*, 1991, pp. 2796–2808. AIAA Paper 91-0996.

[2] Anderson, E. H., G. H. Blackwood, and J. P. How, "Passive Damping in the MIT SERC Controlled Structures Testbed," *Proceedings, International Symposium on Active Materials and Adaptive Structures*, Alexandria, VA, Nov. 1991.

[3] Anderson, E. H., N. W. Hagood, and J. M. Goodliffe, "Self-Sensing Piezoelectric Actuation: Analysis and Application to Controlled Structures," *Proceedings, AIAA Structures, Structural Dynamics, and Materials Conference*, Dallas, TX, Apr. 1992.

[4] Ashkenazi, A. and A. E. Bryson Jr., "Control Logic for Parameter Insensitivity and Disturbance Attenuation," *AIAA Journal of Guidance, Control, and Dynamics*, Vol. 5, No. 4, July 1982, pp. 383–388.

[5] Aubrun, J.-N., "Theory of the Control of Structures by Low-Authority Controllers," *AIAA Journal of Guidance and Control*, Vol. 3, No. 5, Sept–Oct 1980, pp. 444–451.

[6] Balas, M. J., "Trends in Large Space Structure Control Theory: Fondest Hopes, Wildest Dreams," *IEEE Trans. on Automatic Control*, Vol. AC–27, No. 3, June 1982, pp. 522–535.

[7] Basar, T. and H. Selbuz, "Closed-Loop Stackelberg Strategies with Applications in the Optimal Control of Multilevel Systems," *IEEE Trans. on Automatic Control*, Vol. AC–24, No. 2, Apr. 1979, pp. 166–179.

[8] Bellman, R., *Introduction to Matrix Analysis*, McGraw-Hill Book Company, New York, 1970.

[9] Bernstein, D. S., E. G. Collins, Jr., and D. C. Hyland, "Real Parameter Uncertainty and Phase Information in the Robust Control of Flexible Structures," *Proceedings, IEEE Conference on Decision and Control*, Honolulu, HI, 1990, pp. 379–380.

[10] Bernstein, D. S., L. D. Davis, S. W. Greeley, and D. C. Hyland, "Numerical Solution of the Optimal Projection/Maximum Entropy Design Equations for Low-Order Robust Controller Design," *Proceedings, IEEE Conference on Decision and Control*, Ft. Lauderdale, FL, Dec. 1985, pp. 1795–1798.

[11] Bernstein, D. S. and S. W. Greeley, "Robust Controller Synthesis Using the Maximum Entropy Design Equations," *IEEE Trans. on Automatic Control*, Vol. AC–31, No. 4, Apr. 1986, pp. 362–364.

[12] Bernstein, D. S. and W. M. Haddad, "LQG Control with an $\mathcal{H}_\infty$ Performance Bound: A Riccati Equation Approach," *IEEE Trans. on Automatic Control*, Vol. AC–34, No. 3, Mar. 1989, pp. 293–305.

[13] Bernstein, D. S. and D. C. Hyland, "The Optimal Projection Approach to Robust, Fixed-Structure Control Design," in *Mechanics and Control of Space Structures* (Junkins, J. L., ed.), pp. 237–293, AIAA, Washington, D. C., 1990.

[14] Bernstein, D. S. and D. C. Hyland, "Compartmental Modeling and Power Flow Analysis for State Space Systems," *Proceedings, First International Workshop on Robust Control* (Bhattacharyya, S. P. and L. H. Keel, eds.), San Antonio, TX, CRC press, Mar. 1991.

[15] Bhattacharyya, S. P. and L. H. Keel, eds., *Proceedings of the First International Workshop on Robust Control*, (San Antonio, TX), CRC press, Mar. 1991.

[16] Blackwood, G. H., C.-C. Chu, J. L. Fanson, and S. W. Sirlin, "Uncertainty Modelling for the Control of an Active Structure," *Proceedings, Winter Annual Meeting of the ASME*, 1989, pp. 43–51.

[17] Blackwood, G. H., R. N. Jacques, and D. W. Miller, "The MIT Multipoint Alignment Testbed: Technology Development for Optical Interferometry," *Proceedings, SPIE Conference on Active and Adaptive Optical Systems*, San Diego, CA, July 1991.

[18] Boyd, S. P. and C. H. Barratt, *Linear Controller Design: Limits of Performance*, Prentice-Hall, Englewood Cliffs, NJ, 1991.

[19] Chen, G.-S., B. J. Lurie, and B. K. Wada, "Experimental Studies of Adaptive Structures For Precision Performance," *Proceedings, 30th Structures, Structural Dynamics and Materials Conference*, Mobile, AL, Apr. 1989, pp. 1462–1472.

[20] Chen, G.-S., B. J. Lurie, and B. K. Wada, "Bridge Feedback for Active Damping Augmentation," *Proceedings, AIAA Dynamics Specialist Conference*, Long Beach, CA, Apr. 1990, pp. 502–510.

[21] Crawley, E. F., M. S. Barlow, and M. C. van Schoor, "Variation in the Modal Parameters of Space Structures," *Proceedings, AIAA Structures, Structural Dynamics, and Materials Conference*, Apr. 1992.

[22] Crawley, E. F. and S. R. Hall, "The Dynamics of Controlled Structures," Tech. Rep. SERC #10-91-I, M.I.T. Space Engineering Research Center, July 1991.

[23] Donoghue Jr., W. F., *Distributions and Fourier Transforms*, Academic Press, New York, 1969.

[24] Dosch, J. J., D. J. Inman, and E. Garcia, "A Self-Sensing Piezoelectric Actuator for Collocated Control," *Journal of Intelligent Materials, Systems and Structures*, Vol. 3, Jan. 1992, pp. 166–185.

[25] Dowell, E. H. and Y. Kubota, "Asymptotic Modal Analysis and Statistical Energy Analysis of Dynamical Systems," *Journal of Applied Mechanics*, Vol. 52, 1985, pp. 1–9.

[26] Doyle, J., K. Zhou, and B. Bodenheimer, "Optimal Control with Mixed $\mathcal{H}_2$ and $\mathcal{H}_\infty$ Performance Objectives," *Proceedings, American Control Conference*, Pittsburgh, PA, 1989, pp. 2065–2070.

[27] Doyle, J. C., "Analysis of Feedback Systems with Structured Uncertainties," *IEE Proceedings*, Vol. 129, Part D, No. 6, Nov. 1982, pp. 242–250.

[28] Doyle, J. C., K. Glover, P. P. Khargonekar, and B. A. Francis, "State-Space Solutions to Standard $\mathcal{H}_2$ and $\mathcal{H}_\infty$ Control Problems," *IEEE Trans. on Automatic Control*, Vol. AC–34, No. 8, Aug. 1989, pp. 831–847.

[29] Fan, M. K. H., A. L. Tits, and J. C. Doyle, "Robustness in the Presence of Mixed Parametric Uncertainty and Unmodeled Dynamics," *IEEE Trans. on Automatic Control*, Vol. AC–36, No. 1, Jan. 1991, pp. 25–38.

[30] Fano, R. M., "Theoretical Limitations on the Broadband Matching of Arbitrary Impedances," *Journal of the Franklin Institute*, Jan., and Feb. 1950, pp. 57–83, 139–154.

[31] Francis, B. A., *A Course in $\mathcal{H}_\infty$ Control Theory*, Springer-Verlag, 1987.

[32] Frisch, U., "Wave Propagation in Random Media," in *Probabilistic Methods in Applied Mathematics* (Bharucha-Reid, A. T., ed.), Vol. 1, pp. 75–197, Academic Press, NY, 1968.

[33] Fuhrmann, P. A., "Elements of Factorization Theory From a Polynomial Point of View," in *Three Decades of Mathematical System Theory*, pp. 148–178, Springer-Verlag, 1989.

[34] Gangsaas, D., K. R. Bruce, J. D. Blight, and U.-L. Ly, "Application of Modern Synthesis to Aircraft Control," *IEEE Trans. on Automatic Control*, Vol. AC–31, No. 11, Nov. 1986, pp. 995–1014.

[35] Ghosh, B. K. and C. I. Byrnes, "Simultaneous Stabilization and Simultaneous Pole Placement by Non-switching Dynamic Compensation," *IEEE Trans. on Automatic Control*, Vol. AC–28, No. 6, June 1983, pp. 735–741.

[36] Graham, A., *Kronecker Products and Matrix Calculus: with Applications*, Ellis Horwood Limited, 1981.

[37] Greeley, S. W., D. J. Phillips, and D. C. Hyland, "Experimental Demonstration of the Maximum Entropy/Optimal Projection Design Theory for Active Vibration Control," pp. 1462–1467.

[38] Grimble, M. J., "LQG Optimal Control Design for Uncertain Systems," *IEE Proceedings-D*, Vol. 139, No. 1, Jan. 1992, pp. 21–30.

[39] Grocott, S. C. O., D. G. MacMartin, and D. W. Miller, "Experimental Implementation of a Multiple Model Technique for Robust Control of the MACE Test Article," Submitted to the *Third International Conference on Adaptive Structures*, Nov. 1992.

[40] Guicking, D., J. Melcher, and R. Wimmel, "Active Impedance Control in Mechanical Structures," *Acustica*, Vol. 69, 1989, pp. 39—52.

[41] Haddad, W. M. and D. S. Bernstein, "On the Gap Between $\mathcal{H}_2$ and Entropy Perfomance Measures in $\mathcal{H}_\infty$ Control Design," *Proceedings, IEEE Conference on Decision and Control*, Dec. 1989, pp. 1506–1508.

[42] Haddad, W. M. and D. S. Bernstein, "Robust Stabilization with Positive Real Uncertainty: Beyond the Small Gain Theorem," *Proceedings, IEEE Conference on Decision and Control*, Honolulu, HI, 1990, pp. 2054–2059.

[43] Hagedorn, P. and J. T. Schmidt, "On the Active Vibration Control of Distributed Parameter Systems," *Proceedings,* 6^{th} VPI&SU/AIAA *Symposium on Dynamics and Control of Large Structures*, 1987, pp. 359–373.

[44] Hagood, N. W., *Cost Averaging Techniques for Robust Control of Parametrically Uncertain Systems*, Ph.D. thesis, Department of Aeronautics and Astronautics, M.I.T., Cambridge, MA, June 1991.

[45] Hagood, N. W., "Cost Averaging Techniques for Robust Control of Parametrically Uncertain Systems," Presented at *AIAA Guidance, Navigation and Control Conference*, Aug. 1991. AIAA Paper 91-2605.

[46] Hall, S. R., D. G. MacMartin, and D. S. Bernstein, "Covariance Averaging in the Analysis of Uncertain Systems," To appear, *IEEE Transactions on Automatic Control*, 1992.

[47] Hodges, C. H. and J. Woodhouse, "Theories of Noise and Vibration Transmission in Complex Structures," *Reports on Progress in Physics*, Vol. 49, 1986, pp. 107–170.

[48] Hopkins Jr., W. E., "Optimal Control of Linear Systems with Parameter Uncertainty," *IEEE Trans. on Automatic Control*, Vol. AC-31, No. 1, Jan. 1986, pp. 72–74.

[49] Horn, R. A. and C. R. Johnson, *Matrix Analysis*, Cambridge University Press, Cambridge, UK, 1985.

[50] How, J. P. and S. R. Hall, "Connection between the Popov Criterion and Upper Bounds for Real Parametric Uncertainty," 1992. Preprint.

[51] Hsia, W.-S., "Stochastic Model of the NASA/MSFC Ground Facility for Large Space Structures with Uncertain Parameters – The Maximum Entropy Approach," Tech. Rep. NASA-CR-181489, NASA, 1987.

[52] Hyland, D. C., "Maximum Entropy Stochastic Approach to Controller Design for Uncertain Structural Systems," *Proceedings, American Control Conference*, Arlington, VA, June 1982, pp. 680–688.

[53] Keane, A. J. and W. G. Price, "Statistical Energy Analysis of Strongly Coupled Systems," *Journal of Sound and Vibration*, Vol. 117, No. 2, 1987, pp. 363–386.

[54] Lazarus, K. B. and E. F. Crawley, "Multivariable High-Authority Control of Plate-Like Structures," *Proceedings, AIAA Structures, Structural Dynamics, and Materials Conference*, Apr. 1992.

[55] Ly, U.-L., A. E. Bryson, and R. H. Cannon, "Design of Low-order Compensators using Parameter Optimization," *Automatica*, Vol. 21, No. 3, 1985, pp. 315–318.

[56] Lyon, R. H., "Statistical Analysis of Power Injection and Response in Structures and Rooms," *The Journal of the Acoustical Society of America*, Vol. 45, No. 3, Mar. 1969, pp. 545–565.

[57] Lyon, R. H., *Machinery Noise and Diagnostics*, Butterworth Publishing, June 1987.

[58] Lyon, R., *Statistical Energy Analysis of Dynamical Systems: Theory and Applications*, The MIT Press, Cambridge MA, 1975.

[59] Mace, B. R., "Active Control of Flexural Vibrations," *Journal of Sound and Vibration*, Vol. 114, No. 2, 1987, pp. 253–270.

[60] Maciejowski, J. M., *Multivariable Feedback Design*, Addison-Wesley, Wokingham, England, 1989.

[61] MacMartin, D. G. and S. R. Hall, "Control of Uncertain Structures using an $\mathcal{H}_\infty$ Power Flow Approach," *AIAA Journal of Guidance, Control, and Dynamics*, Vol. 14, No. 3, May–June 1991, pp. 521–530.

[62] MacMartin, D. G. and S. R. Hall, "Structural Control Experiments using an $\mathcal{H}_\infty$ Power Flow Approach," *Journal of Sound and Vibration*, Vol. 148, No. 2, July 1991, pp. 223–241.

[63] MacMartin, D. G., S. R. Hall, and D. Mustafa, "On a Cost Functional for $\mathcal{H}_2/\mathcal{H}_\infty$ Minimization," *Proceedings, IEEE Conference on Decision and Control*, Honolulu, HI, Dec. 1990, pp. 1010–1012.

[64] MacMartin, D. G., D. W. Miller, and S. R. Hall, "Structural Control using Active Broadband Impedance Matching," in *Recent Advances in Active Control of Sound and Vibration*, Apr. 1991, pp. 604–617.

[65] Medanic, J., "Closed-loop Stackelberg Strategies in Linear-Quadratic Problems," *IEEE Trans. on Automatic Control*, Vol. AC–23, No. 4, Aug. 1978, pp. 632–637.

[66] Mercadal, M., *$\mathcal{H}_2$, Fixed Architecture, Control Design for Large Scale Systems*, Ph.D. thesis, Department of Aeronautics and Astronautics, M.I.T., Cambridge, MA, June 1990.

[67] Miller, D. W., *Modelling and Active Modification of Wave Scattering in Structural Networks*, Ph.D. thesis, Department of Aeronautics and Astronautics, M.I.T., 1988. (Space Systems Laboratory Report #12–88).

[68] Miller, D. W. and S. R. Hall, "Experimental Results Using Active Control of Travelling Wave Power Flow," *AIAA Journal of Guidance, Control, and Dynamics*, No. 2, Mar–Apr 1991, pp. 350–359.

[69] Miller, D. W., S. R. Hall, and A. H. von Flotow, "Optimal Control of Power Flow at Structural Junctions," *Journal of Sound and Vibration*, Vol. 140, No. 3, 1990, pp. 475–497.

[70] Miller, D. W., E. Saarmaa, and R. N. Jacques, "Preliminary Structural Control Results from the Middeck Active Control Experiment (MACE)," *Proceedings, AIAA Structures, Structural Dynamics, and Materials Conference*, Apr. 1992.

[71] Miller, D. W. and A. H. von Flotow, "A Travelling Wave Approach to Power Flow in Structural Networks," *Journal of Sound and Vibration*, Vol. 128, No. 1, 1989, pp. 145–162.

[72] Miyazawa, Y., "Robust Flight Control System Design with Multiple Model Approach," *Proceedings, AIAA Guidance, Navigation, and Control Conference*, Portland, OR, Aug. 1990, pp. 874–882.

[73] Mustafa, D., "Relations Between Maximum-entropy/$\mathcal{H}_\infty$ Control and Combined $\mathcal{H}_\infty$/LQG Control," *Systems and Control Letters*, Vol. 12, 1989, pp. 193–203.

[74] Mustafa, D., *Minimum Entropy $\mathcal{H}_\infty$ Control*, Springer-Verlag, 1990.

[75] Nelson, P. A., A. R. D. Curtis, S. J. Elliot, and A. J. Bullmore, "The Active Minimization of Harmonic Enclosed Sound Fields, Part I:Theory," *Journal of Sound and Vibration*, Vol. 117, No. 1, 1987, pp. 1–13.

[76] O'Neal, M. and D. Eldred, "The JPL Phase-B Testbed," *Symposium on Active Materials and Adaptive Structures*, 1991.

[77] Pearson, R. K. and T. L. Johnson, "Energy Equipartition and Fluctuation-Dissipation Theorems for Damped Flexible Structures," *Quarterly of Applied Mathematics*, Vol. 45, 1987, pp. 223–238.

[78] Pierce, A. D., *Acoustics: an Introduction to its Physical Principles and Applications*, McGraw-Hill, New York, 1981.

[79] Preumont, A., J.-P. Dufour, and C. Malékian, "Active Damping by a Local Force Feedback with Piezoelectric Actuators," *AIAA Journal of Guidance, Control, and Dynamics*, No. 2, March–April 1992, pp. 390–395.

[80] Redman-White, W., P. A. Nelson, and A. R. D. Curtis, "Experiments on the Active Control of Flexural Wave Power Flow," *Journal of Sound and Vibration*, Vol. 112, No. 1, 1987, pp. 187–191.

[81] Rhee, I. and J. L. Speyer, "A Game Theoretic Controller and its Relationship to $\mathcal{H}_\infty$ and Linear-Exponential-Gaussian Synthesis," *Proceedings, 28th IEEE Conf. on Decision and Control*, Dec. 1989, pp. 909–915.

[82] Rotea, M. A. and P. P. Khargonekar, "$\mathcal{H}_2$-optimal Control with an $\mathcal{H}_\infty$-constraint: The State Feedback Case," *Automatica*, Vol. 27, No. 2, 1991, pp. 307–316.

[83] Rotea, M. A. and P. P. Khargonekar, "Mixed $\mathcal{H}_2/\mathcal{H}_\infty$ Control via Convex Programming," *Proceedings, American Control Conference*, Boston, MA, June 1991, pp. 1149–1154.

[84] Rudin, W., *Principles of Mathematical Analysis*, McGraw-Hill, New York, 1976.

[85] Scales, L. E., *Introduction to Non-Linear Optimization*, Springer-Verlag, New York, 1985.

[86] Scheuren, J., "Active Control of Bending Waves in Beams," *Proceedings, Internoise*, Munich, Sept. 1985, pp. 591–594.

[87] Simaan, M. and J. B. Cruz, "On the Stackelberg Strategy in Nonzero-Sum Games," *Journal of Optimization Theory and Applications*, Vol. 11, No. 5, 1973, pp. 533–555.

[88] Skudrzyk, E., "The Mean-value Method of Predicting the Dynamic Response of Complex Vibrators," *The Journal of the Acoustical Society of America*, Vol. 67, No. 4, Apr. 1980, pp. 1105–1135.

[89] Slater, G. L., A. Bosse, and Q. Zhang, "Robustness of Positive Real Controllers for Large Space Structures," *AIAA Journal of Guidance, Control, and Dynamics*, Vol. 15, No. 1, Jan–Feb 1991, pp. 58–64.

[90] Steinbuch, M. and O. Bosgra, "Necessary Conditions for Static and Fixed Order Dynamic Mixed $\mathcal{H}_2/\mathcal{H}_\infty$ Optimal Control," *Proceedings, American Control Conference*, Boston, MA, 1991, pp. 1137–1142.

[91] Steinbuch, M., S. G. Smit, G. Schootstra, and C. Bosgra, "μ-Synthesis of a Flexible Mechanical Servo System," *Proceedings, American Control Conference*, Boston, MA, 1991, pp. 593–598.

[92] Stengel, R. F. and L. R. Ray, "Stochastic Robustness of Linear Time-Invariant Control Systems," *IEEE Trans. on Automatic Control*, Vol. AC–36, No. 1, Jan. 1991, pp. 82–86.

[93] Van Valkenburg, M. E. and B. K. Kinariwala, *Linear Circuits*, Prentice-Hall, 1982.

[94] Vaughan, D., "Application of Distributed Parameter Concepts to Dynamic Analysis and Control of Bending Vibrations," *Journal of Basic Engineering*, June 1968, pp. 157–166.

[95] von Flotow, A. H., "The Acoustic Limit of Structural Dynamics," in *Large Space Structures: Dynamics and Control*, pp. 213–238, Springer-Verlag, 1988.

[96] von Flotow, A. H. and B. Schäfer, "Wave-Absorbing Controllers for a Flexible Beam," *AIAA Journal of Guidance, Control, and Dynamics*, Vol. 9, No. 6, Nov.–Dec. 1986, pp. 673–680.

[97] Wie, B. and D. S. Bernstein, "A Benchmark Problem for Robust Control Design," *Proceedings, American Control Conference*, San Diego, CA, May 1990, pp. 961–962.

[98] Wie, B. and D. S. Bernstein, "Benchmark Problems for Robust Control Design," *Proceedings, American Control Conference*, Boston, MA, June 1991, pp. 1929–1930.

[99] Yeh, H.-H. and S. S. Banda, "Necessary and Sufficient Conditions for Mixed $\mathcal{H}_2$ and $\mathcal{H}_\infty$ Optimal Control," *Proceedings, IEEE Conference on Decision and Control*, Honolulu, HI, Dec. 1990.

[100] Young, P. M., M. P. Newlin, and J. C. Doyle, "μ Analysis with Real Parametric Uncertainty," *Proceedings, IEEE Conference on Decision and Control*, Brighton, England, Dec. 1992, pp. 1251–1256.

[101] Zhou, K., J. Doyle, K. Glover, and B. Bodenheimer, "Mixed $\mathcal{H}_2$ and $\mathcal{H}_\infty$ Control," *Proceedings, American Control Conference*, San Diego, CA, May 1990, pp. 2502–2507.

[102] Zhou, K., K. Glover, B. Bodenheimer, and J. Doyle, "Mixed $\mathcal{H}_2$ and $\mathcal{H}_\infty$ Performance Objectives I: Robust Performance Analysis," Submitted to the *IEEE Trans. on Automatic Control*, 1992.